Hamaus

An Experiment to Search Exotic Resonances in Proton -Antiproton Collisions at CERN's LEAR

A Track Reconstruction Program and its Application to Simulated Data

Helen Korsmo

A thesis submitted to the
Faculty of the Department of Physics of the
University of Oslo in partial fulfillment
of the requirements for the degree
Cand.Scient.
February 1990

An Experiment to Search Exotic Resonances in Proton -Antiproton Collisions at CERN's LEAR

A Track Reconstruction Program and its Application to Simulated Data

Helen Korsmo

A thesis submitted to the
Faculty of the Department of Physics of the
University of Oslo in partial fulfillment
of the requirements for the degree
Cand.Scient.
February 1990

To my mother and the memory of my father.

Abstract

The experiment PS202 (JETSET) at CERN's LEAR will search for gluonic resonances in proton antiproton collisions with an internal gas jet target inserted in the LEAR ring. In this thesis I give a short overview of the field of gluonium physics, followed by a description of the JETSET experiment. We have developed a track fitting program for the experiment, and tested it on Monte Carlo events. I describe the program in detail, as well as presenting the results for mass resolution, and background rejection efficiency of the detector. The appendix gives a summary of the main results, and does also present some new results.

Aknowledgements

I would like to thank my supervisor, Bjarne Stugu, for his help and guidance during the work with my thesis, and for reading through all the versions of the manuscript, giving a lot of suggestions for improvements.

I also want to thank the other students and employees at the Particle Physics Group at the University of Oslo, especially fellow student Elias Bergan, for many clarifying discussions, and Lars Bugge, who managed to keep the Vax computers working, sometimes under very difficult conditions.

Helen Karsmo

Oslo, 1. February 1990

Contents

List of Figures

List of Tables

Chapter 1

Glueballs

The QCD theory for strong interactions predicts the existence of a new form of matter, glueballs. In the JETSET experiment at CERN we will search these particles, for which there so far exists no clear evidence .

This chapter will explain why we expect that glueballs exist, and the theoretical predictions we have about their mass, quantum number, production and decay properties. The possibility of observing gluonium states and distinguishing them from quarkonium(ordinary mesons) will be discussed.

A short summary of glueball-candidates seen so far in experiments will be given, and we will conclude with an outline of what is special about our experiment, and why we expect that it will provide valuable information.

1.1 The Colour Force

In this section the history of events that led to QCD, and its main properties will be described.More details as well as the original references are given in [6],[18],and [7].

Before 1950 only a few elementary particles were known.They were the electron, the muon, and the photon, and the strongly interacting particles, the proton, the neutron and the pion .

The electromagnetic interaction between particles was well understood, through the theory of quantum electrodynamics, QED. The strong force , not so well understood , was described by the exchange of virtual pions by Yukawa in 1935.

However , when high energy accelerators were built in the 50's and 60's a large number of new strongly interacting particles were found, these could not be understood as elementary particles.

M.Gell-Mann and Y.Ne'eman showed in 1961 that the hadrons could be described by the so called "Eightfold Way".All hadrons can be classified in eight and ten dimensional representations of SU(3), which can be interpreted as products of the fundamental three dimensional representation. In 1964 Gell-Mann and G.Zweig assigned real particles to the triplet, and called them quarks.Quarks have spin 1/2 and fractional electric charge. The three quarks in the triplet have different flavour, up,down and strange, and the flavour SU(3) symmetry is only exact if we ignore quark masses. In later years one has found evidence for two more flavours, charm and bottom.

One of the particles the eightfold way predicted, and that was discovered in 1964 is the Ω^-, which consists of three s quarks. However this state seems to break the Pauli exclusion principle because we have three identical fermions with parallel spin of 1/2. Greenberg solved this problem by introducing a new degree of freedom, called colour.He postulated that there exist three colours,R,B,Y and anticolours, and that real particles are colour singlets ($RBG, \overline{RBG}, R\overline{R} + B\overline{B} + G\overline{G}$). Also the ratio

$$R = \frac{\sigma(e^+e^- \rightarrow hadrons)}{\sigma(e^+e^- \rightarrow \mu^+\mu^-)}$$

indicated the existence of quark colours.This ratio is equal to the sum of the quark charges for all flavours $\sum e_i^2$.However the result gets in agreement with experiment only if we multiply by 3, implying that each quark flavour comes in three different types.

It turns out that colour also explains the force between quarks. The free Lagrangian for quarks is the ordinary Dirac Lagrangian

$$\mathcal{L}_0 = \overline{\Psi}(i\gamma^\mu\partial_\mu - m)\Psi \tag{1.1}$$

where Ψ is a three dimensional column vector in colour space.Here we consider only one flavour.

We now assume a local $SU(3)_{colour}$ symmetry, (different from $SU(3)_{flavour}$), in the same way as local U(1) gauge invariance is assumed in QED. The local phase transformations will be of the form

$$\Psi(x) \rightarrow e^{i\alpha_a(x)T_a}\Psi(x) \tag{1.2}$$

where T_a, a=1,..8, are $\lambda_a/2$,the λ's are the eight 3×3 Gell-mann matrices,

and $\alpha(x)$ some function of x. Since the generators T_a do not commute, the theory is non-Abelian.

The free Lagrangian of equation 1.1 is not gauge invariant, but the following Lagrangian is

$$\mathcal{L} = -\frac{1}{2}G^a_{\mu\nu}G^{\mu\nu}_a + i\overline{\Psi}\gamma^\mu D_\mu\Psi + \overline{\Psi}m\Psi. \tag{1.3}$$

D_μ is the covariant derivative

$$D_\mu = \partial_\mu - ig_s G^a_\mu T_a \tag{1.4}$$

and $G^a_{\mu\nu}$ is the field strength tensor,

$$G^a_{\mu\nu} = \partial_\mu G^a_\nu - \partial_\nu G^a_\mu + g_s f_{abc} G^b_\nu G^c_\mu. \tag{1.5}$$

G^a_μ are the eight vector boson fields, or gluons, which transforms as

$$G^a_\mu \rightarrow G^a_\mu + \frac{1}{g_s}\partial_\mu\alpha_a + f_{abc}\alpha_b G^c_\mu. \tag{1.6}$$

A mass term for the gluons, $\frac{1}{2}m^2 G^a_\mu G^\mu_a$ is not consistent with gauge invariance, and therefore gluons must be massless.

It can be shown that the binding is attractive for colour singlets, and less attractive or repulsive for other combinations. While we can have charged electrical objects, it is postulated that a particle with net colour (e.g.a free quark) can not be observed.The reason for this is that the force is not dependent of the inverse square of the distance like in electrostatics, it increases or is constant with distance.Figure 1.1 shows the field lines between electon-positron, and quark-antiquark. However this is not a fundamental feature of QCD.

From the Lagrangian in equation 1.3 we get couplings of quarks and gluons, but also self couplings of gluons corresponding to the vertices shown in figure 1.2.These gluon -gluon vertices arise because the group is non-abelian. The eight gluons have colour charges

$$R\overline{B}, B\overline{R}, R\overline{G}, B\overline{G}, \overline{R}G, \overline{B}G, (B\overline{B} - R\overline{R})/\sqrt{2}, \text{and}(R\overline{R} + B\overline{B} - 2G\overline{G})/\sqrt{6}.$$

Because gluons can interact with other gluons it is possible to get bound, colour less states containing only gluons, called glueballs.

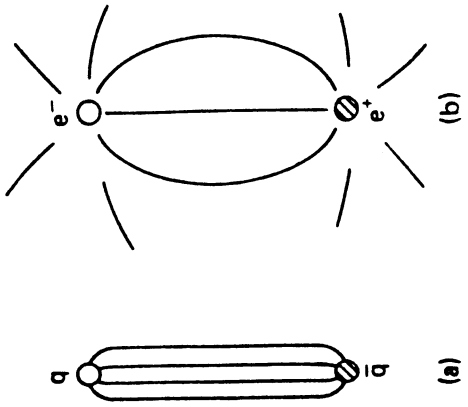

Figure 1.1: Field-lines for coulomb and colour field(from [6])

A problem in QCD arises from the fact that the coupling constant g_s increases at large distanses.In QED it is possible to make detailed calculations because the coupling constant is so small that we can use perturbation theory. In QCD the vacum polarisation of both quarks and gluons will give an increase of g_s at small momentum transfer, or long distances. It is then very difficult to calculate the masses of the particles.

1.2 Looking for Glueballs

Because of the special properties of the colour force, QCD predicts not only bound states of coloured quarks like $q\overline{q}$, and qqq, but also bound states of gluons, gg, ggg called glueballs, and of quarks and gluons,for example $g\overline{q}q$, which are called hybrids and meiktons. If we don't find evidence for these particles, it could mean that we do not have a proper understanding of the colour force.

When so many mesons and baryons have been discovered during the last thirty years why haven't we seen any glueballs ? There can be several reasons for this.

- Glueballs might be so broad that they can't be disentangled from

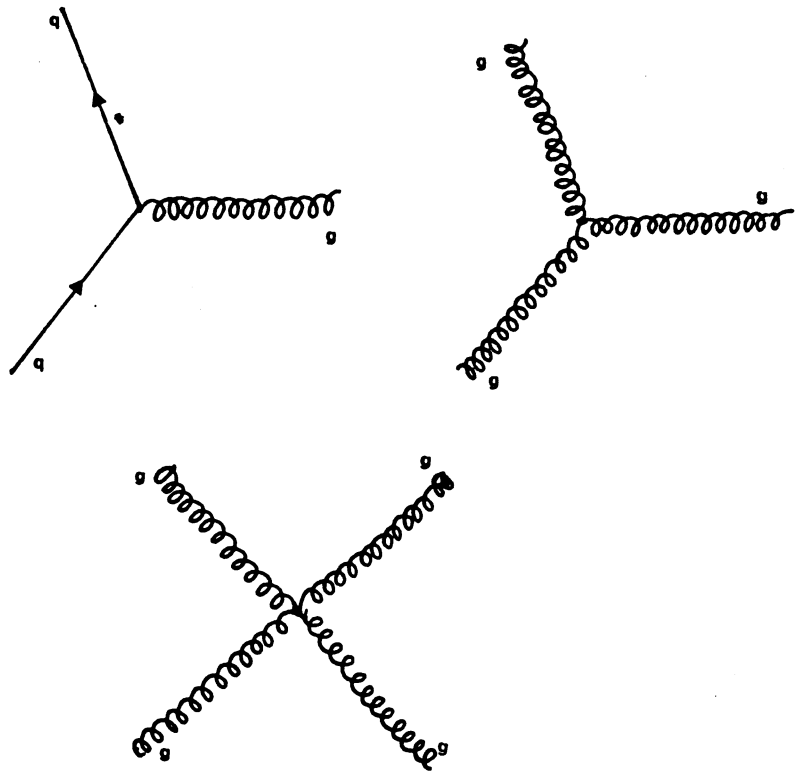

Figure 1.2: QCD- vertices

quarkonium-states.

- We may have seen glueballs, and mistaken them for quarkonium.
- There might be only a few processes which produce glueballs and these processes haven't been studied thoroughly yet.
- It is possible that pure glueballs don't exist, but that they mix with quark-antiquark states.But this would give one more degree of freedom and therefore another particle with same quantum-numbers.

What should we look for when we try to find glueballs?

- Particles that can not be mesons.This means either that they have exotic quantum numbers, $J^{PC} = 0^{+-}, 0^{--}, 1^{-+}$, not allowed for $q\overline{q}$ states, or that we can't fit the particles into any meson multiplets with given quantum-numbers.
- Flavour independent decays.Glueballs are flavour singlets and couple with equal strength to all flavours.
- Supressed radiative decays and no production in $\gamma\gamma$ collisions. Since glueballs don't have electic charge they do not couple to photons.
- Widths of about 10 Mev is predicted by the OZI rule but this is controversial(see section 1.2.2).

1.2.1 Glueball Properties

Quantum Numbers

Gluons are vector bosons , they have spin 1, so glueballs have integer spin. They make up a colour octet which transforms into itself under charge conjugation, $8 = \overline{8}$. The colourneutral gg will be a singlet in $8 \otimes 8$ with c =-1, where c is the eigenvalue of the charge conjugation operator C. The three gluon state ggg can be a singlet in $8 \otimes 8 \otimes 8$ with c =-1 or c=+1.

In the bag model [5] massless spin 1 gluons are put into a spherical bag.Boundary conditions give a transverse electric mode $(TE)_L$ with parity $(-1)^{L+1}$and transverse magnetic $(TM)_L$ with parity $(-1)^L$ where L is

l	J^{pc}		
0	0^{++}	2^{++}	
1	0^{-+}	1^{-+}	2^{-+}
2	2^{++}	0^{++}	4^{++}
3	2^{-+}	3^{-+}	4^{-+}

Table 1.1: Quantum-numbers of glueballs(from [21])

the total angular momentum of the gluon. Lowest lying are TE1 = 1^+, TE2 = 2^-,$TM1 = 1^-$. Table 1.1 shows the possible J^{PC} for gg states, from space-spin colour symmetry .Here l is the orbital angular momentum, and J the total angular momentum. There are two states forbidden for $q\bar{q}$, 1^{-+} [1] and 3^{-+} .Three gluons states ggg may have any J^{pc} combination while f.ex. 0^{--},0^{+-} and others are forbidden for $q\bar{q}$.

Masses

There are several models to predict the masses of glueballs.

- The bag model.
- Potensial models.
- Flux-tube models.
- Lattice QCD calculations

In the **bag model** [5] we have as already mentioned a spherical bag with the boundary condition that no gluon flux passes across the surface, Then the lowest mass glueballs are $(TE)_1(TE)_1$, with $J^{pc} = 0^{++}, 2^{++}$, and $(TE)_1(TM)_1$, $J^{pc} = 0^{-+}, 2^{-+}$. The lowest mass state for three gluons is $(TE)_1(TE)_1(TE)_1$. The mass of the lightest glueball is predicted at about 1 GeV. Interactions between the gluons might shift the energy upwards by some hundreds of MeV. However the result is that the lightest glueball is 0^{++}, and then in order of increasing mass: $0^{-+}, 2^{++}, 2^{-+}$.The ggg states are heavier, above 2 GeV.

[1] Note that 1^{-+} is only possible for glueballs if we treat gluons as massive spin 1 quanta with three helicity states.

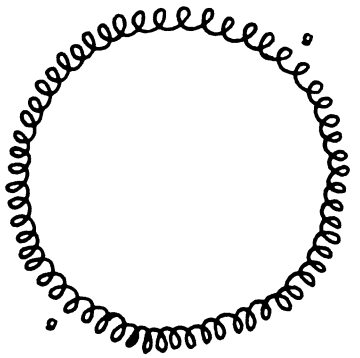

Figure 1.3: Flux-tube model of glueball

The **potential model** assumes two massive spin 1 gluons interacting through a potential. Cornwall-Soni [8] assume that the gluons interact via a breakable string, the mass m is generated via the strong gluon forces.The potental is

$$v(r) = 2m[1 - e^{-r/r_0}] \tag{1.7}$$

Barnes [20] uses a model where the long range confining potential is a scalar, linear at large distances. The result is that the lightest state is 0^{++} with $M = 1.23 \cdot 2m_g$, where m_g is the effective mass of the gluon which is unknown. Barnes has chosen it to be 500 GeV. Diekmann [1] calculates the effective gluon mass in the following way

$$m_g \approx \frac{colour factor 8 \otimes 8}{colour factor 3 \otimes 3} \cdot m_q \approx 700 MeV \tag{1.8}$$

Glueballs can be regarded as **flux tubes** [5], like the one in figure 1.1 with the quarks removed, and the ends of the tube joined.See figure 1.3.The energy of the various excitations (rotational, vibrational and radial) can be calculated.The mass of the lightest glueball 0^{++} turns out to be about 1.5 GeV.The next lightest glueballs are 1^{+-} and 2^{++} [5].

In **lattice gauge theories**[5] one does Monte-Carlo simulation of the gluon interactions.The lightest glueball is 0^{++}, with a mass of about 1 GeV, and then $0^{-+}, 2^{++}$.

Table 1.2 shows some mass-predictions for three of the models.

The conclusion is that there seems to be general agreement that the lightest glueball has quantum numbers 0^{++}, and mass between 0.5 and 1.5 GeV. Things get more unclear with higher masses but probably the next in order of mass are 0^{-+} and 2^{++}.

Glueball masses from a bag model (in MeV) [249] (C_{TE}, C_{TM}: gluon self-energy with respect to the cavity).

C_{TE}/C_{TM} \ J^{PC}	$(TE)^2$ 0^{++}	$(TE)^2$ 2^{++}	(TE) 0^{-+}	(TM) 2^{-+}	$(TM)^2$ 0^{++}	$(TM)^2$ 2^{++}
1/2	670	1750			1930	2640
1	1140	2120	1440	2300	1550	2300
2	1560	2470			1330	1940

Glueball masses from a potential model (in MeV) [248].

$m(0^{++}) = 1100\text{-}1200$
$m(0^{-+}) = 1300\text{-}1400$
$m(1^{++}) = 1400\text{-}1550$
$m(2^{++}) = 1550\text{-}1650$
$m(2^{-+}) = 1700\text{-}1800$

Glueball masses from a lattice calculation (in MeV) [251].

$m(0^{++}) = 740 \pm 90$	
$m(0^{-+}) = 1420^{+240}_{-180}(!)$	
$m(2^{++}) = 1620 \pm 100$	
$m(1^{-+}) = 1730 \pm 220$	← exotic states
$m(0^{--}) = 2880 \pm 300$	
$m(2^{--}) = 3420 \pm 300$	
$m(1^{++}) = 2980 \pm 300$	

Table 1.2: Glueball masses(from[1])

1.2.2 Decays

As already mentioned, glueballs have equal coupling to all flavours, and decay to isoscalar flavour singlet states. We should expect equal branching ratios for $gg \to \omega\omega, gg \to \phi\phi$ and $gg \to \pi\pi$. However the gluon-interaction may be mass dependent.In that case we expect equal coupling to up and down but not to the strange quark. Helicity conservation arguments suggest that glueballs will decay to strange particles more often than to particles consisting of only up and down quarks. For glueballs with charge conjugation +1(-1) we have the allowed decays to strange mesons.

$$G^- \to K_V^* \overline{K}, K_V^* \overline{K_T}. \tag{1.9}$$

$$G^+ \to K\overline{K}, K_V^* \overline{K_V^*}, K_T^* \overline{K}, K_L K_S. \tag{1.10}$$

The following reaction is not allowed: $G^+ \to \eta\eta$.

A nonet of quarkonium states can decay to:

$$(q\overline{q}) \to K\overline{K}, K_V^* \overline{K}, K_V^* K_V^*, K_T^*, \eta\eta. \tag{1.11}$$

K_V means a vector, and K_T a tensor meson.

Glueballs can go to states with both strange or non-strange-mesons.

$$G^+ \to \omega\omega, \phi\phi, \omega\eta, \pi\pi. \tag{1.12}$$

Type	J^{PC}	typical decays
(1) TE TE	$0^{-+}; 2^{-+}$	$\pi\pi$; $K\bar{K}$; $\eta\eta$; $\eta'\eta'$; $\rho\rho$; $\omega\omega$; $K^*\bar{K}^*$; $\phi\phi$; $\eta\eta'$; f_0f_0
(2) TE TM	$0^{+-}; 1^{+-}; 2^{+-}$	$\pi\pi$; $K\bar{K}_0$; $\eta f_0(975)$; $\eta' f_0$; ρb_1; K^*K_1
(3) TM TM	$0^{++}; 2^{++}$	same as (1)
(4) TE TE TM	$0^{-+}; 1^{--}; 3^{--}$	πa_0; $K\bar{K}_0$; $\eta' f_0$; $\pi\rho$; $K\bar{K}^*$; $\eta\omega$; $\eta'\phi$; ωf_2; ...
(5) TE TE TM	$0^{++}; 1^{++}; 2^{++}$	same as (1) + πa_0; $K\bar{K}_0$; $\eta f_0(975)$; ...
	$1^{-+}; 2^{-+}; 3^{-+}$	$\pi\rho$; $K\bar{K}^*$; $\eta\omega$; $\eta'\phi$; πb_1; $K\bar{K}_1$; ηf_1; ...
(6) TE TE TM	$0^{--}; 1^{--}; 2^{--}$	same as (2)
	$1^{--}; 2^{--}; 3^{--}$	πb_1; $K\bar{K}_1$; ρa_2; $\bar{K}^*K_2^*$; ωf_1; $f_1 f_2'$; ...
(7) TM TM TM	$0^{++}; 1^{++}; 3^{++}$	same as (1) + πb_1; $K\bar{K}_1$; ρa_1; ρa_2; ...

Table 1.3: Glueball decay modes(from[1]).

$$G^- \rightarrow \omega\eta, \phi\eta, \rho\pi. \tag{1.13}$$

Quarkonium decays are restricted by the OZI rule and we can have the following decays:

$$(u\bar{u}, d\bar{d}) \rightarrow \omega\omega, \omega\eta, \rho\rho. \tag{1.14}$$

$$(s\bar{s}) \rightarrow \phi\phi, \phi\eta. \tag{1.15}$$

A particle decaying only into one of the two classes of strange meson pairs according to either equation 1.9,or equation 1.10, but both types of channels in equation 1.14 and equation 1.15 would indicate a glueball. Table 1.3 shows glueball decay modes.

Since gluons are electrically neutral they don't couple to photons, and glueballs therefore have supressed radiative decays.They can only go to γ's in higher order diagrams.

From the OZI rule we can get the width of glueballs[2]. Figure 1.4shows OZI-forbidden and -allowed decays. The relation between the widths is

$$f^2 = \frac{\Gamma_{ozi}}{\Gamma_{hadron}} \tag{1.16}$$

If we assume that OZI -forbidden reactions go through glueballs we get:

$$\Gamma_{gg} = f \cdot \Gamma_{hadron} = \sqrt{\Gamma_{ozi} \cdot \Gamma_{hadron}} \approx 10 - 30 MeV. \tag{1.17}$$

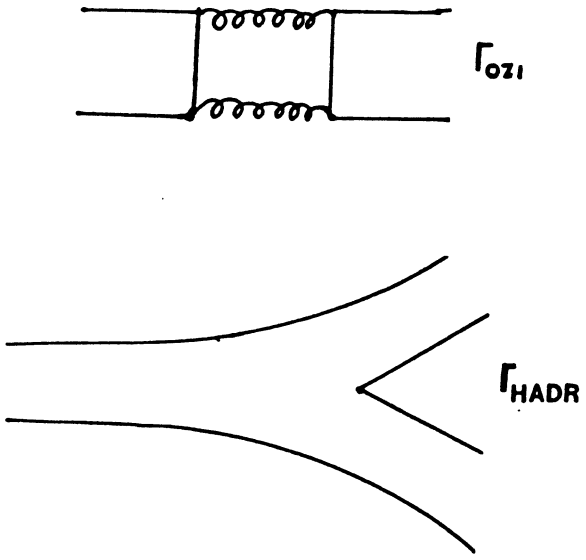

Figure 1.4: OZI-forbidden and -allowed decays.

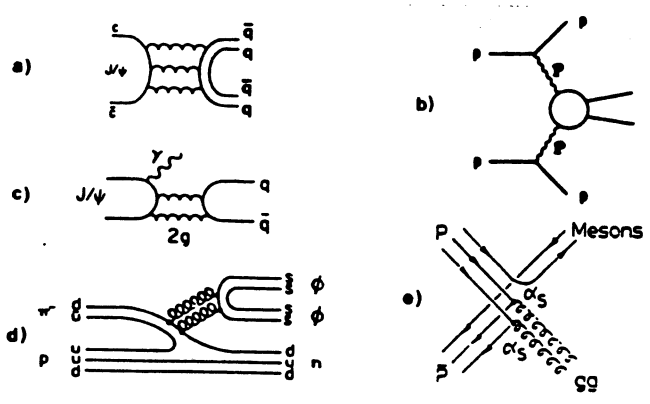

Figure 1.5: Glueball-production(from[13])

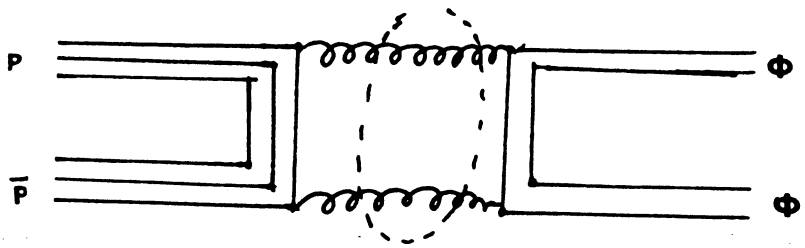

Figure 1.6: The reaction $p\bar{p} \rightarrow \phi\phi$

1.2.3 Production

We know three ways glueballs can be produced(see figure 1.5).

- J/Ψ decay:The c and $\bar{c}$ annihilate through gluon states. $J/\Psi \rightarrow ggg$ or $J/\Psi \rightarrow gg\gamma$.
- Double diffraction of protons.Gluons surrounding the protons fuse , first they make a glueball, which then go to mesons.
- OZI violating modes f.ex in $\pi^- p$ and $p\bar{p}$ collisions , where one or more quarks annihilate.We then expect coloured gluons to be produced.In one of the reactions we will study at JETSET, $p\bar{p} \rightarrow \phi\phi$, all three quarks annihilate, and we hope to find a gluonic resonance there.(figure 1.6)

candidate	J^{PC}	mass MeV	width MeV	reaction	experiment
$S^*(975)$	0^{++}	975	16	$pp \to pp\pi\pi$ (double pomeron) $J/\Psi \to \phi\pi\pi$ $\pi p \to \pi p\pi\pi$	ISR-AFS Mark III WA76
G(1590)	0^{++}	1590	200	$\pi p \to \eta\eta n$ (ozi- violating) $\pi p \to \eta\eta' n$	GAMS
$\iota(1460)$	0^{-+}	1460	100	$J/\Psi \to \gamma K_S^0 K\pi$	Mark II,III
$\theta(1720)$	2^{++}	1720	100	$J/\Psi \to \gamma KK$ $J/\Psi \to \gamma\eta\eta$ $J/\Psi \to \gamma\pi\pi$ $J/\Psi \to \omega K^+K^-$	Crystal Ball
g(2011) g(2297) g(2339)	2^{++} 2^{++} 2^{++}	2011 2297 2339	202 149 315	$\pi^- p \to \phi\phi n$ (ozi-violating) $\pi^- Be \to \phi\phi X$? (ozi-violating)	BNL/CCNY WA67
$\Xi(2230)$	2^{++}	2230	20	$J/\Psi \to \gamma K_S^0 K_S^0$ $J/\Psi \to \gamma K^+K^-$	Mark III

Table 1.4: Possible glueballs seen in experiments

1.2.4 Glueball Candidates

There are so far no unambigious sign of glueballs, but there are more states than can be fitted into the existing $q\overline{q}$ multiplets. Table 1.4 list some of the candidates, together with reactions where they are seen .

The $\iota(1460)$ is one of the strongest candidates.If it is correct that it has $J^{PC} = 0^{-+}$ then it does not fit into any existing $q\overline{q}$ multiplet.However some experiments have seen another particle E(1420) with almost the same mass, and $J^{PC} = 1^{++}$, which fits into a $q\overline{q}$ multiplet. The θ is also a good candidate.It's decay implies that it is a $s\overline{s}$, but there already exist a $s\overline{s}$ in this mass region, the f(1550). However, a lot of experiments and analysis on the data have to be done before we can be sure to have found a glueball.

1.3 JETSET Physics

The first reaction to be studied at JETSET is $p\bar{p} \rightarrow \phi\phi$. This reaction is OZI-forbidden, and hopefully a good source for glueballs. All three quarks in the proton will annihilate with the antiquarks in the antiproton, and go to $\phi\phi$ through a multi gluon intermediate state. At a center of mass energy of about 2 GeV we will try to find a resonant behaviour of the cross section. Other experiments have found interesting unexplained states in this mass region, eg. the three g-states seen at Brookhaven, and the ξ seen by MARK III(table 1.4 MARK III has also seen other peaks in their experiments. JETSET has several advantages which will give a cleaner picture.

- We hope to achieve higher statistics than the other experiments (see section 2.1).
- The mass resolution will be determined by the beam parameters and not the mass resolution of the detector. The uncertainty will be about $\sigma(M_{\phi\phi}) \approx 1.0 MeV/c^2$ Since the width is predicted to be about 10-30 MeV for glueballs the measured width will not be smeared out by the detector mass resolution.
- A full solid angle detector and high statistics will enable us to find the quantum numbers.

Chapter 2

The JETSET Experiment

In the first chapter we discussed glueballs, why they should exist and what we know about them. We saw that a gluon-rich channel is

$p\overline{p} \rightarrow \phi\phi \rightarrow K^+K^-K^+K^-$

To search for resonances in this reaction we need anti-protons in a focused beam with well determined momentum of about 1 GeV, which can easily be changed in small steps. This is provided by the LEAR, Low Energy Antiproton Ring.We also need a high density proton target , which will give the necessary luminosity to provide us with sufficiently high statistics. The JETSET experiment uses a molecular hydrogen gas jet target for the protons. This is inserted into the LEAR ring, where we have circulating anti-protons.

We will try to find resonances in $p\overline{p} \rightarrow \phi\phi$ by measuring the reaction rate as a function of LEAR beam-momentum. Other experiments have seen interesting structures in the $\phi\phi$ mass spectrum in the 2.0-2.4 GeV region. We will scan with small steps in the beam momentum $0.6GeV/c \leq P_{\overline{p}} \leq 2.0GeV/c$, corresponding to a centre of mass energy from 1.96 GeV to 2.43 GeV.

It is necessary with a detector which can to filter out the large amounts of background events at trigger level, and to recognize $\phi\phi$ events off-line.

Some of the background reactions are:

- $p\overline{p} \rightarrow K^+K^-K^+K^-$
- $p\overline{p} \rightarrow \pi^+\pi^-\pi^+\pi^-$
- $p\overline{p} \rightarrow \pi^+\pi^-K^+K^-$

- $p\overline{p} \rightarrow \pi^+\pi^-p\overline{p}$
- $p\overline{p} \rightarrow \pi^+\pi^-\pi^+\pi^-\pi^0$
- $p\overline{p} \rightarrow \pi^+\pi^-\pi^+\pi^-\pi^0\pi^0$
- $p\overline{p} \rightarrow \pi^+\pi^-K^+K^-\pi^0$

All these reactions have much higher cross sections than

$$p\overline{p} \rightarrow \phi\phi \rightarrow K^+K^-K^+K^-$$

The non-resonant

$$p\overline{p} \rightarrow 4K$$

cross-section is poorly known, so we will try to measure that as well.

In this chapter the setup of the experiment , the gas-jet target, the detector and the triggering and event-selection will be described.

2.1 The Antiproton Beam

The antiprotons we need for the experiment will be produced by bombarding 26 GeV/c protons from the proton synchroton PS on a tungsten target. Antiprotons with a momentum of about 3.5 GeV/c will be selected by dipole magnets to the AAC, Antiproton Accumulating Complex. The AAC consists of the Antiproton COLlector ring, ACOL and the Antiproton Accumulator, AA. Here the antiprotons will be collected, accumulated and stochastically cooled. Stochastic cooling is a method to give uniform momenta to the antiprotons. Pickup electrodes measure the location of the charge at one point in the orbit.At the opposite point a correction voltage is applied. Because the signal is transmitted across the ring it will arrive faster than the antiprotons which have to go round the arc. When we have a bunch consisting of about 4×10^{10} antiprotons with momentum 3.5 GeV/c circulating in the AA it is transferred to the PS where it is decelerated to 0.609 GeV/C before it is sent into the LEAR ring. Here the beam momentum can be varied between 0.6 Gev/c and 2 GeV/c. Continuous stochastic cooling will give a low momentum uncertainty $\frac{\Delta p}{p} \approx 10^{-3}$. Low beta quadropoles focus the beam.This is important because we want the beam dimensions to be smaller than the target dimensions.

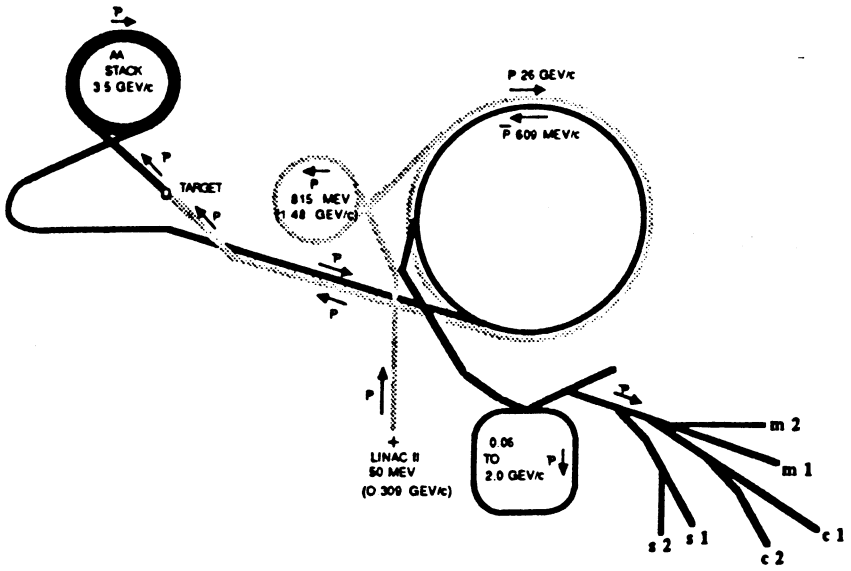

Figure 2.1: Antiproton production for LEAR (from[15])

The $\overline{p}$ revolution frequency will be 3.2×10^6 Hz. Figure 2.1 shows the layout of the antiproton production system. In figure 2.2 we see the LEAR ring with the location of the jet-target in the south straight section, low beta quadropoles to focus the beam, and the stochastic cooling system.

2.2 The Gas Jet Target and the Beam Pipe.

The beam pipe will be a corrogated structure of 0.3 mm stainless steel. The target for the experiment consists of a supersonic hydrogen beam, which crosses the LEAR vacum pipe , where it interacts with the antiproton beam. Hydrogen gas is kept in a vessel at low temperature T_0 and high pressure P_0.It is injected into the vacum through a trumpet shaped nozzle with small aperture.To focus the jet it will pass through three slits before it reaches the vacum pipe. After traversing the vacum pipe the gas is absorbed by a sink pump system.

Figure 2.3 gives a view of the target, with the source at the top and the

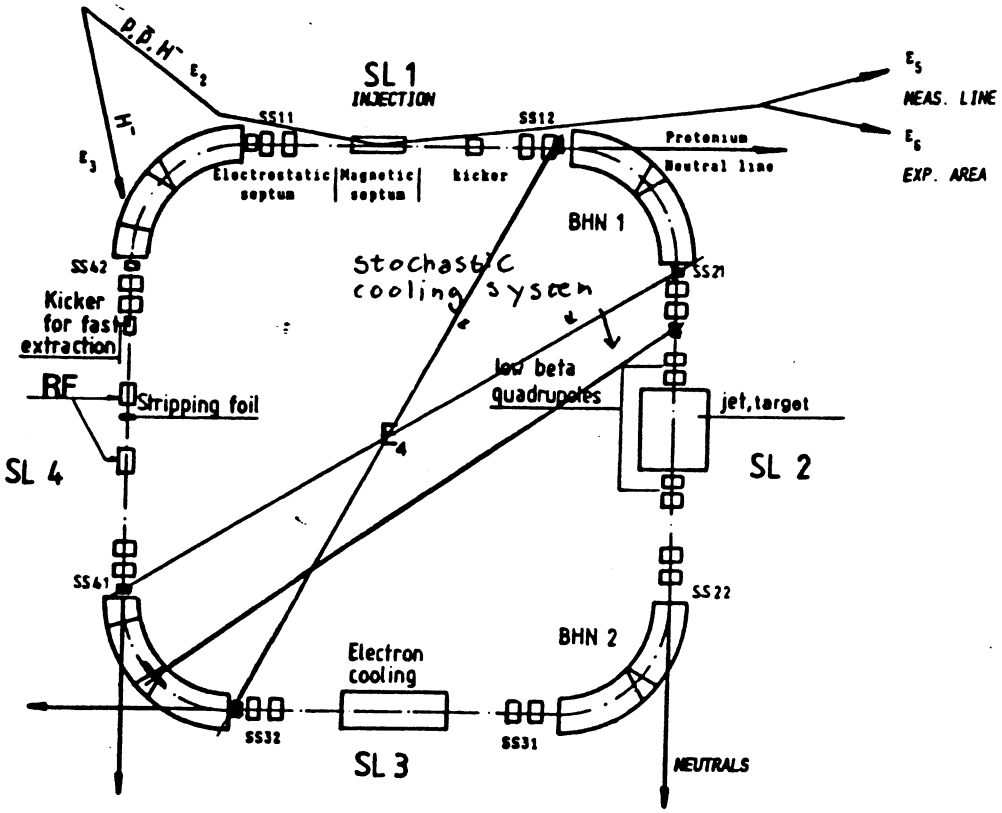

Figure 2.2: LEAR ring(from[11])

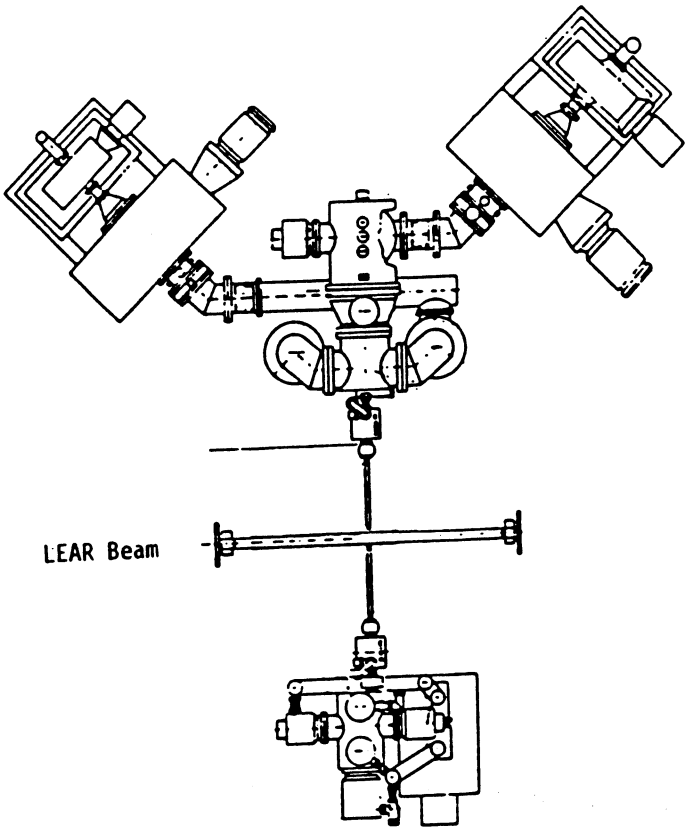

Figure 2.3: Jet target(from [3]).

sink at the bottom.

No work is done by the expanding gas, the expansion is adiabatic, and there will be no change of entropy.During the expansion the gas will cross the vapour pressure curve.It will supersaturate and clusters of about $10^5 - 10^6$ molecules will be formed.Hence the density in the interaction area will increase, and less of the H_2 will be lost in the vacum tube.

The density is determined by the temperature and pressure of the gas and the shape of the nozzle.By optimizing these parameters we can obtain

$$\rho = 8 \cdot 10^{13} atoms/cm^2$$

The luminosity is given by

$$L = \rho N_{\overline{p}} f$$

where

$$N_{\overline{p}} = \text{number of antiprotons in the beam .}$$

$$f = \text{revolution frequency of the antiprotons.}$$

There are $4 \cdot 10^{10}$ antiprotons in the injected beam which circulate the ring $3.2 \cdot 10^6$ times pr. second. This gives a maximum luminosity of

$$L = 10^{31} cm^{-2} s^{-1} = 10^{-2} nb^{-1} s^{-1}.$$

With this luminosity the total interaction rate will be

$$\frac{dN}{dt}_{tot} = L \cdot \sigma_{tot} = 10^6 Hz,$$

assuming $\sigma(p\overline{p} \rightarrow anything) = 100mb$). The cross section for $p\overline{p} \rightarrow \phi\phi$ is not known , but if we assume $\sigma(\phi\phi) = 0.1\mu barn$ we get one $\phi\phi$ event pr. second. The luminosity will vary with time as

$$L = L_0 e^{-t/\tau}$$

where τ is the beam lifetime.

If we have two fills of $4 \cdot 10^{10}$ antiprotons each day we get an integrated luminosity

$$\int_0^{24h} Ldt \approx 500nb^{-1}$$

assuming 100 percent detection efficiency. In one day we will get about $5 \cdot 10^4$ $p\overline{p} \rightarrow \phi\phi$ events.

If we produce a resonance , its mass is given by

$$M = \sqrt{(E_{\overline{p}} + m_p)^2 - P_{\overline{p}}^2} = \sqrt{2m_p^2 + 2m_p\sqrt{m_p^2 + P_{\overline{p}}^2}} \tag{2.1}$$

The mass uncertainty will be determined by the uncertainty in the momentum of the antiproton $S_{P_{\overline{p}}}$, and is given by

$$S_M = \frac{m_p P_{\overline{p}}}{M\sqrt{m_p^2 + P_{\overline{p}}^2}} S_{P_{\overline{p}}} \tag{2.2}$$

The stochastic cooling system will provide a momentum spread of

$$\Delta P/P \approx 10^{-3}$$

This gives an uncertainty in the invariant mass for one event:

$$P = 2GeV, \quad S_M = 0.7MeV$$

$$P = 0.6GeV, \quad S_M = 0.15MeV$$

If we have N events at the same beam momentum where this resonance is produced,the uncertainty will be

$$\sigma_M = S_M/\sqrt{N}$$

2.3 The Detector

The detector will surround the beam pipe and gas jet.It will be divided into a barrel and a forward part. The detector components will have a matching geometry, cylindrical in the barrel, and wedge -shaped or phi-planes in the forward part. The volume will be about 1 m^3. The geometric acceptanse will be

$$0 \leq \phi \leq 360^o, 8^o \leq \theta \leq 130^o.$$

The plan is to have two phases for the detector, the phase II will be an improved and more advanced version, where a solenoidal magnetic field will surround the detector. In phase II we will also look at reactions like $p\overline{p} \rightarrow \phi\omega$.There are also plans to get polarized protons. Figure 2.4 shows the detector. The straw chambers will give track information for momentum detemination. The RICH and dE/dx counters will give $\pi/K/p$ identification by measuring β.The threshold cerenkov counter will identify fast charged pions, while the calorimeter will recognize neutral pions, by reconstructing the 2 γ mass. In the following the individual detector components will be described.

2.3.1 The Straw(Drift-Tube) Tracker

The straw chambers consist of cylindrical drift tubes glued together. The tubes will be made of aluminium and filled with the gas be AR/CO_2.In the middle there will be an anode wire made of tungsten.

The diameter of the tubes will be 8 mm, and they will be about 400 mm long. The anode wires will have a diameter of 30 μm, and resistance 1 kΩ/m. The wall thickness will be about 50 μm , the amount of material seen by a crossing particle will be about $10^{-3}X_0$ per straw.This gives little multiple scattering which makes the track reconstructon easier.

When a charged particle traverses the tube, the gas in it will ionize .The electrons will drift toward the positive electrode. The distance of the track from the wire is determined by measuring the drift time using a scintillator signal as time = 0.

We can not tell which side of the wire the track passed. These ambiguities will disappear if the straw tubes are placed such that the wires in each adjacent layer are displaced by half a tube. Then the transverse coordinate can be measured with resolution $\sigma_t \approx 200\mu m$. The longitudinal coordinate

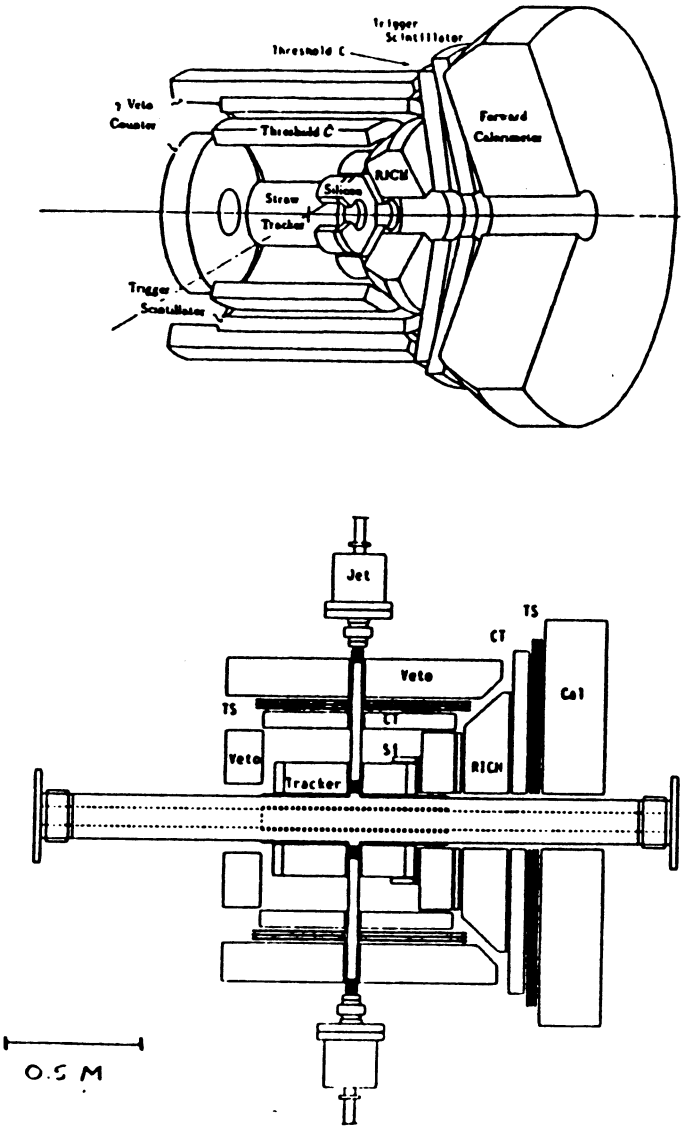

Figure 2.4: JETSET detector(from [3]).

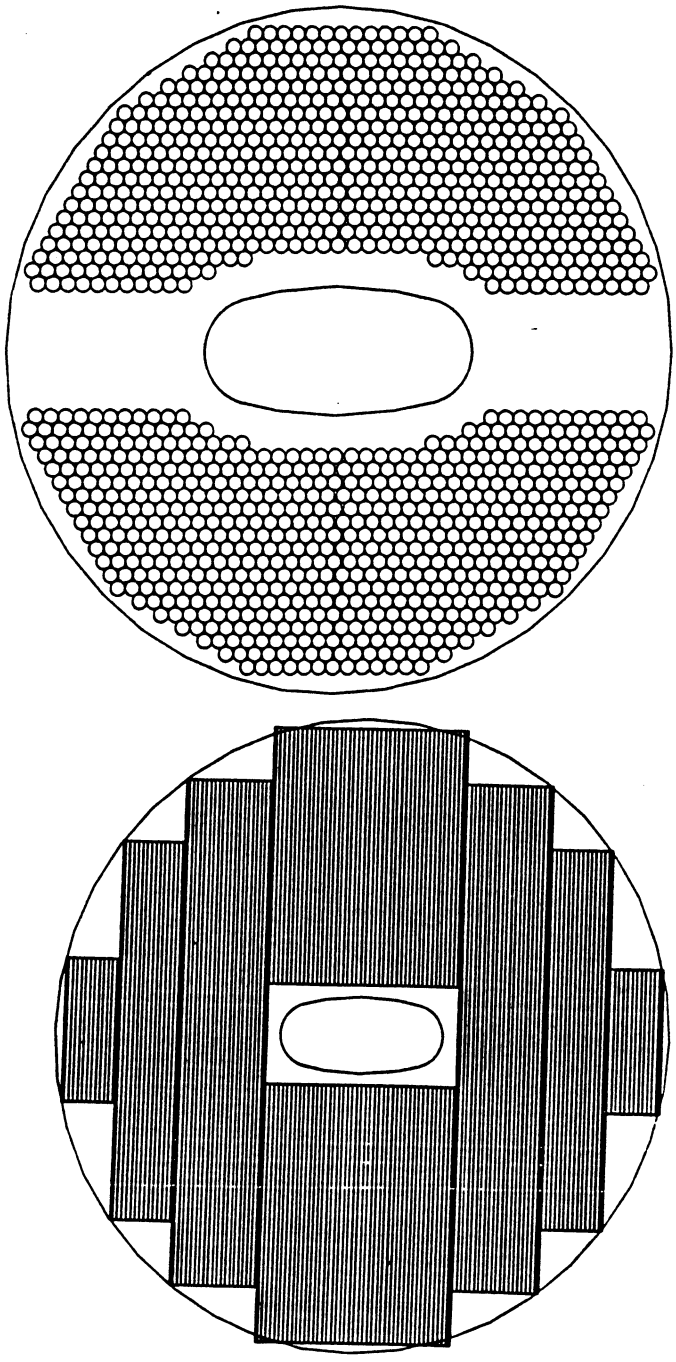

Figure 2.5: Straw tubes, barrel and forward(from [19]).

is measured by comparing the sizes of pulses received at the two ends of the wire. Then

$$z = \frac{Q_1 - Q_2}{Q_1 + Q_2}$$

This charge division method will give the longitudinal coordinate with an accuracy of about 1% of the straw length.

In the barrel we will have 1720 straws parallel to the beam tube, which will give azimuthal (ϕ) and z coordinates for tracks with $\theta \geq 45^o$. In the forward direction there will be 12 layers, perpendicular to the beam direction, and with straws parallel to x and y See figure 2.5.

The information from the straw tubes will be used for offline analysis to reconstruct the charged tracks.

2.3.2 The dE/dx Silicon Counters

The dE/dx silicon counters will be located just outside the straw tube tracker. By measuring the energy loss they will give the value of $\beta = v/c$. For a charged particle the energy loss is given by the Bethe-Block formula.

$$\frac{dE}{dx} = D\frac{z\rho}{A\beta^2}(\ln\frac{2m_e c^2\beta^2\gamma^2}{I} - \beta^2) \tag{2.3}$$

where

I = ionization potental
$D = 4\pi N_0 r_e^2 m_e c^2$
N_0 = avogadros number
r_e = electron radius
m_e = electron mass
Z = atomic number
A = atomic weight
ρ = density$[kg/m^3]$

Each silicon detector has a dimension $1.95 \cdot 2.4cm^2$. In phase II we plan to have detectors in the barrel region as well, with a cylindrical geometry, of rectangular pads parallel to the beam. In the forward direction there will be two planar circular counter arrays. In order to improve our triggering capabilities a third silicon plane equipped with fast electonics was foreseen in the forward diresction. This detector would need a lot of development

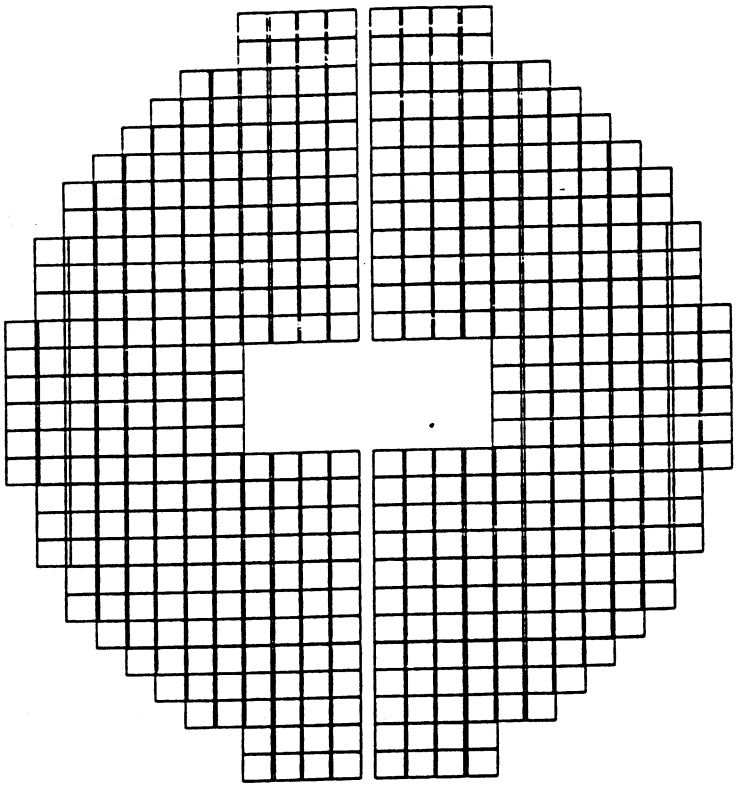

Figure 2.6: The dE/dx counters (from [19]).

work, and is replaced by a set of small scintillators placed along the beam pipe.See section 2.3.7 The dE/dx counters will help to distinguish 4K events from background, especially $p\bar{p}\pi^{+}\pi-$. The geometry of the detectors are shown in figure 2.6 .

2.3.3 The Threshold Cerenkov Counter.

Cerenkov counters give a signal when the speed of the traversing particle is higher than the speed of light in the medium. $v_{threshold} = v_c = c/n$, where n is the refraction index. In our Cerenkov we will have liquid freon, which have

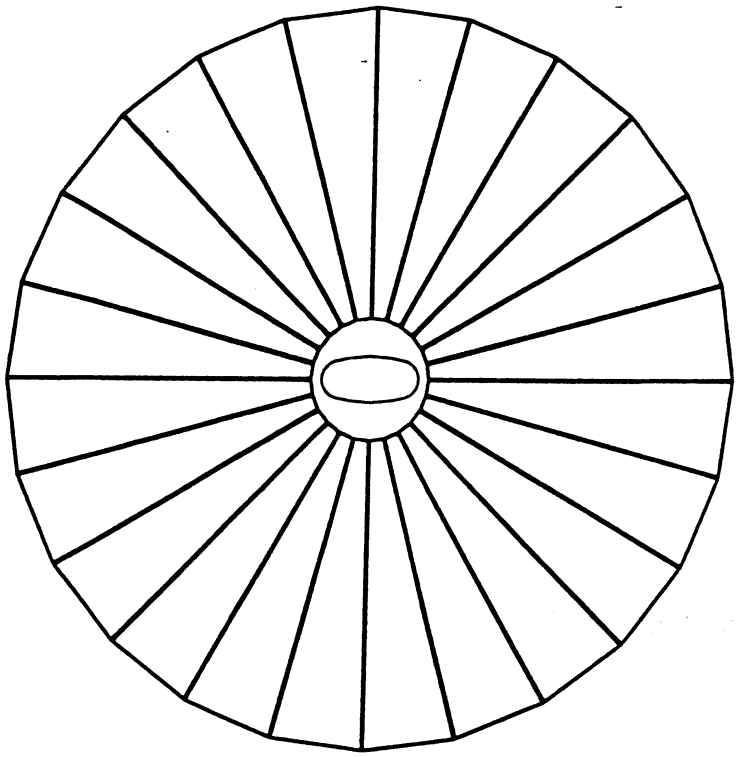

Figure 2.7: Forward Cerenkov counters(from[19]).

n =1.26, $\beta_{th} = 0.8$. Since pions are lighter than kaons they are much faster at a given energy,and they will usually have a β above the Cerenkov threshold. This means that we can reject most of the charged pions at trigger level. The barrel counter will have a radius of 29 cm and consist of 24 wedges with a trapezoidal cross section of 3.5 cm, length 60 cm . In the forward region there will be 24 pie shaped wedges, with an outer radius 30 cm, and a thickness of 2 cm. Figure 2.7 shows the geometry of the forward Cerenkov counters.

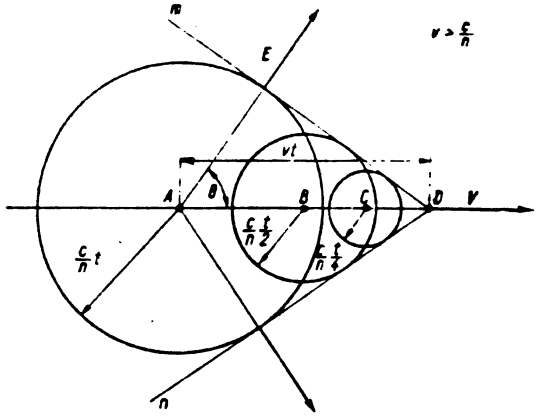

Figure 2.8: Cerenkov wave front.

2.3.4 The Ring Imaging Cerenkov (RICH) Counter.

The Cerenkov light is sent out in a cone shaped wave front.

From the figure 2.8 we see that the opening angle is given by.

$$\cos\theta = \frac{\frac{c}{n}t}{\beta ct} = \frac{1}{\beta n} \tag{2.4}$$

This gives us another β-measurement in addition to that from the dE/dx. In the RICH detecor we will have a 1 cm radiator layer of CaF_2 or quartz.Then the photons are allowed to drift 6 cm, before they are detected by the photon detector.The photon detector consists of TMAE gas carried in methane , where the photons will be converted to photo-electrons.They are detected by a 2D "honeycomb" arrangement of wire chambers. Here we will get a ring image, in this way we can measure θ (figure 2.9).

The RICH counter will be used in phase II.

2.3.5 The EM-Calorimeter.

The purpose of the electromagnetic calorimeter is to measure the energy of γ's which go into the detector. In this way we can detect π^0's or other neutral mesons which would have escaped unnoticed otherwise. The calorimeters consists of plastic scintillation fibers embedded in Pb plates and packed together in towers. The fibers point toward the interaction region. The $\gamma's$ will loose all their energy by electromagnetic interactions in the lead. The energy

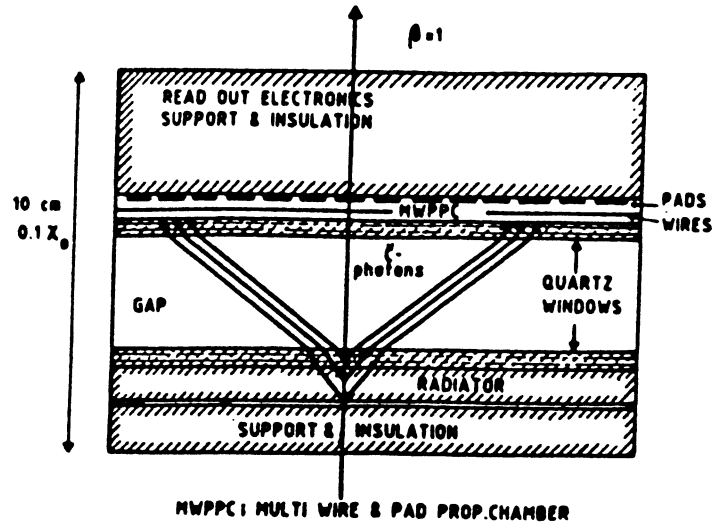

Figure 2.9: Rich counter.

resolution is $\sigma_E/E \approx \frac{0.06}{\sqrt{E(GeV)}}$ [4]. The coordinates can be measured with resolution $\sigma_{xy} \approx 5mm$. There will be 336 towers in the forward direction, grouped in 8 theta rings with 24-28 modules pr. ring in the phi direction. The geometry is shown in figure 2.10. In phase II the EM-calorimeter will be extended to the barrel region.

2.3.6 The γ-Veto Counter.

The veto counter will be placed in the barrel region to detect photons from decays of neutral mesons. It consists of plastic scintillator fibers and Pb . and will be wedge shaped and segmented into 24 elements in the azimuthal direction.

2.3.7 The Fast Charged Trigger Counters

The fast charged trigger-counters consists of three layers of scintillation counters in the barrel and forward direction, positioned outside the threshold Cerenkov, and one layer close to the beam pipe. Scintillators emit light when struck by a charged particle.Because they are very fast and have good time resolution they are effective for timing (t_0 for straws) and as trigger counters. They will be used to determine the charged multiplicity, and in the next level the segmentation permits a possible fast kinematics trigger,

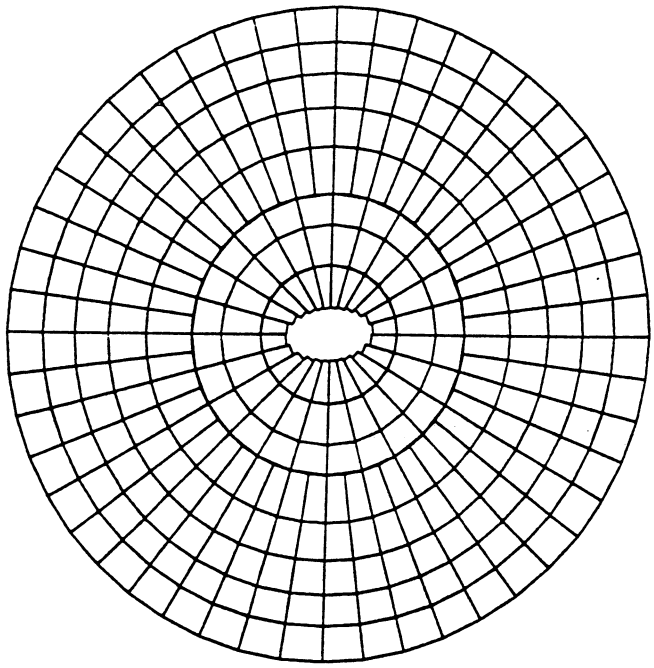

Figure 2.10: The EM-calorimeter (from [19]).

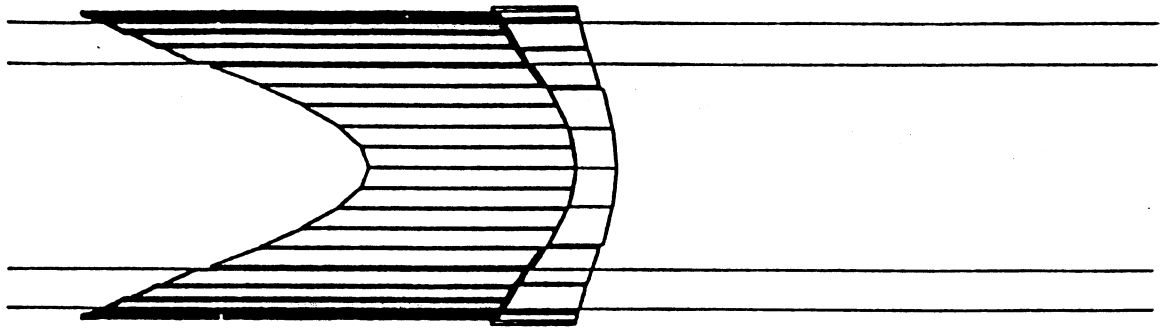

Figure 2.11: Pipe scintillators (from[19]).

where $\theta - \phi$ coordinates will be measured.The layer close the beam pipe has 40 scintillators that cover the angle $15 < \theta < 45$ and 20 scintillators that cover the angle $45 < \theta < 65$,all with a thickness of 0.2 cm.To cover the same angular region around the ellipse the scintillators will have varying length as shown in figure 2.11. In the barrel one of the outer layers will consist of straight scintillators parallel to the beam axis, the other two will be twisted in opposite directions.This gives 300 ($276 + 2 \times 12$ half cells in each end) independent cells which will give information about the position. In the forward detector there will be 48 wedge shaped elements in one of the layers, the other two will each have 24 spirally shaped scintillators in oposite directions. See figure 2.12 and 2.13 for the geometry of the trigger counters.

We have done some tests of prototypes of these detectors, at the T11 beam at CERN's PS .The prototypes were made with NE 110 equivalent material, and had a thickness of 5 mm.The T11 beam consists of $p, \pi^+, \pi^-, e^+, e^-$ at momentum 0.6 GeV/c-3.0 GeV/c.

Figures 2.14 and 2.15 show tests of light collection and timing properties

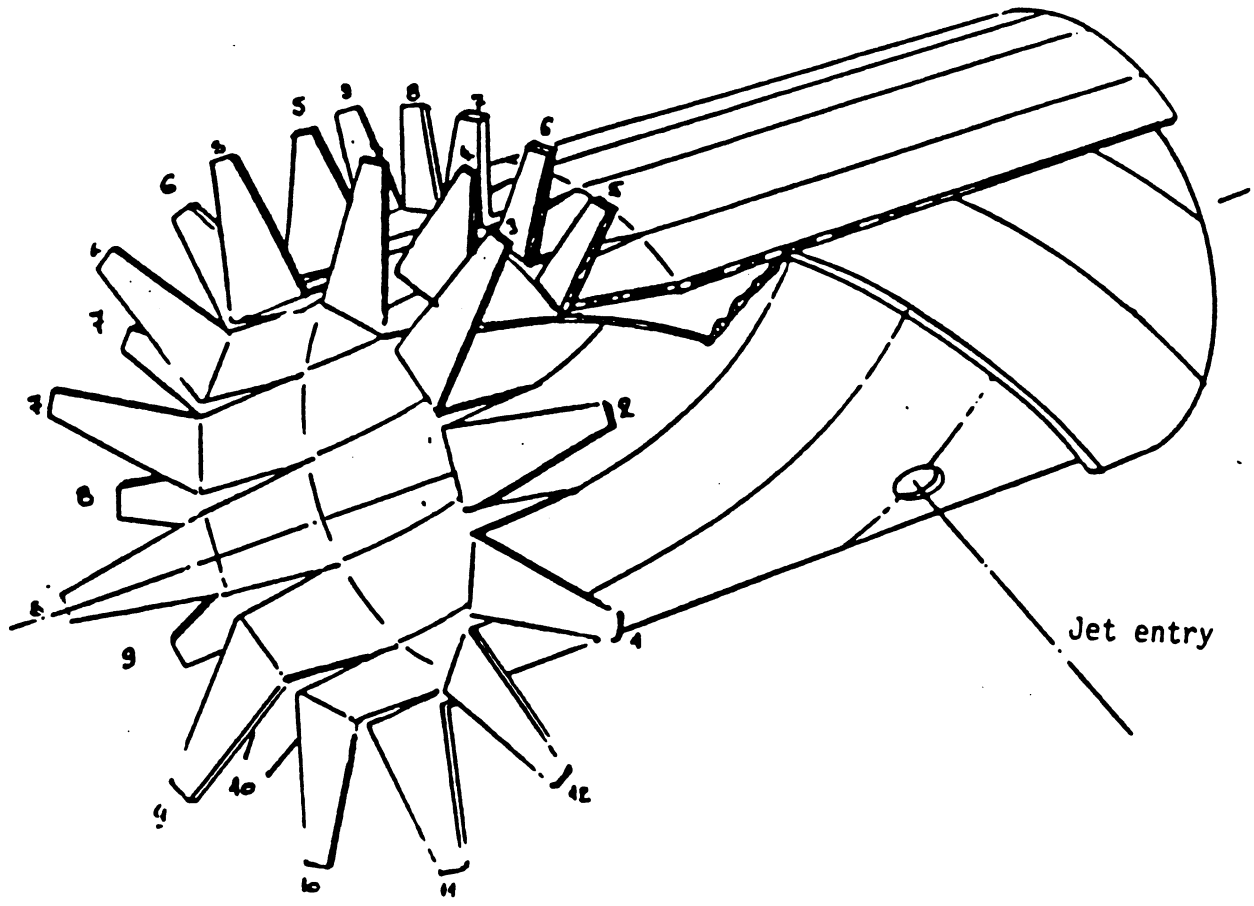

Figure 2.12: Trigger scintillators, barrel (from[17]).

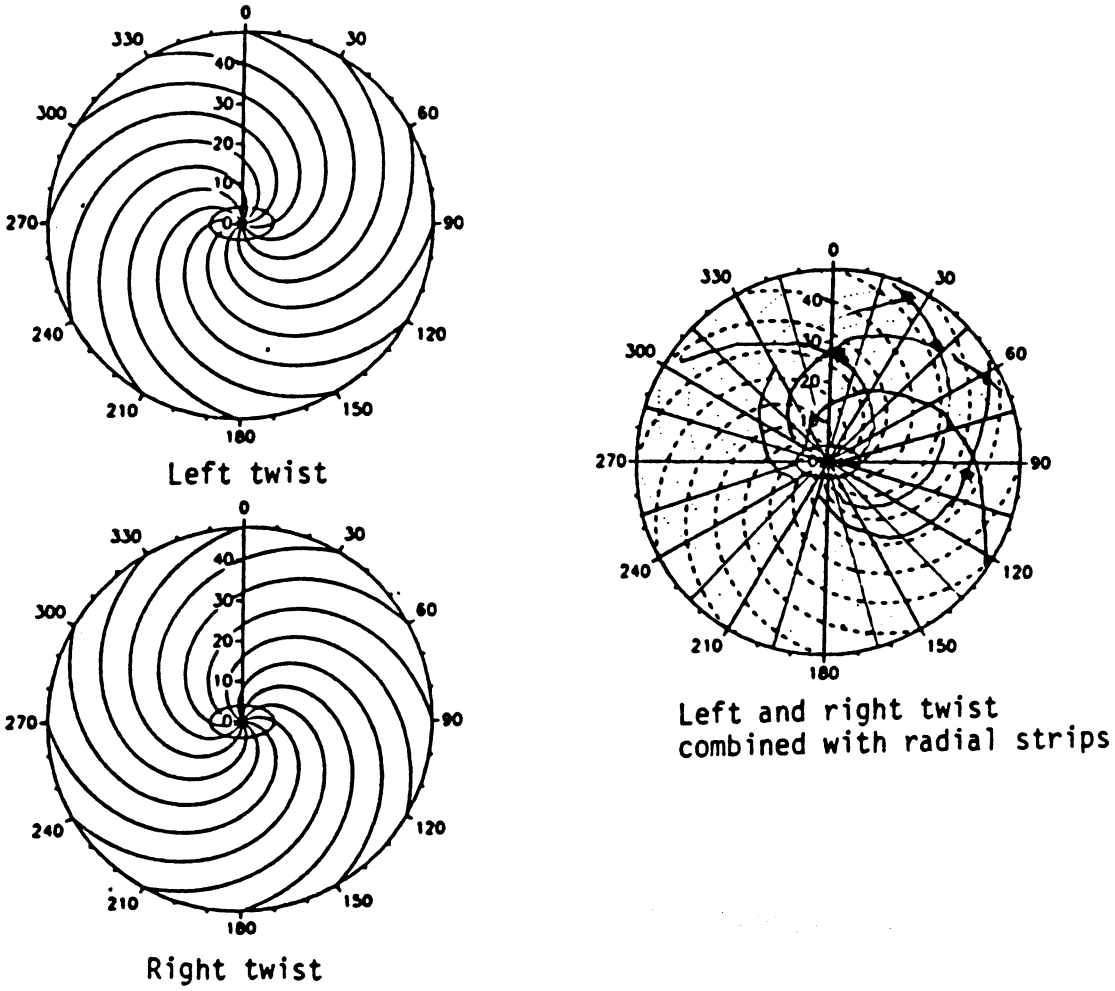

Figure 2.13: Trigger scintillators, forward(from[17]).

for these detectors.The scintillators were moved at different positions with respect to the beam.We see a linear dependence of pulseheight and time of travel for the produced light on the position. Time resolution found by the full width half maximum of the TDC spectra was of the order of 1-2 ns.Typically 20-40 photo-electrons were detected.We can calculate the number of photons that is produced, this should be about 11000.This means that the light collection efficiency is about 1-2 percent.

Inefficiencies for the detectors were found to be of the order of 10^{-4}.

We have also found that it's possible to get a crude measurement of the energy loss.Figure 2.16 shows ADC spectrum for protons and pions,at beam momentum 0.9 GeV/c.The energy loss is larger for the protons.Figure 2.17 shows how the pulse height depends on the momenta for pions and protons,with error bars equal to the FWHM of the ADC spectrum. However, because of a large Landau tail it will be difficult to use this to separate different kind of particles online.

Similar tests have been done with the spirally shaped forward counters, which also gave similar results.

2.3.8 The Magnetic Field

In a second phase we hope to have a magnetic field in the detector. The magnetic field in JETSET will be uniform with direction parallel to the beam.The path of charged particles will then follow a helix

$$P\cos\lambda = const \cdot qBR$$

where

$B = B_Z$ = value of the magnetic field
R = radius of the helix
q = charge of the particle
λ = pitch angle
$P\cos\lambda$ = transverse momentum.

Since we know β from dE/dx measurements, we can distinguish between $\pi/p/K$ if we measure the momentum. The momentum will also be used to get the invariant mass of pairs of kaons in 4K events.We can then find the events which are $p\overline{p} \rightarrow \phi\phi \rightarrow 2K^{+}2K^{-}$. The following magnets have been suggested.

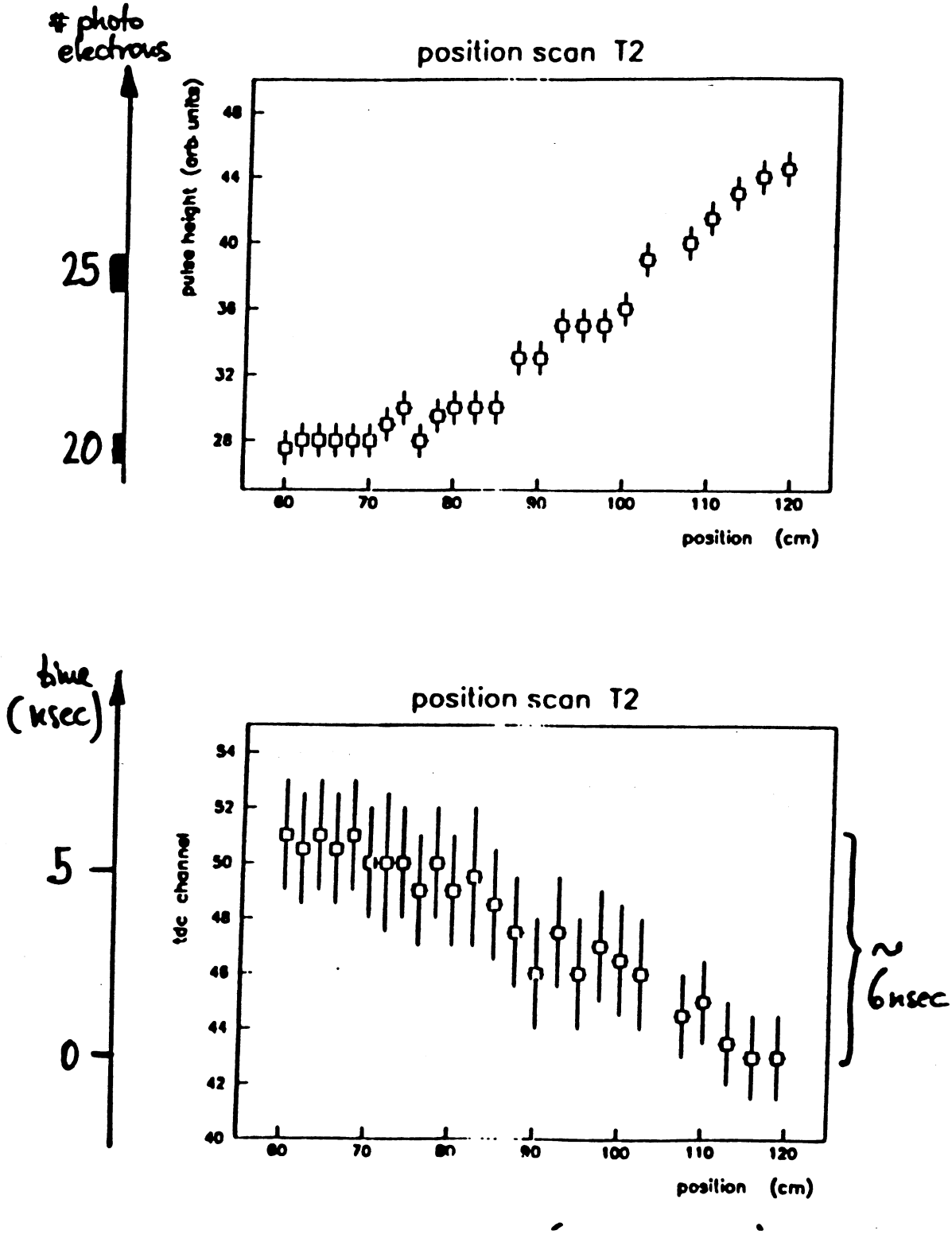

Figure 2.14: Position scans of straight scintillator with 90° light guide.

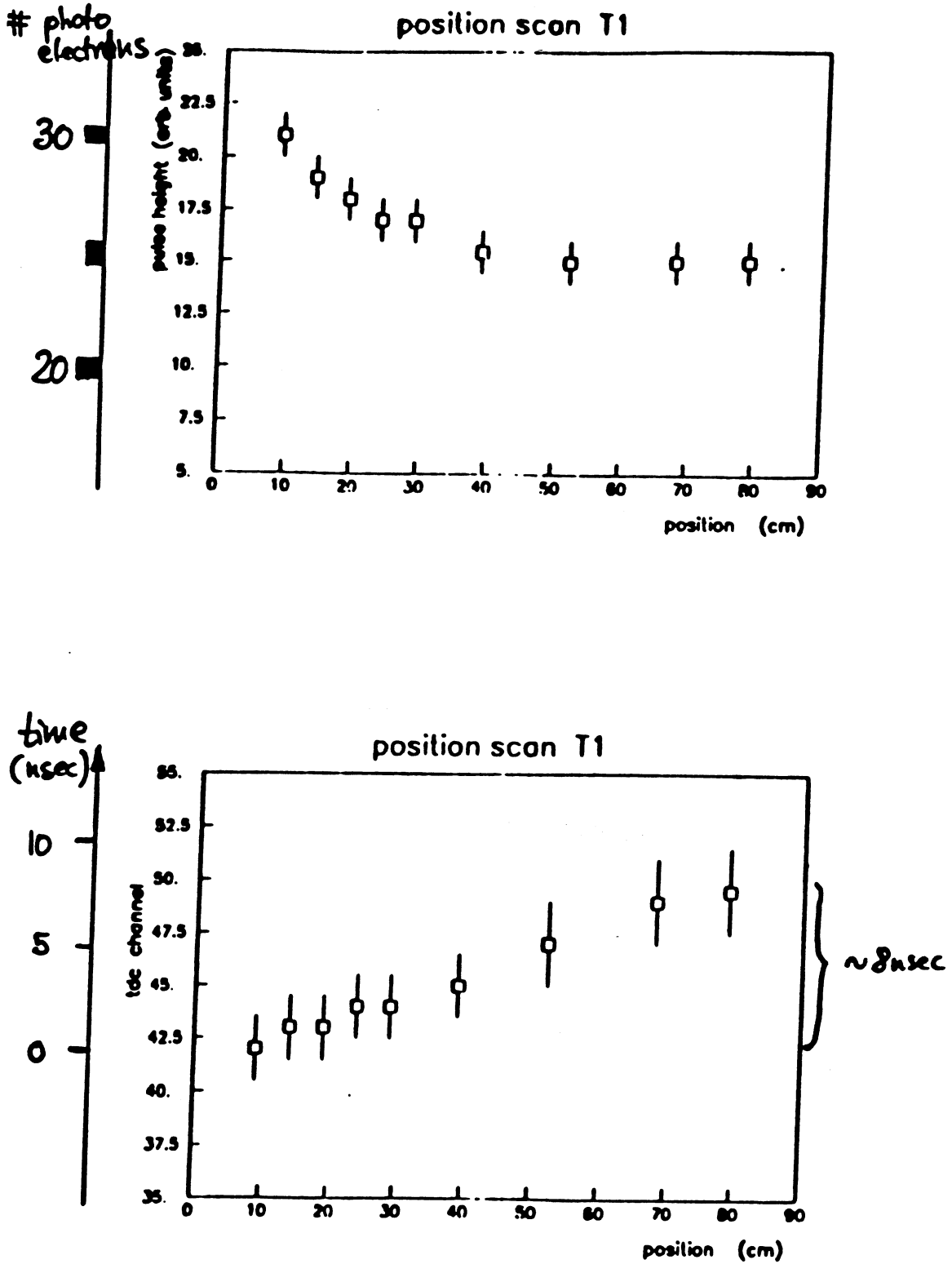

Figure 2.15: Position scans of twisted scintillator with straight light guide.

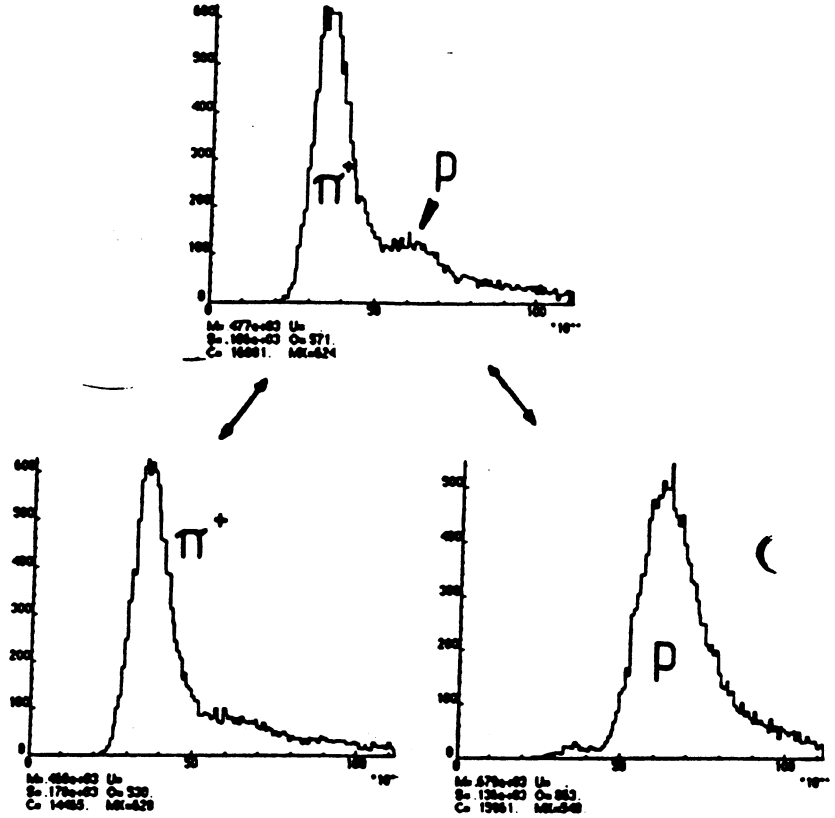

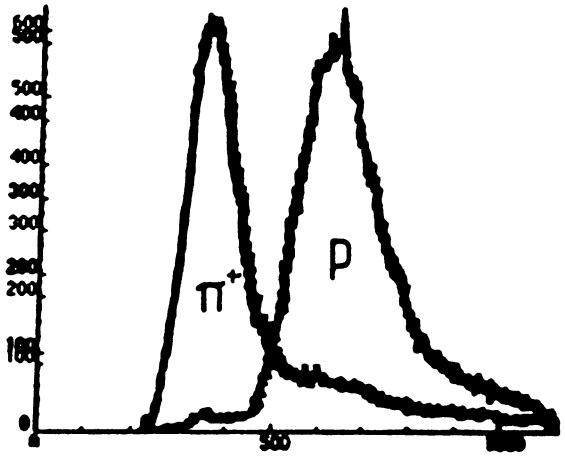

Figure 2.16: ADC spectrum for straight scintillator.

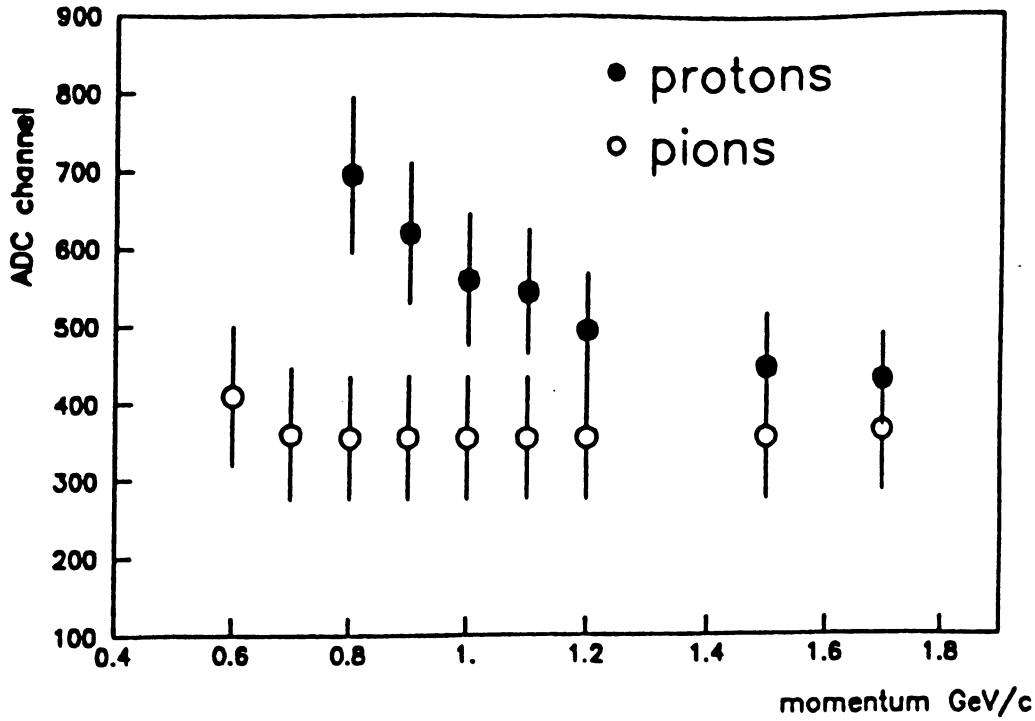

Figure 2.17: Pulseheight dependence on momenta.

- A 4 Tesla superconducting solenoid.
- A weak field 0.5 T solenoid.
- A 1.5 T warm magnet.

A higher field gives a better momentum determination but is also more expensive to obtain.The choice will probably be the 1.5 Tesla.Tests have shown that with this we can obtain a nearly uniform field [9]. The choice of magnet would also depend on whether LEAR can operate satisfactory at the highest field values. The field will be made by two Cu coils wounded around the JETSET detector and contained in a cylinder of length 1.72 m .The cylinder will be surrounded by a thick iron yoke, open at the sides to provide passage for the gas jet target and detector readout. The coils will have inner radius 0.70 m, outer radius 0.95 meter. Each coil will have 210 turns , a current of 5000 A will then give the wanted field strenght.

Figure 2.18 shows the magnet setup.

2.4 Triggering.

We have seen in section 2.1 that the number of $p\overline{p}$ interactions will be about 10^6 each second.Of these we only expect about one $\phi\phi$ event. A selective trigger is necessary to get rid of most of the background events and bring the rate down to less than 100 Hz, which can be written to tape. At the time of writing the complete trigger design is not decided. There will be three levels , the first and probably the second based on fast electonics, and the third on transputer processing.

Deadtime is the time when the readout electonics are blocked by data-acquisition and triggering, during this time new events can not be recorced.In order to reduce the deadtime as much as possible , the first level trigger should give a large rejection factor.We wil here describe one possible trigger setup (see section 5.2 for Monte Carlo studies).

- Level 1 Here the selection criteria will be
  - Multiplicity of four charged particles all forward of $\theta = 90$ and one or less with $\theta > 45$ (3 forward,1 in barrel, or 4 forward). Kaons

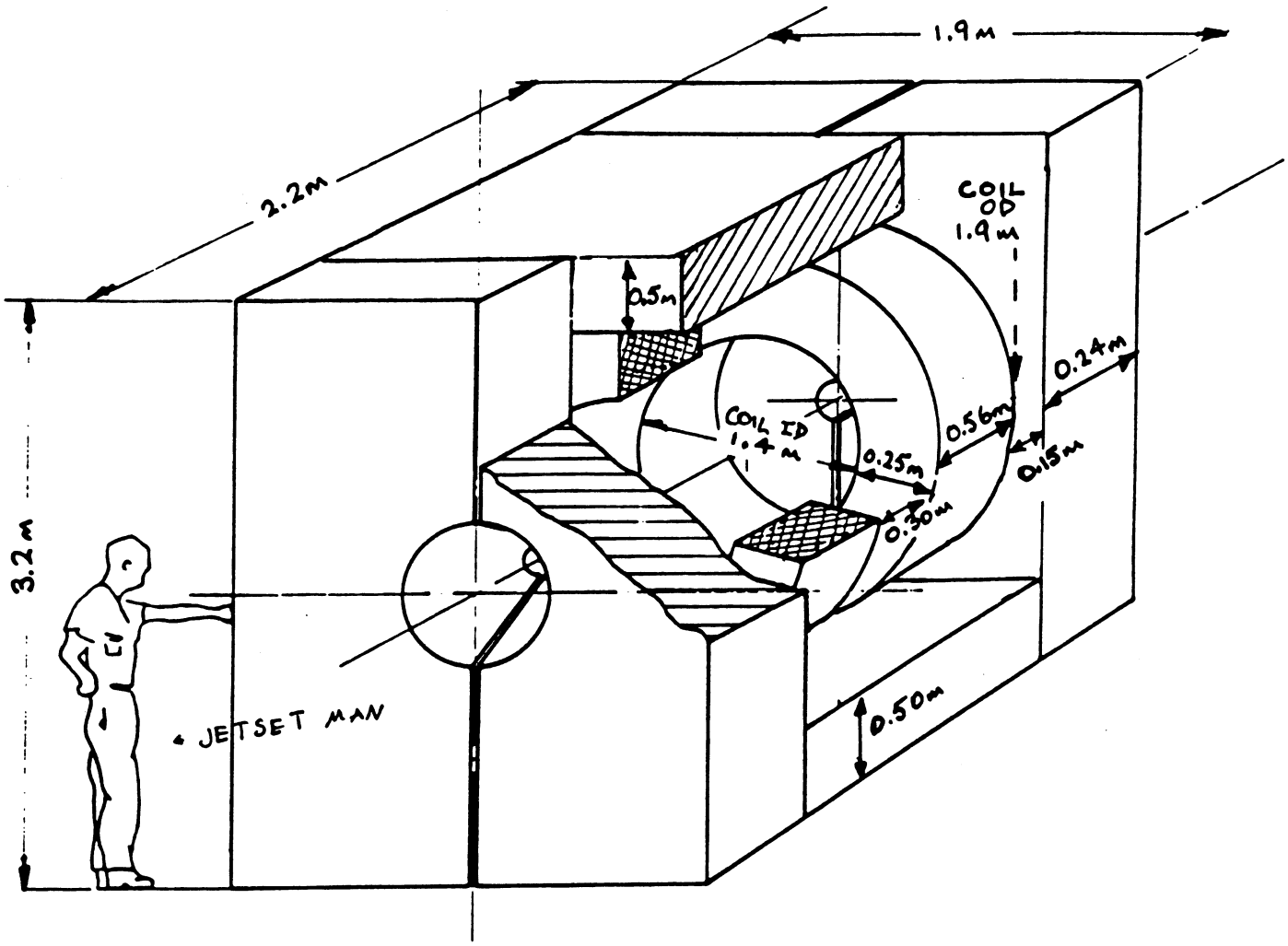

Figure 2.18: JETSET magnet.From[9].

, being heavier than pions will go mostly in the forward direction because of momentum conservation.

The multiplicity will be determined by the trigger scintillators.

- No γ's .π_0's will mostly decay to gammas, so we have to veto on those.This is done if there is a signal in the electromagnetic calorimeter or the γ veto counter, but no signal in the scintillator elements directly in front.
- Not more than one particle with $\beta > 0.8$, which is the threshold of the Cerenkov counter. This is also to get rid of the fast pions.

This level will take about 300 ns and reduce the rate from 1 MHz, to a few kHz.

- Level 2 Here the θ distribution of the particles will be tested, a kinematical cut $\Sigma\theta < 170$ has been proposed, simulations have showed that this generally holds for 4K events.REF This will probably be useful also when we have a magnetic field. Theta will be determined by the trigger scintillator pixels. A problem will be the so called ghosts ; with three or four tracks in the forward direction we will have ambigiuties when there is a false coincidence in the three scintillator levels. Several solutions have been proposed to this problem. Forward Silicon pads can be used in defining the tracks. Also a combinatorial logic incorporated in the pixel defining electronics is proposed (see [14]). Another method is to feed all possible pixel combinations into the coincidence matrix without removing the ghosts.The event will be accepted if any set of pixels fulfill the conditions. In this level the rate will be reduced to about 100 Hz, in 4 μs.

- Level 3 For the dE/dx counters one has proposed for a 4K final state.
  - Total transverse momentum conservation
  - Energy conservation
  - Angle-velocity $(\theta - \beta)$ correlation.

  However , with the present readout of the silicon(Amplex), fast triggering is not possible.

Information from all the detector components will be correlated. At this level digitized readout from the detectors will be assimilated by transputers into an event which will be analysed in μVax computers.This processing will take about 5 ms, but it is in parallell with the other levels, so little additional deadtime will be introduced for each event.

2.5 Data Acquisition

Each of the detector components will be controlled by an independent Valetplus system, with readout buses like FASTbus and CAMAC . In case of a positive trigger , event information will be read out from the FASTbus/CAMAC modules and written to tape. Then they can be further analyzed off-line.The $\phi\phi$ events will be filtered out from 4K and other background events which have managed to get through the trigger. In chapter 4 we will discuss how well this can be done.

Chapter 3

The Simulation Programs

Because of the increasing complexity of particle physics experiments, design studies are very important.Before starting to build the detecor components we do a lot of Monte Carlo simulations. This is to check that we have the optimal detector set up, efficient trigger cuts, and to test that our reconstruction and analysis programs work. In particle physics applications, Monte-Carlo programs generate events of any reaction we want. Then these events go through a program which simulates the whole detector. In this chapter the simulation programs we have used will be described.

3.1 The Event Generator EVGEN

3.1.1 The Fowl Program

The FOWL program was used to generate the wanted events.In this program the Monte-Carlo method is used to calculate phase space distributions arising from particle interactions.The events are generated according to Lorentz invariant phase-space. Figure 3.1 shows a simple flow chart for FOWL. As input for the program we must have a file containing information about the events we want to study in the form of data cards.The required data cards are shown in figure 3.2. The user must also supply the subroutines Start,User and Finish.

W 505

CERN COMPUTER CENTRE
PROGRAM LIBRARY

Amended: 20.1.1970

LONG WRITE-UP

Organization of the Program

The basic structure of FOWL is outlined in the following simplified subroutine diagram:

PROGRAM FOWL - Main program, serves only to fix the length of blank COMMON and define input/output options (CD

SUBROUTINE FOWLMP - Basic controlling subroutine, which makes the following subroutine calls:

REDATA - reads all data cards
START* - for initialization if necessary

for each event {
BEAMIN - chooses beam momentum if variable
GENEV - generates event (momentum vectors)
USER* - calculates desired quantities and wei
TRANCH - accumulates weights in histogram and scattergram bins

FINISH* - for manipulations of final results if necessary
OUTPUT - controls all output (histograms, scat grams, punched cards, etc.)

* = written by user

Figure 3.1: The FOWL program

CERN COMPUTER CENTRE W 505

PROGRAM LIBRARY

Amended: 20.1.1970

LONG WRITE-UP

Required Data Cards

The first three data cards contain the following information:

1. First card - General information - Format I10,2F10.0,I10
   - NEVTOT - Maximum number of events to be generated
   - TLIMIT - Maximum calculation time in minutes (should be smaller than the job time limit to allow for printing)
   - TLIM2 - no longer used.
   - NDUMP - Number of individual events to be dumped (see section E-DUM
2. Second card - Beam - Format 4F10
   - PRM - Beam particle mass
   - TARBM - Target particle mass
   - PBM - Beam momentum
   - DPBM - Spread in beam momentum (half-width of Gaussian) (see section L)

   } (in GeV)
3. Third card - Outgoing particles - Format I10,(7F10),(8F10)
   - NP - Number of outgoing particles (maximum 18)
   - AMASS(1) ... AMASS(NP) - Masses of outgoing particles (in GeV). If more than seven particles, continue on second card (8F10) and if more tha fifteen, on a third card (3F10)

Figure 3.2: Data cards for FOWL

3.1.2 The EVGEN Program

We want to simulate the reaction

$$p\bar{p} \rightarrow \phi\phi \rightarrow K^+K^-K^+K^-$$

,and background reactions listed on page 20.

The program consists of a call to FOWL,and the following user subroutines.

Start

Reads in particle kinds generated by FOWL,decay products, and size of the interaction region.The user can supply in the data file ,life time of the generated particles, and masses of the decay products.She must also give the size of the beam- target interaction voulume.

User

Calculates momentum of decay products.Calculates vertex for decay products and primary particles.Transform to JETSET reference system.Write events to a file readable by the GEANT JETSET Monte Carlo program. Optional:Call to the subroutine ANALYS.Here various calculation can be done to study the distribution of angle and velocity for the particles,and to study the effects of the various trigger requirements.Acceptance cuts can be applied before the events are written to file.

Finish

Write statistics and output histograms.

3.2 The Jetset Monte Carlo

3.2.1 The Geant Program Package

Geant3 is a program package which enables us to

- Track particles through a setup to study the acceptance and simulate the detector response

- Get a graphical representation of the setup and trajectories

We will briely describe this package: The setup is described by using a structure of geometrical volumes,each volume filled by a medium.The particles are tracked through the detector, and physical effects like interactions with matter,decay,and bending in a magnetic field are taken into account. When a particle hits a sensitive detector, this is recorded and the detector response is simulated.This information is written to a file, which can then be read by an analysis program. For each event we can also draw the particle tracks through the detector. A simplified program flow chart for GEANT is shown in figure 3.3

The user must write the main program and some of the subroutines.In the initialization phase she must provide the code to define the geometrical setup and the tracking medium parameters.The setup is described through a set of volumes where each volume has one of several basic shapes and the user gives the dimension and a local reference system.The physical properties are given by the MATERIAL parameters,and some additional information in the TRACKING MEDIUM. A unique initial volume must be defined with a reference system called the master reference system.Volumes can be positioned inside each other, in a hierarchical structure. In the event processing the user must supply code to generate or read in an event.Each particle is tracked until it stops, decays, interacts, or escapes the detector.One subroutine (GCTRACK) loops over all geometrical volumes, and another (GTVOL) over succesive steps.The particle is tracked according to it's type, and all physical prosesses (i.e. energy loss,multiple scattering, decay) and the bending in the magnetic field are calculated. At the end of each step the user dependent subroutine GUSTEP is called. For a sensitive detector the hits will be stored in the data structure JHITS .(The tracking medium parameter ISVOL defines whether a detector is sensitive or not.)When the event is processed it can be written to a file in the subroutine GUOUT.

A file with datacards is also necessary.Here the user can set various flags to control the run,for example she can turn all physical processes on or off and decide which volumes she want to include, and whether they are sensitive or not, according to her own taste.

GEANT 3.10 USER'S GUIDE BASE 010

Author(s) : F.Bruyant
Origin : GEANT3

Submitted: 01.10.
Revised: 20.05.

Simplified Program Flow Chart

```
MAIN (user)
|
|- GZEBRA initialisation of ZEBRA system, dynamic core allocation
|- UGINIT (user)
|   |
|   |- GINIT   initialisation of GEANT3 variables
|   |- GFFGO   interpretation of data cards
|   |- GZINIT  initialisation of ZEBRA core divisions and link areas
|   |- GPART   creation of the 'particle' data structure JPART
|   |- GMATE   creation of the 'material' data structure JMATE
|   |- 'user code' description of the geometrical setup, of the sensitive detectors
|   |              creation of data structures JVOLUM, JTMED, JROTM, JSETS
|   |- GPHYSI preparation of cross-section and energy loss tables for all used materials
|
|- GRUN loop over events
|   |
|   |   GTRIGI initialisation for event processing
|   |   GTRIG  event processing
|   |   |
|   |   |- GUKINE (user) generation (or input) of event initial kinematics
|   |   |- GUTREV (user)
|   |   |   |- GTREVE (loop over tracks, including any secondaries generated)
|   |   |   |   |- GUTRAK (user)
|   |   |   |   |   |- GTRACK control tracking of current track
|   |   |   |   |   |   |- GMEDIA find current volume/tracking medium
|   |   |   |   |   |   |- GTVOL  loop over successive media seen by the particle
|   |   |   |   |   |   |   |- GTGAMA/GTELEC/.... tracking of particle according to type
|   |   |   |   |   |   |   |   |-GUSTEP (user) recording of hits in data structure JHITS
|   |   |   |   |   |   |   |   |                and of space points in data structure JXYZ
|   |   |- GUDIGI computation of digitisations and recording in data structure JDIGI
|   |   |- GUOUT  output of current event
|   |
|   |- GTRIGC clearing of memory for next event
|
|- UGLAST (user)
|   |
|   |- GLAST  standard GEANT3 termination.
|
stop
```

Figure 3.3: GEANT flow chart

3.2.2 The JSMC Program

This program reads events from the EVGEN program,and tracks particles through the JETSET detector.The following elements of the experimental setup can be simulated.

- The beam pipe
- The straw tubes
- The electromagnetic calorimeter
- The trigger scintillation counters
- The threshold Cerenkov
- The dE/dx counters
- (The Rich counter)
- (The silicon microstrips)

When we want to test the reconstruction programs that we will describe in the next chapter,we will only include the beam pipe,scintillators, and the straw tubes in the simulation.Only the straw tubes will be defined as active detectors. The reconstruction programs RETNREC and HELREC reconstruct the tracks from hits in the straw tubes.We must include the beampipe and the inner scintillators, because the multiple scattering that takes place in the material here will affect the track reconstruction. We will now describe how the detector elements are described in the JSMC program.(All sizes given in cm.)

Simulation of the Beam Pipe

The beampipe in JETSET is an ellipse with half axes 8.2 cm and 4.2 cm. In JSMC it is described as 4 tube sections with the following parameters (in cm and degrees)

Section	1	2	3	4
Internal radius	2.786	20.584	2.786	20.584
External radius	2.801	20.599	2.801	20.599
Length	140	140	140	140
Φ upper limit	-75	75	105	255
Φ lower limit	75	105	255	285
Material	Iron			

The 4 sections are then positioned to make an ellipse.

Simulation of the Beam Pipe Scintillators

These detectors are described with 24 boxes with the following parameters.

length	16.0
width	1.6
thickness	0.2
material	plastic

Simulation of the Straw Tubes

The straw tubes contain three elements,the straw walls, the fill gas, and the anode wire.They are described by three tubes inside each other. In the current geometry we use the following parameters

Wire radius	0.0035
Wall thickness	0.0030 -0.0060
Feedtrough length	0.0500
Outer radius	0.4
Length	39.5
Material walls	aluminium
Material wire	tungsten
Chamber gas	70 % argon 30 % C4H10

In the barrel we have 51 layers and a total radius of enclosure 18.0 cm. The endcap is a tube with

Outer radius	8.2
Inner radius	18.0
Length	0.4
Material	Aluminium

In the forward part we have 2 x-chambers and 2 y-chambers at z-positions 21.0,23.9,26.8,29.7, and a radius of enclusure 28.0 .

The geometrical parameters are read in from a separate file called DBASE so they can easily be changed if we want to see the effects of a different geometry.

Output of an Event

After processing an event the following information will be written to the file that will later be read by the reconstruction programs.

- The coordinates for the interaction point (vertex)
- Momentum and direction for all the tracks at vertex
- For each hit: x,y,z,reference to track,reference to the detector

3.3 Summary

For each reaction we want to study we must first run the program EVGEN with the necessary data cards in another file EVGDAT.The output is written to an EVENT file. The JSMC program reads the EVENT file .It also reads the file DBASE with the geometrical parameters,and the data cards file JSMC-DAT.The output is written to a file HITS.This can be read by the reconstruction program, which will be described in the next chapter.

Chapter 4

The Reconstruction Program

4.1 The Method of Least Squares

We have N measurements $y_1, ...y_N$,and a theoretical model which predicts the true values of the measurements $f_i = f_i(\theta_1, ...\theta_M)$ i=1,...N, in terms of the M parameters $\theta_1, ...\theta_M$.

$$\underline{y} = \begin{pmatrix} y_1 \\ y_2 \\ . \\ . \\ . \\ y_N \end{pmatrix} \qquad \underline{\theta} = \begin{pmatrix} \theta_1 \\ \theta_2 \\ . \\ . \\ . \\ \theta_M \end{pmatrix} \qquad \underline{f} = \begin{pmatrix} f_1 \\ f_2 \\ . \\ . \\ . \\ f_N \end{pmatrix} \tag{4.1}$$

The least squares principle says that the best values of the parameters θ minimize the quantity

$$X^2 = [\underline{y} - \underline{f}]^T (\Sigma)^{-1} [\underline{y} - \underline{f}] \tag{4.2}$$

Σ is the covariance matrix

$$\Sigma = \begin{pmatrix} \sigma_1^2 & \sigma_{12} & . & . \\ \sigma_{21} & \sigma_2^2 & . & . \\ . & . & . & . \\ \sigma_{N1} & . & . & \sigma_N^2 \end{pmatrix}. \tag{4.3}$$

It's inverse Σ^{-1} is called the weight matrix,W . If Σ is diagonal then we can write

$$X^2 = \sum_{i=1}^{N} w_i(y_i - f_i)^2 \tag{4.4}$$

where w_i is the weight of the measurement i ,$w_i = 1/\sigma_i^2$. The covariance matrix will be described in more detail in section 4.1.1.

If we can make a reasonable first guess $\theta_1^0, ..., \theta_M^0$ of the parameters,we may expand the f_i in a Taylor series retaining only the 0. and 1. order terms.

$$f_i(\theta_1, \theta_2 .....\theta_M) = f_i(\theta_1^0, \theta_2^0 .....\theta_M^0) + \sum_{j=1}^{M} \frac{\partial f_i}{\partial \theta_j} \triangle\theta_j \tag{4.5}$$

or in matrix form

$$\underline{f}(\underline{\theta}) = \underline{f}(\underline{\theta}^0) + A\triangle\underline{\theta} \tag{4.6}$$

where A is the matrix of derivatives;

$$A = \begin{pmatrix} \frac{\partial f_1}{\partial \theta_1} & \frac{\partial f_1}{\partial \theta_2} & \cdot & \frac{\partial f_1}{\partial \theta_M} \\ \frac{\partial f_2}{\partial \theta_1} & \cdot & \cdot & \cdot \\ \cdot & \cdot & \cdot & \cdot \\ \frac{\partial f_N}{\partial \theta_1} & \frac{\partial f_N}{\partial \theta_2} & \cdot & \frac{\partial f_N}{\partial \theta_M} \end{pmatrix} \tag{4.7}$$

Then X^2 can be written:

$$X^2 = [\underline{y} - \underline{f}(\underline{\theta}^0) - A\triangle\underline{\theta}]^T W[\underline{y} - \underline{f}(\underline{\theta}^0) - A\triangle\underline{\theta}]. \tag{4.8}$$

We want to find the minimum of X^2 ,that is we have to solve

$$\frac{\partial X^2}{\partial \triangle\underline{\theta}} = 0 \tag{4.9}$$

The solution is

$$\triangle\underline{\theta} = (A^T W A)^{-1} \cdot A^T W(\underline{y} - \underline{f}) \tag{4.10}$$

This gives us a better set of track parameters

$$\underline{\theta} = \underline{\theta}^0 + \triangle\underline{\theta} \tag{4.11}$$

If the linear model is only approximate,we have to use an iterative method. The new parameters $\underline{\theta}$ are used as starting parameters $\underline{\theta}^0$ in a new least

squares fit.This procedure is repeated k times until $\mid X^2_{k-1} - X^2_k \mid < \epsilon$,where ϵ is some small number.If we have done an apropriate choice of parameters ,and their starting values are not too far from the real parameters this will not take too many iterations,and we will soon get small X^2.It may happen that $X^2_k > X^2_{k-1}$. This means that the minimum value has been passed over.We can then set $\underline{\theta} = \underline{\theta}^0 + 1/2\triangle\underline{\theta}$ and try an iteration with these values.

4.1.1 The Covariance Matrix

General Theory

The variance $V(y_i)$ of a random variable y_i is the expectation value

$$\sigma_i^2 =< (y_i - < y_i >)^2 >= \int (y_i - < y_i >)^2 P(y_i) dy_i \tag{4.12}$$

σ_i is called the standard deviaton.P(y) is the probability density.

The covariance cov(i,j) of the two random variables y_i, y_j is

$$\sigma_{ij} =< y_i - < y_i >>< y_j - < y_j >>= \tag{4.13}$$

$$\int (y_i - < y_i >)^2 (y_j - < y_j >)^2 P(y_i) P(y_j) dy_i dy_j \tag{4.14}$$

Application to Track Fitting

In track fitting the measurements are measured coordinates from the detectors, for instance drift chambers.The distribution of the measured coordinate y_i will often be gaussian,with the mean equal to the true value and standard deviaton proportional to the precision of detector. Taking only the measurement errors into account we will get a diagonal covariance matrix as input for the least squares fit.

However other effects may cause deviations of measurements from our track model,for example multiple Coulomb scattering of the particle along its trajectory.In this case the covariance matrix will be non diagonal. How to calculate this covariance matrix will be described in more detail in section 4.6.

4.2 Track-model

4.2.1 Geometry of the JETSET Detector

In chapter 2 the JETSET detector was described in detail.The part of it to be used in the track and momentum reconstruction is the precision barrel tracker and precision forward tracker.This consists of straw counters as described in chapter 2.3.1. Parameters for a typical setup of the straws can be seen on page 3.2.2

Figure 4.1 shows the position of the straws in the detector. The barrel consists of straw counters parallel to the beam direction.We have assumed that we do measurements with R = $\sqrt{x^2 + y^2}$ fixed, and measure the coordinates Rϕ and z. Since the transverse resolution in the straws is much better than the longitudinal resolution,$\sigma_{R\phi} \ll \sigma_z$,the ϕ-measurement will have much larger weight than the z- measurement.

In the forward direction we will have layers perpendicular to the beam axis, and parallell to x or y. Here the measurements will have z fixed, and one coordinate x or y have large weight,the other one much smaller. (See figure 4.2). One has to take into account the possibility that the layers are slightly rotated with respect to the x and y axes,i.e. that the straws lie along some direction u, or v, where uv is a rotated coordinate system in the xy-plane.

In this chapter we describe track fitting procedures both for the non magnetic detector and for the case of a homogenous magnetic field,parallel to the beam axis.

4.2.2 Equations of Motion and Parametrization

Straight Tracks

In the case of no magnetic field the equations of motions will be very simple, the particles will follow straight tracks:

$$\begin{aligned} x &= x^0 + v_x t \\ y &= y^0 + v_y t \\ z &= z^0 + v_z t \end{aligned} \tag{4.15}$$

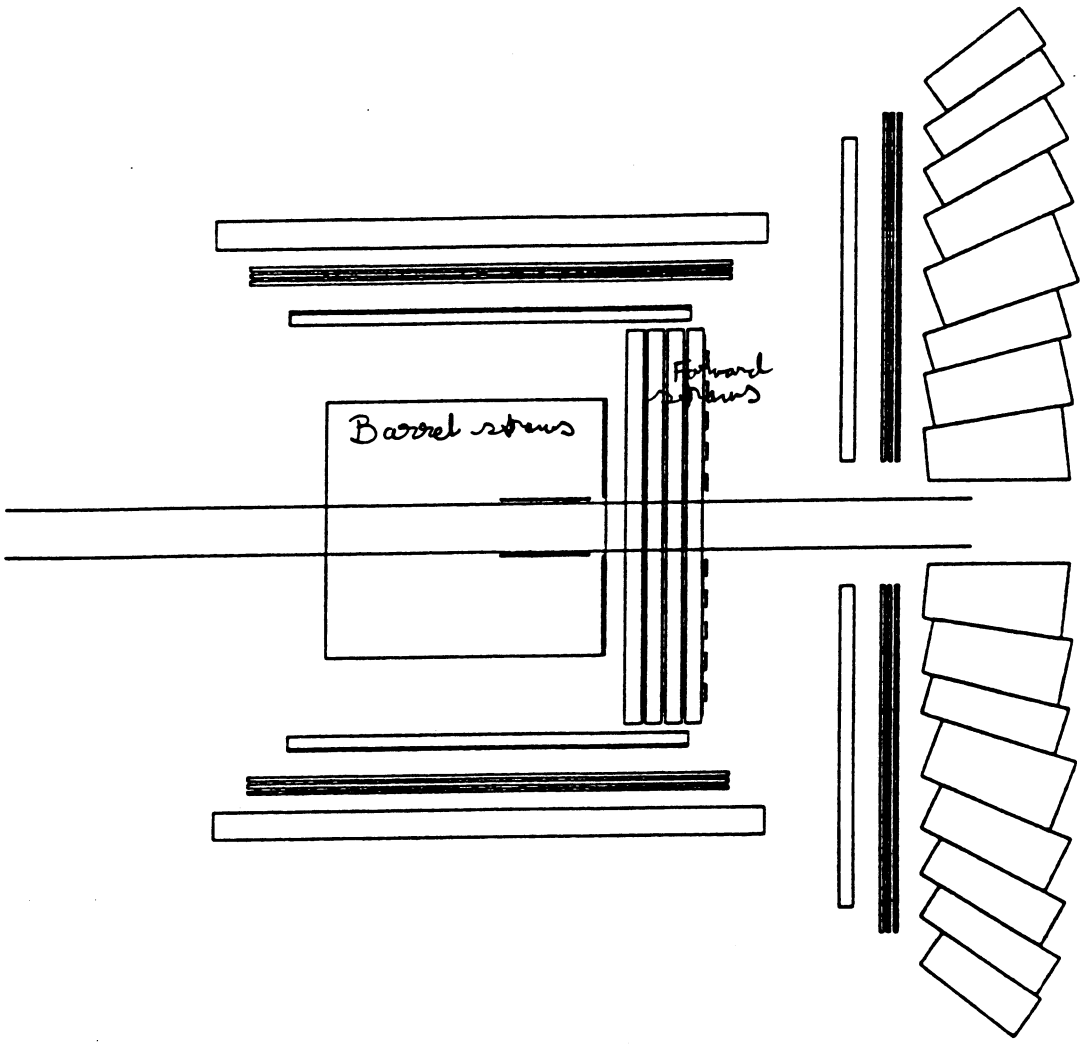

Figure 4.1: Position of straws in the detector.

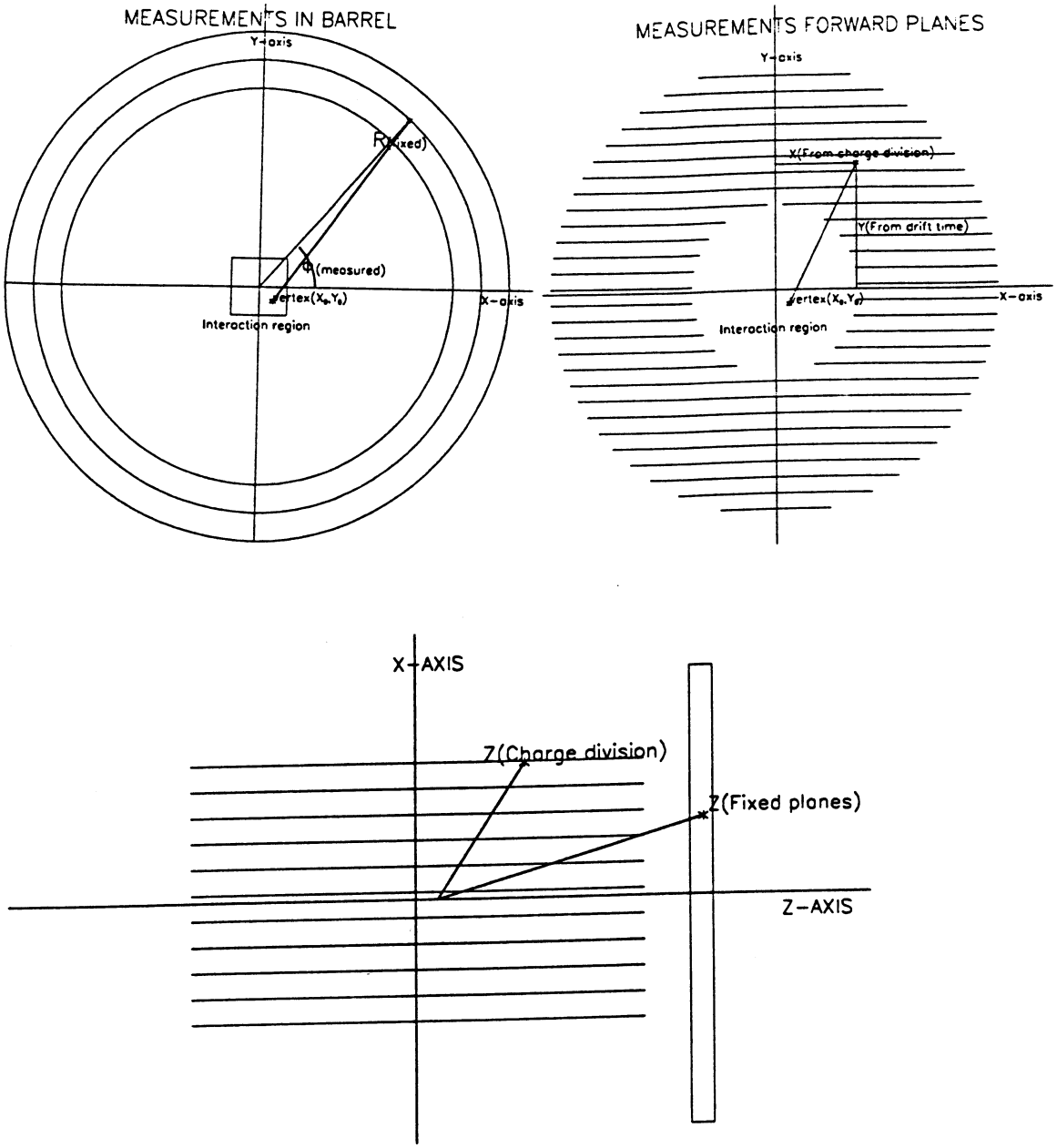

Figure 4.2: Position measurement in straws.

We assume that we have measured x and y for each hit,and that z is known with almost no uncertainty.The predicted values will be:

$$x = x^0 + \frac{v_x}{v_z}(z - z^0)$$
$$y = y^0 + \frac{v_y}{v_z}(z - z^0). \tag{4.16}$$

When we have four tracks we want to find eleven parameters
-x^0, y^0, z^0 ,the common vertex
-$\frac{v_x}{v_z}, \frac{v_y}{v_z}$ at vertex for the four tracks.

Magnetic Field

With a homogenous magnetic field the particles follow helix-shaped paths: The force on a particle in a static magnetic field $\underline{B}(\underline{x})$ is

$$\underline{F} = q\underline{v} \times \underline{B} \tag{4.17}$$

where q is the particle charge,and $\underline{v}$ it's velocity. So the equation of motion will be:

$$m\gamma\frac{d^2\underline{x}}{dt^2} = c^2\kappa q\underline{v} \times \underline{B}. \tag{4.18}$$

Here κ is a proportionality factor dependent of the system of units used, and γ the relativistic factor $\gamma = \frac{1}{\sqrt{1-\beta^2}}\beta = v/c$. That is

$$\frac{d^2\underline{x}}{ds^2} = q/p\frac{d\underline{x}}{ds} \times \underline{B}. \tag{4.19}$$

where

s is path-length, $\frac{ds}{dt} = v$
$\underline{p} = m\gamma\underline{\beta}c$ is the momentum,
p is its abolute value.

In a homogenous magnetic field $\underline{B} = B\underline{e}_z$

$$\frac{d^2x}{ds^2} = (\kappa q/p)\frac{dy}{ds}B \tag{4.20}$$
$$\frac{d^2y}{ds^2} = -(\kappa q/p)\frac{dx}{ds}B \tag{4.21}$$
$$\frac{d^2z}{ds^2} = 0. \tag{4.22}$$

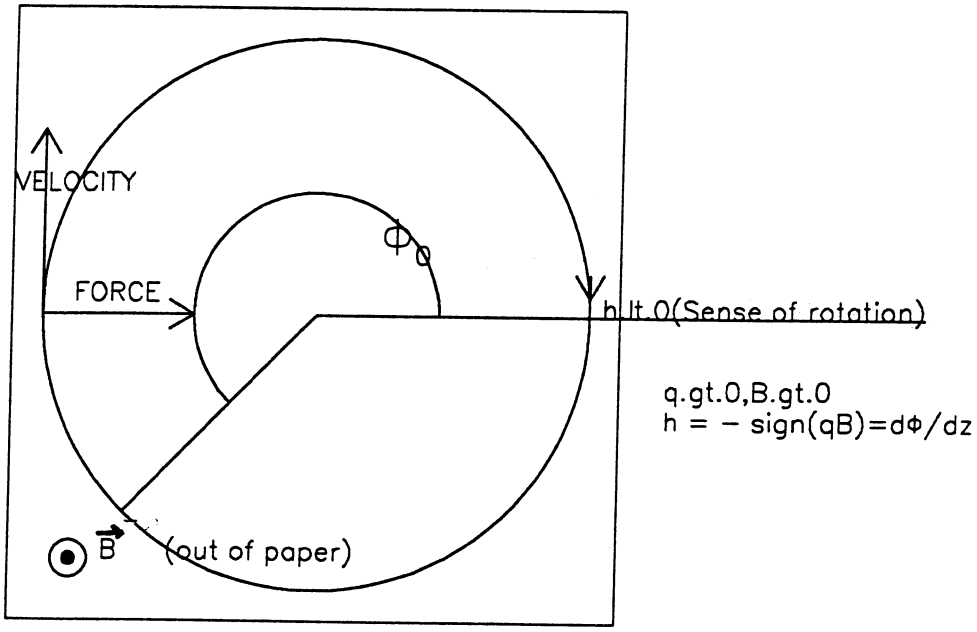

Figure 4.3: Force on particle and sense of rotation.

which gives solutions

$$x(s) = x^0 + R_H(cos(\Phi^0 + hscos\lambda/R_H) - cos\Phi^0 \quad (4.23)$$

$$y(s) = y^0 + R_H(sin(\Phi^0 + hscos\lambda/R_H) - sin\Phi^0 \quad (4.24)$$

$$z(s) = z^0 + sin\lambda s \quad (4.25)$$

where

s = path length along helix
$\underline{x}^0$ = starting point at $s = s^0$
λ = slope angle = $\arcsin dz/ds$
R_H = radius of helix = $\frac{P\cos\lambda}{abs(\kappa qB)}$
Φ_0 = azimuthal angle of starting point
= $\arctan dy/dx_{s=0}$
h = sense of rotation
= $\partial\Phi/\partial z = -sign(qB)$ (see fig 4.3).

The equations for x and y, in terms of z will be

$$x = x^0 + R_H(\cos(\phi_0 + h/R_H\frac{z - z^0}{\tan\lambda}) - \cos\phi_0)$$

$$y = y^0 + R_H(\sin(\phi_0 + h/R_H \frac{z - z^0}{\tan\lambda}) - \sin\phi_0). \tag{4.26}$$

In the case of four tracks we want to find fifteen parameters -x^0, y^0, z^0 ,the common vertex
-$\Phi_0, \tan\lambda, h/R_H$ at vertex for the four tracks.
Figures 4.4, and 4.5 shows the parameters for curved tracks.

4.2.3 Measurement Errors

The resolution for the straws with measurements in the transverse/longitudinal direction are assumed to be

$\sigma_t = 0.02cm, \sigma_l = 0.2cm$

In the forward direction one coordinate (x or y) has error σ_t,the other σ_l. In the barrel measurements with ϕ,z measured we transform to x,y measurements by setting:

$$\begin{aligned} z &= z_{measured} \\ x_{measured} &= R\cos\phi_{measured} \\ y_{measured} &= R\sin\phi_{measured} \end{aligned} \tag{4.27}$$

The rule for error propagation says:

$$\sigma_x = (\frac{\partial x}{\partial z_m})^2\sigma_{z_m}^2 + (\frac{\partial x}{\partial \phi_m})^2\sigma_{\phi_m}^2 \tag{4.28}$$

$$\frac{\partial x}{\partial \phi_m} = R(-\sin\phi_m)$$

$$\frac{\partial x}{\partial z_m} = \cos\phi_m \frac{\partial R}{\partial z_m} = \cos\phi_m \tan\theta$$

$$\tan\theta = R/z_m$$

$$\sigma_\phi = \sigma t/R \tag{4.29}$$

$$\sigma_x = (\sin\phi_m)^2\sigma_t^2 + (\cos\phi_m R/z_m)^2\sigma_l^2 \tag{4.30}$$

See figure 4.6.Similarly, the error in y will be

$$\sigma_y = (\cos\phi_m)^2\sigma_t^2 + (\sin\phi_m R/z_m)^2\sigma_l^2 \tag{4.31}$$

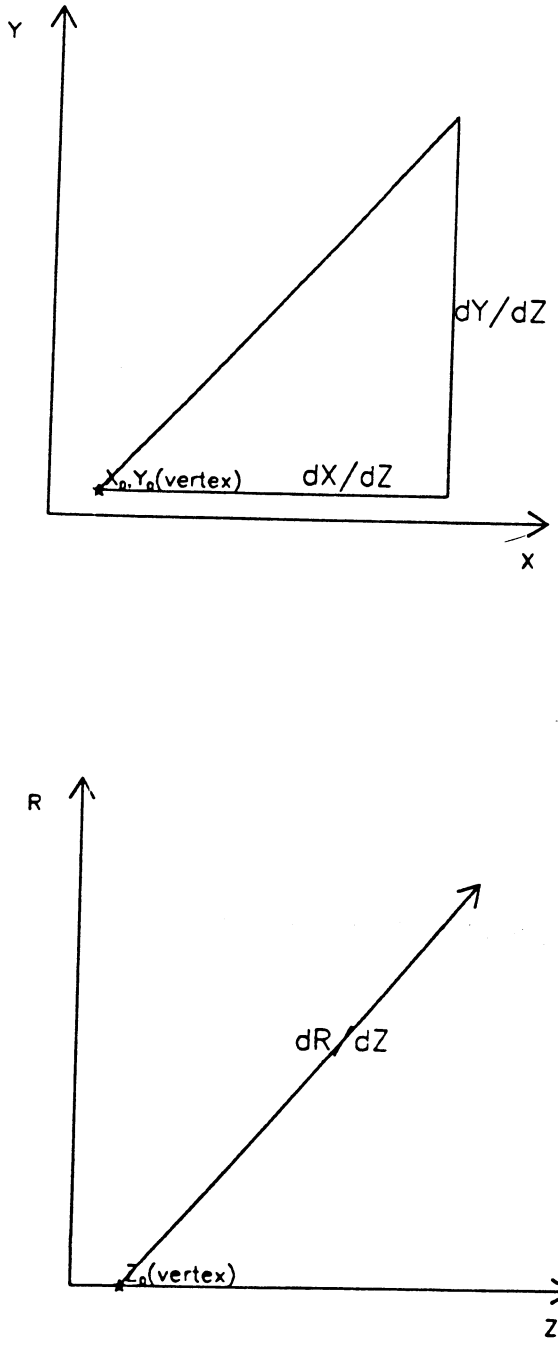

Figure 4.4: Parameters for track fitting,straight tracks

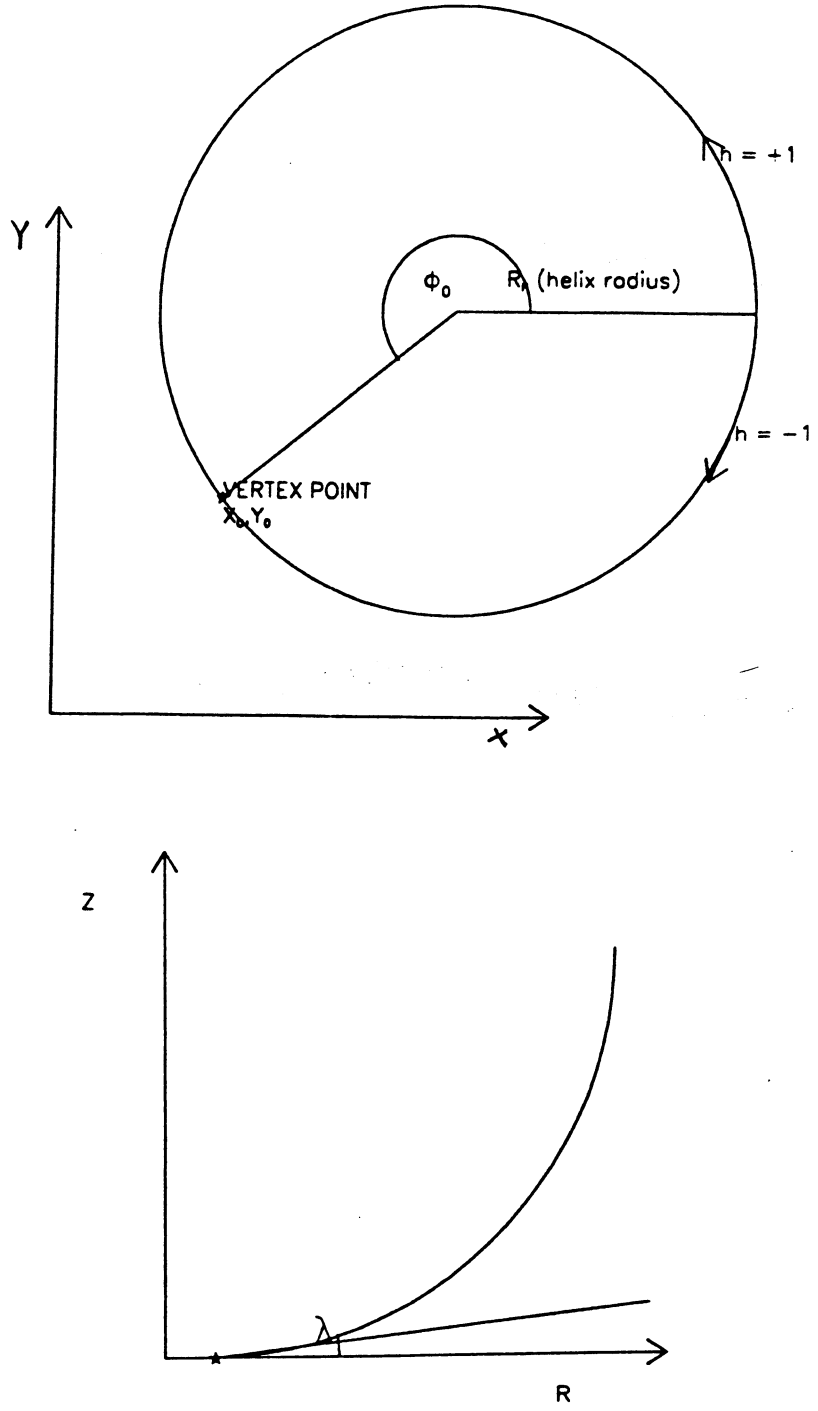

Figure 4.5: Parameters for track fitting,curved tracks

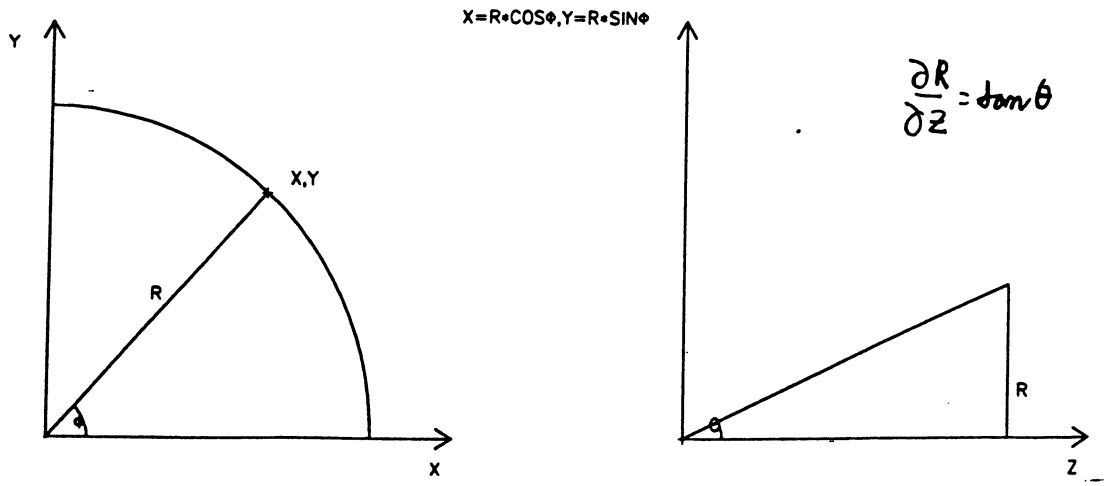

Figure 4.6: Transformation of measured coordinates

4.3 The Track-Vertex Fit

We have the following information to start with: Measured coordinates for the tracks with errors,approximate vertex position,beam momentum and magnetic field strength.

From this we want to find the vertex coordinates,and the momentum at vertex for all the particles, by using the method of least squares already explained.We have used a method where all the tracks (four in our case) are fitted at the same time, through a common vertex. If there is a magnetic field, the momenta can be found directly from this. Otherwise we can only find the directions.Then the method described in section 4.4 is used to determine the momenta.

In general we have for the measurement vector $\underline{f}_j$ for track number j,

$$\underline{f}_j = \underline{f}_j(\underline{z}_j, \underline{a}_j, \underline{r}) \tag{4.32}$$

In our case for each hit in the detector we will have two measurements f. Z is a fixed value for each measurement (the position of the detector),and
$\underline{a}_j$ are track parameters (momentum,direction for track j)
$\underline{r}$ are common vertex parameters

Then we can write
$\underline{f} = \underline{f}(\underline{z}, \underline{\theta})$
$\underline{\theta} = (\underline{r}, \underline{a}_1, , , \underline{a}_4)$
$\theta_1, , \theta_3 = x_0, y_0, z_0$
$\theta_4, , \theta_{npar} = a_{j,itp}$,$j = 1, ntrack, itp = 1, ntp$
ntp is the number of parameters for each track ,2 for straight tracks, and 3 for curved tracks.
$a_{j,itp} = \theta_k$, $k = 3 + ntp(j-1) + itp$

4.3.1 Matrix Calculation

In section 4.1 we saw that when we start with parameters θ we get improvements

$$\Delta\underline{\theta} = (A^T W A)^{-1} \cdot A^T W(\underline{y} - \underline{f}) \tag{4.33}$$

N_i is the number of hits for each track.In our straw tubes each hit will produce two coordinate measurement X_m and Y_m (from drift time and charge division). The total number of measurements will be $NMEAS = 2(N_1+N_2+N_3+N_4) = 2N$ The vector of residuals ,$(\underline{y} - \underline{f})$ has dimension $NMEAS$,and is given by

$$\mathbf{Res} = (\underline{\mathbf{y}} - \underline{\mathbf{f}}) = \begin{pmatrix} \mathbf{Res1} \\ \mathbf{Res2} \\ \mathbf{Res3} \\ \mathbf{Res4} \end{pmatrix} = \begin{pmatrix} X_m(1,1) - X_c(1,1) \\ Y_m(1,1) - Y_c(1,1) \\ X_m(2,1) - X_c(2,1) \\ \cdot \\ \cdot \\ Y_m(N_1,1) - Y_c(N_1,1) \\ - - - - - - - - - - \\ \cdot \\ \cdot \\ - - - - - - - - - - \\ \cdot \\ \cdot \\ - - - - - - - - - - \\ X_m(1,4) - X_c(1,4) \\ \cdot \\ \cdot \\ Y_m(N_4,4) - Y_c(N_4,4) \end{pmatrix} \tag{4.34}$$

$X_m(i,j), X_c(i,j)$ and $Y_m(i,j), Y_c(i,j)$ are measured and calculated values of X, Y for hit number i, track number j.

The matrix **A** of derivatives will have the form

$$\mathbf{A} = \begin{pmatrix} \mathbf{A_{10}} & \mathbf{A_{11}} & 0 & 0 & 0 \\ \mathbf{A_{20}} & 0 & \mathbf{A_{22}} & 0 & 0 \\ \mathbf{A_{30}} & 0 & 0 & \mathbf{A_{33}} & 0 \\ \mathbf{A_{40}} & 0 & 0 & 0 & \mathbf{A_{44}} \end{pmatrix} \tag{4.35}$$

It has dimension $NMEAS\times$ number of parameters .

$$\mathbf{A_{j0}} = \begin{pmatrix} \frac{\partial X_c(1,j)}{\partial X^0} & \frac{\partial X_c(1,j)}{\partial Y^0} & \frac{\partial X_c(1,j)}{\partial Z^0} \\ \frac{\partial Y_c(1,j)}{\partial X^0} & \frac{\partial Y_c(1,j)}{\partial Y^0} & \frac{\partial Y_c(1,j)}{\partial Z^0} \\ \cdot & \cdot & \cdot \\ \cdot & \cdot & \cdot \\ \frac{\partial X_c(N_j,j)}{\partial X^0} & \frac{\partial X_c(N_j,j)}{\partial Y^0} & \frac{\partial X_c(N_j,j)}{\partial Z^0} \\ \frac{\partial Y_c(N_j,j)}{\partial X^0} & \frac{\partial Y_c(N_j,j)}{\partial Y^0} & \frac{\partial Y_c(N_j,j)}{\partial Z^0} \end{pmatrix} \tag{4.36}$$

$$\mathbf{A_{jj}} = \begin{pmatrix} \frac{\partial X_c(1,j)}{\partial a_{j1}} & \frac{\partial X_c(1,j)}{\partial a_{j2}} & \cdot \\ \frac{\partial Y_c(1,j)}{\partial a_{j1}} & \frac{\partial Y_c(1,j)}{\partial a_{j2}} & \cdot \\ \cdot & \cdot & \cdot \\ \cdot & \cdot & \cdot \\ \frac{\partial X_c(N_j,j)}{\partial a_{j1}} & \frac{\partial X_c(N_j,j)}{\partial a_{j2}} & \cdot \\ \frac{\partial Y_c(N_j,j)}{\partial a_{j1}} & \frac{\partial Y_c(N_j,j)}{\partial a_{j2}} & \cdot \end{pmatrix} \tag{4.37}$$

a_{jk} is parameter k for track j.

W is the weight matrix $\mathbf{\Sigma^{-1}}$.It has dimension NMEAS,$\times$ NMEAS,and the block form

$$W = \begin{pmatrix} \mathbf{W_{11}} & \cdot & \cdot & \cdot \\ \cdot & \mathbf{W_{22}} & \cdot & \cdot \\ \cdot & \cdot & \mathbf{W_{33}} & \cdot \\ \cdot & \cdot & \cdot & \mathbf{W_{44}} \end{pmatrix} \tag{4.38}$$

$\mathbf{W_{jj}}$ is the weight matrix for one track .There is no covariance between the different tracks.

We define a vector DELTA=$A^TW(\underline{y}-\underline{f})$ size npar and a matrix $ATA = (A^TWA)$,size npar $\times$ npar.

$$DELTA = \begin{pmatrix} \sum \mathbf{A_{j0}^T W_{jj} ResJ} \\ \mathbf{A_{11}^T W_{11} Res1} \\ . \\ \mathbf{A_{44}^T W_{44} Res4} \end{pmatrix} \tag{4.39}$$

$$ATA = \begin{pmatrix} \sum \mathbf{A_{j0}^T W_{jj} A_{j0}} & \mathbf{A_{10}^T W_{11} A_{11}} & . & . & \mathbf{A_{40}^T W_{44} A_{11}} \\ \mathbf{A_{11}^T W_{11} A_{10}} & \mathbf{A_{11}^T W_{11} A_{11}} & 0 & 0 & 0 \\ . & . & . & . & . \\ . & . & . & . & . \\ \mathbf{A_{44}^T W_{44} A_{40}} & 0 & 0 & 0 & \mathbf{A_{44}^T W_{44} A_{44}} \end{pmatrix} \tag{4.40}$$

If we have a diagonal weight matrix

$$\mathbf{W_{jj}} = \begin{pmatrix} \frac{1}{\sigma_x(1,j)^2} & 0 & 0 & 0 & 0 \\ 0 & \frac{1}{\sigma_y(1,j)^2} & 0 & 0 & 0 \\ 0 & 0 & \frac{1}{\sigma_x(2,j)^2} & 0 & 0 \\ .0 & 0 & 0 & . & 0 \\ 0 & 0 & 0 & 0 & \frac{1}{\sigma_y(N_j,j)^2} \end{pmatrix} \tag{4.41}$$

where $\frac{1}{\sigma_x(i,j)^2}$ is the weight,w(i,j),for the x -measurement for hit i,track j then we get the following expressions.

$$DELTA(k) = \begin{cases} \text{...For k=1,.,3} \\ \sum_{j=1}^{ntrack}[\sum_{i=1}^{nhits(j)} w_x(i,j)\frac{\partial x_c}{\partial \theta_k}(x_c(i,j)-x_m(i,j))+ \\ ..y \text{ terms}] \\ \text{...For k= 4,.,npar} \\ \sum_{i=1}^{nhits(j)} w_x(i,j)\frac{\partial x_c}{\partial \theta_k}(x_c(i,j)-x_m(i,j))+ \\ ..y \text{ terms} \end{cases} \tag{4.42}$$

$$ATA(k,l) = \sum_{j=1}^{ntrack}\Big(\sum_{i=1}^{nhits(j)} w_x(i,j)\frac{\partial x_c}{\partial \theta_k}\frac{\partial x_c}{\partial \theta_l} + ..y \text{ terms}\Big) \tag{4.43}$$

The reconstruction procedure will then be like this:

-PROCEDURE TRVREC
- Find starting parameters
- $x_0, y_0, z_0, (a_1, ., a_{itp})_j, j = 1, ntrack$
- from detector hits.
- k = 0
- start: k = k+1
- For j = 1,ntrack
- For i = 1,nhits(j)
- $x_c = ..$
- $y_c = ..$
- For ipar = 1,npar
- For jpar = 1,npar
- DELTA(ipar) = DELTA(ipar) +....
- ATA(ipar,jpar) = ATA(ipar,jpar) +...
- $X^2 = X^2 + (\Delta x \times w_x)^2 + (\Delta y \times w_y)^2$
- if $\mid X^2_{k-1} - X^2_k \mid < \epsilon$ GO TO END of trvrec.
- if $X^2_{k-1} - X^2_k < 0$ THEN
- $\theta = \theta - 0.5\Delta\theta$
- GO TO start
- ENDIF
- $\Delta\theta = (ATA)^{-1} DELTA$
- $\theta = \theta + \Delta\theta$
- GO TO START
-END of trvrec

The CERNLIB routines RFACT and REQN are used to solve the matrix equation. If we want to use a non diagonal weight matrix with contributions from multiple scattering we must change the whole procedure. See section 4.6. Tables 4.3 and 4.4 shows the derivatives we use in calculatating ATA and DELTA. The start-values are shown in table 4.1 (straight tracks),or table 4.2(curved tracks).

Circle Radius

To find the radius for the projected circle in the XY-plane we use a method proposed in [16]. This gives the position of the center,$x_c(j), y_c(j)$,for the circle, when three points are given,and goes like this:.

- Shift origin to x_1, y_1

$$x_i' = x_i - x_1, , i = 2, 3 \tag{4.44}$$

- Rotate coordinate system,$(y_3' = 0)$

$$d = \sqrt{(x_3')^2 + (y_3')^2} \tag{4.45}$$
$$c_\phi = x_3'/d \tag{4.46}$$
$$s_\phi = y_3'/d \tag{4.47}$$
$$\tilde{x_i} = x_i' c_\phi + y_i' s_\phi, i = 2, 3 \tag{4.48}$$
$$\tilde{y_i} = y_2' c_\phi - x_2' s_\phi, i = 2, 3 \tag{4.49}$$
$$\tag{4.50}$$

- Find the centre and radius:

$$\tilde{x_c} = x_3/2 \tag{4.51}$$
$$\text{check that } \tilde{y_2} \neq 0 \tag{4.52}$$
$$\tilde{y_c} = 1/2 \cdot (\tilde{y_2} - \tilde{x_2}(\tilde{x_3} - \tilde{x_2})/\tilde{y_2})$$
$$r^2 = \tilde{x_c^2} + \tilde{y_c^2} \tag{4.53}$$

- Rotate and shift centre to original system.

$$x_c = \tilde{x_c} c_\phi - \tilde{y_c} s_\phi + x_i \tag{4.54}$$
$$y_c = \tilde{y_c} c_\phi + \tilde{x_c} s_\phi + y_i \tag{4.55}$$

4.4 How to Find the Momenta

4.4.1 Straight Tracks

If we have found the directions of the four outgoing particles,we can find the momenta assuming that the particles have a mass equal to M_K. From

x_0	0
y_0	0
z_0	0
dx/dz	$\frac{x_m(nhits(j),j)}{z_{plane}(nhits(j),j)}$
dy/dz	$\frac{y_m(nhits(j),j)}{z_{plane}(nhits(j),j)}$

Table 4.1: Starting values for parameters,straight tracks.

x_0	0
y_0	0
z_0	0
Φ_0	$\arctan \frac{(-y_c(j))}{(-x_c(j))}$
$\tan\lambda$	$\frac{z_{plane}(nhits(j),j)}{\sqrt{x_m(nhits(j),j)^2+y_m(nhits(j),j)^2}}$
h/R_H	$\frac{sign(\Delta\Phi)}{\sqrt{(x_c(j)-x_m(nhits(j),j))^2+(y_c(j)-y_m(nhits(j),j))^2}}$

Table 4.2: Starting values for parameters,helix formed tracks.

θ/f	$x(z)$	$y(z)$
x_0	1	0
y_0	0	1
z_0	$-dx/dz$	$-dy/dz$
dx/dz	$z-z_0$	0
dy/dz	0	$z-z_0$

Table 4.3: Derivatives, $\frac{\partial f}{\partial\theta}$,straight track

θ/f	$x(z)$	$y(z)$
x_0	1	0
y_0	0	1
z_0	$h/\tan\lambda \sin(\Phi_0 + h/R_H \frac{z-z_0}{\tan\lambda})$	$-h/\tan\lambda \cos(\Phi_0 + h/R_H \frac{z-z_0}{\tan\lambda}$
Φ_0	$R_H(-\sin(\Phi_0 + h/R_H \frac{z-z_0}{\tan\lambda}) + \sin\phi_0)$	$R_H(\cos(\Phi_0 + h/R_H \frac{z-z_0}{\tan\lambda}) - \cos\Phi_0)$
$\tan\lambda$	$\frac{h(z-z_0)}{tan^2\lambda} \sin(\Phi_0 + h/R_H \frac{z-z_0}{\tan\lambda})$	$-\frac{h(z-z_0)}{tan^2\lambda} \cos(\Phi_0 + h/R_H \frac{z-z_0}{\tan\lambda})$
h/R_H	$-hR_H^2(\cos(\Phi_0 + h/R_H \frac{z-z_0}{\tan\lambda}) - \cos\Phi_0)$ $-R_H \frac{(z-z_0)}{tan\lambda} \sin(\Phi_0 + h/R_H \frac{z-z_0}{\tan\lambda})$	$-hR_H^2(\sin(\Phi_0 + h/R_H \frac{z-z_0}{\tan\lambda}) - \sin\Phi_0)$ $+R_H \frac{(z-z_0)}{tan\lambda} \cos(\Phi_0 + h/R_H \frac{z-z_0}{\tan\lambda})$

Table 4.4: Derivatives, $\frac{\partial f}{\partial \theta}$, curved track

momentum conservation we get three equations.

$$P_{inc,i} = \sum_{j=1}^{ntrack} P_i^j, \qquad (i = 1,3) \tag{4.56}$$

$P_{inc,i}$ is the momentum component i of the incident antiproton.
$P_{inc,x}$=$P_{inc,y}$= 0. Manipulating with these equation we get

$$M \begin{pmatrix} P^2 \\ P^3 \\ P^4 \end{pmatrix} = \begin{pmatrix} -C_x^1 P^1 \\ -C_y^1 P^1 \\ P_{inc,z} - C_z^1 P^1 \end{pmatrix} \tag{4.57}$$

Here C_i^j is $\frac{P_i^j}{P^j}$,and M the matrix

$$M = \begin{pmatrix} C_x^2 & C_x^3 & C_x^4 \\ C_y^2 & C_y^3 & C_y^4 \\ C_z^2 & C_z^3 & C_z^4 \end{pmatrix} \tag{4.58}$$

If P^1 is known we can find the three other momenta from:

$$\begin{pmatrix} P^2 \\ P^3 \\ P^4 \end{pmatrix} = M^{-1} \begin{pmatrix} -C_x^1 P^1 \\ -C_y^1 P^1 \\ P_{inc,z} - C_z^1 P^1 \end{pmatrix} \tag{4.59}$$

This can also be written

$$P^j = a_j P^j + b_j$$

From conservation of energy we have that

$$\Delta = E_{inc} + E_{target} - \sum_{j=1}^{ntrack} (m_k^2 + (P^j)^2)^{1/2} = 0 \tag{4.60}$$

We have to scan for different values of P^1 . The second derivative of Δ with respect to P^1 is always negative.

$$\frac{d^2\Delta}{d(P^1)^2} = - \sum_{j=1}^{ntrack} a_j^2 \frac{m_j^2}{[(a_j P^j + b_j)^2 + m_j^2]^{3/2}} \tag{4.61}$$

Figure 4.7 from [12] shows the different forms Δ can have and we see that we can get 0,1 or 2 good solutions ($\Delta = 0$). In this and the next chapter, we have then chosen the correct solution (closest to Monte Carlo values),but [10] explains how it can be found from measurements of the energy loss in silicon detectors.

4.4.2 Curved Tracks

From figure 4.8 we see that the momenta are given from the parameters in the following way.

$$\begin{aligned} P_T &= \frac{|\, B\kappa q \,|}{R_H} \\ \phi &= \Phi_0 + h \cdot \pi/2 \\ P_X &= P_T \cos\phi \\ P_Y &= P_T \sin\phi \\ P_Z &= P_T \tan\lambda \end{aligned} \tag{4.62}$$

After having found the momenta in this way,we can then use the directions at the starting point$(P_X/P_Z, P_Y/P_Z)$ to do a fit with directions as described above.

4.5 The REC Programs.

We have used the programs RETNREC and HELREC to reconstruct monte-carlo events.Events generated by FOWL were used as input to the GEANT

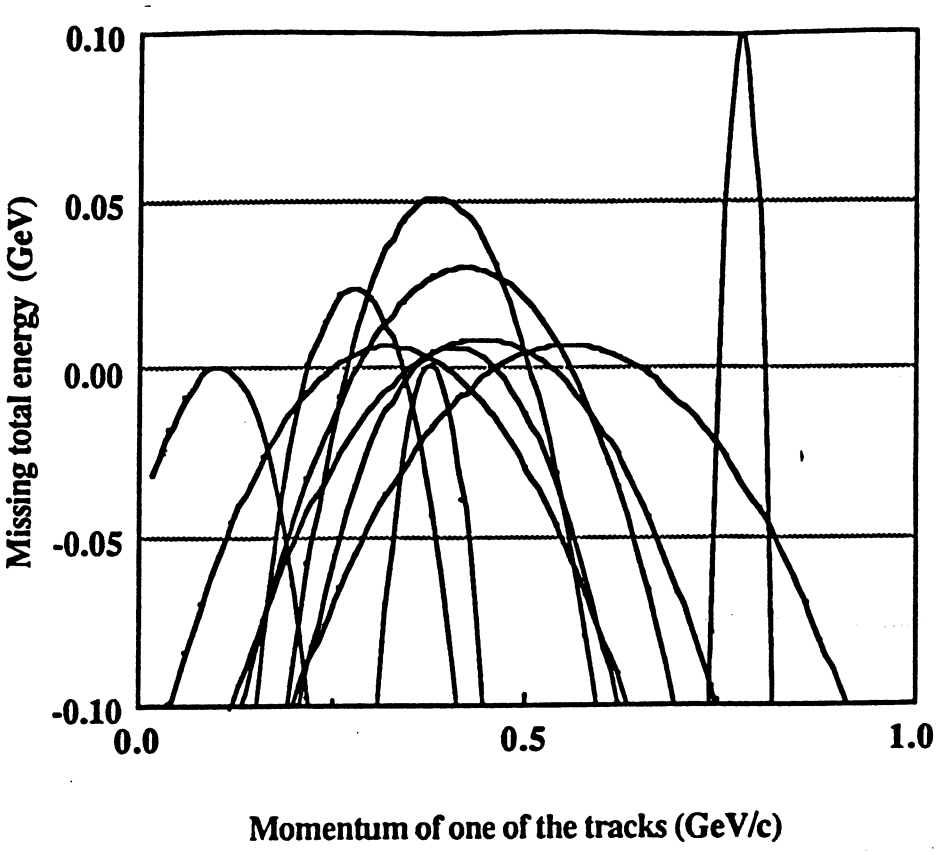

Fig. 7 A few examples of the functional dependence of the "missing energy" from one of the particles momenta.

Figure 4.7: The Δ function (from [12]).

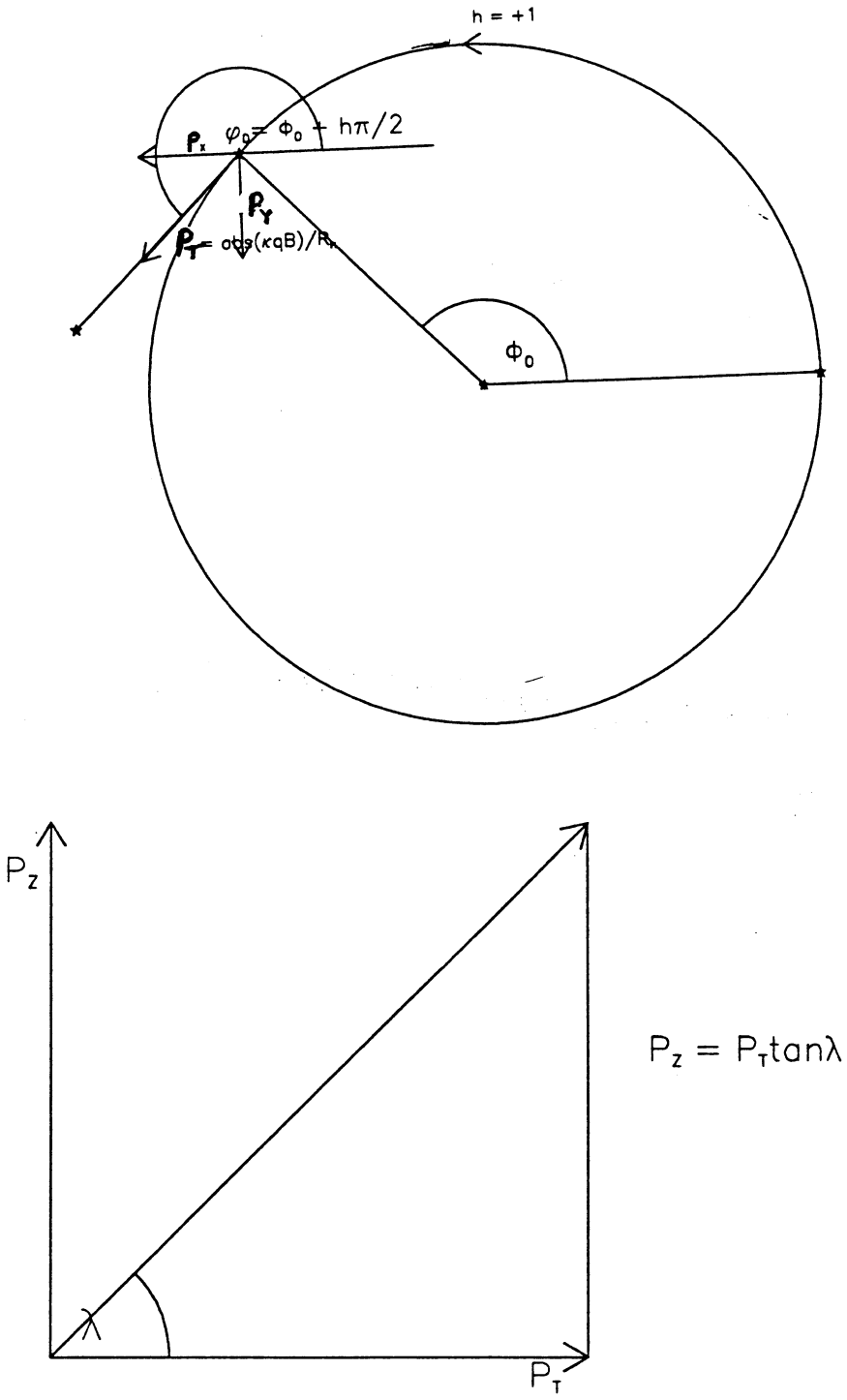

Figure 4.8: Connection between momenta and parameters.

program,which simulated the detector with different physical processes. In the programs gaussian fluctuations were added to the impact points, before reconstruction of the directions and momenta of kaons, and the invariant masses of pairs of tracks. For each hit,we knew the corresponding track which produced it ,so no attempt of pattern recognition was done. To check the program the reconstructed momenta was compared to the 'true' values for the monte-carlo events. We will briefly describe the program RETNREC:

```
-BEGIN
-CALL INITIALIZE
-
-       CALL PARA
-       Reads geometrical parameters for detector element
-
-       CALL READH
-       Reads event file header;magnetic field,momentum of
-       incoming anti-proton etc.
-
-FOR each event DO
-
-       CALL READEV
-       Reads no. of tracks ,vertex and momenta
-       for each track,type of particle (from MC-data),
-       reads no. of hits in each detector ,corresponding track,
-       hit coordinates.
-
-              For strawhits
-              CALL DSTRW
-              Fakes pattern recognition.Assigns each hit to a track,
-              and assign errors according to detector type.
-
-       CALL TRVINP
-       Prepares input for the track reconstruction.
-       Adds gaussian errors to hits to get measured values.
-       Transforms all measurements to X-Y measurements.
-       Calculates errors from multiple scattering.
```

```
-       Finds weights for all measurements.
-
-       CALL TRVREC
-       Described on page 4.3.1.
-
-       If event OK so far
-       CALL EVREC
-
-            CALL KINEM
-            Finds momenta of kaons from directions and the
-            energy and momentum of the antiproton.
-           See section 4.4.
-
-            CALL INVMASS
-            Reconstructs mass of φ particles.
-
-       CALL STATIS
-      Compare reconstructed with generated values,and chi square
-      values with theoretical distribution.
-
-END
```

4.5.1 Results from the Programs

We have generated $\phi\phi$ events in EVGEN, with a beam momenta of 1.5 GeV, and an interaction region of 1 cm^3. The geometry used in the simulation program JSMC is described in section 3.2.2.In each case we generated 1000 events. We then tested the program RETNREC at four different conditions.

1. No multiple scattering in the simulation program,and no errors added in the reconstruction program.All the measurements have equal weights.In this case the reconstructed values should be very close to the generated. The purpose was to check that the program works properly.

2. No multiple scattering in the simulation program,gaussian errors added in the reconstruction program. Weights used are,$w_i = 1/\sigma_i^2$,σ_i .This is the best fit we can achieve. If the multiple scattering is mimimal, and

we have the right covariance matrix, we can get close to this.

3. Multiple scattering in simulation,gaussian errors added in the reconstruction program.The weights used are the same as those in 2.

4. Multiple scattering, and gaussian errors as above, but with an improved fit, taking the multiple scattering into account, by a diagonal error matrix.

The Chisquared Distribution

If the measurement errors follows a gaussian distribution,then the minimum value of X^2 is called chisquared,χ^2, and follows a theoretical chisquare distribution. The mean value of χ^2 should be $\nu = m - n$, where ν is the number of degrees of freedom, m is the number of measurements, and n is the number of parameters.

Figure 4.9 shows the distribution of X^2/ν. The distribution for only gaussian errors added follows closely the theoretical χ^2 curve.From table 4.5 we see that with no scattering or measurement errors we get,as we should expect, an average of about zero,for condition 2 we get $\overline{X^2/\nu} \approx 1$,as expected from the theory.With scattering (conditions 3 and 4) the value is higher than 1 when scattering errors haven't been included in the weights, and lower than 1 with the diagonal error matrix in 4.This is because there is actually a strong correlation between the errors, which has not been taken into account. (See section 4.6).

Reconstructed Parameters

In figure 4.11 ,the reconstructed directions dx/dz and dy/dz we got from using the LSM are compared to the generated Monte Carlo values.In figure 4.10 and figure 4.12 the same is done for the reconstructed momenta and vertex.The average values for the absolute value of$[P_{gen} - P_{rec}]_{abs}$ are shown in table 4.5.

Results from the helix fit, HELREC

In the first phase of JETSET, it will be run without a magnet, but at a later phase, this will probably be added. We have done similar tests as described

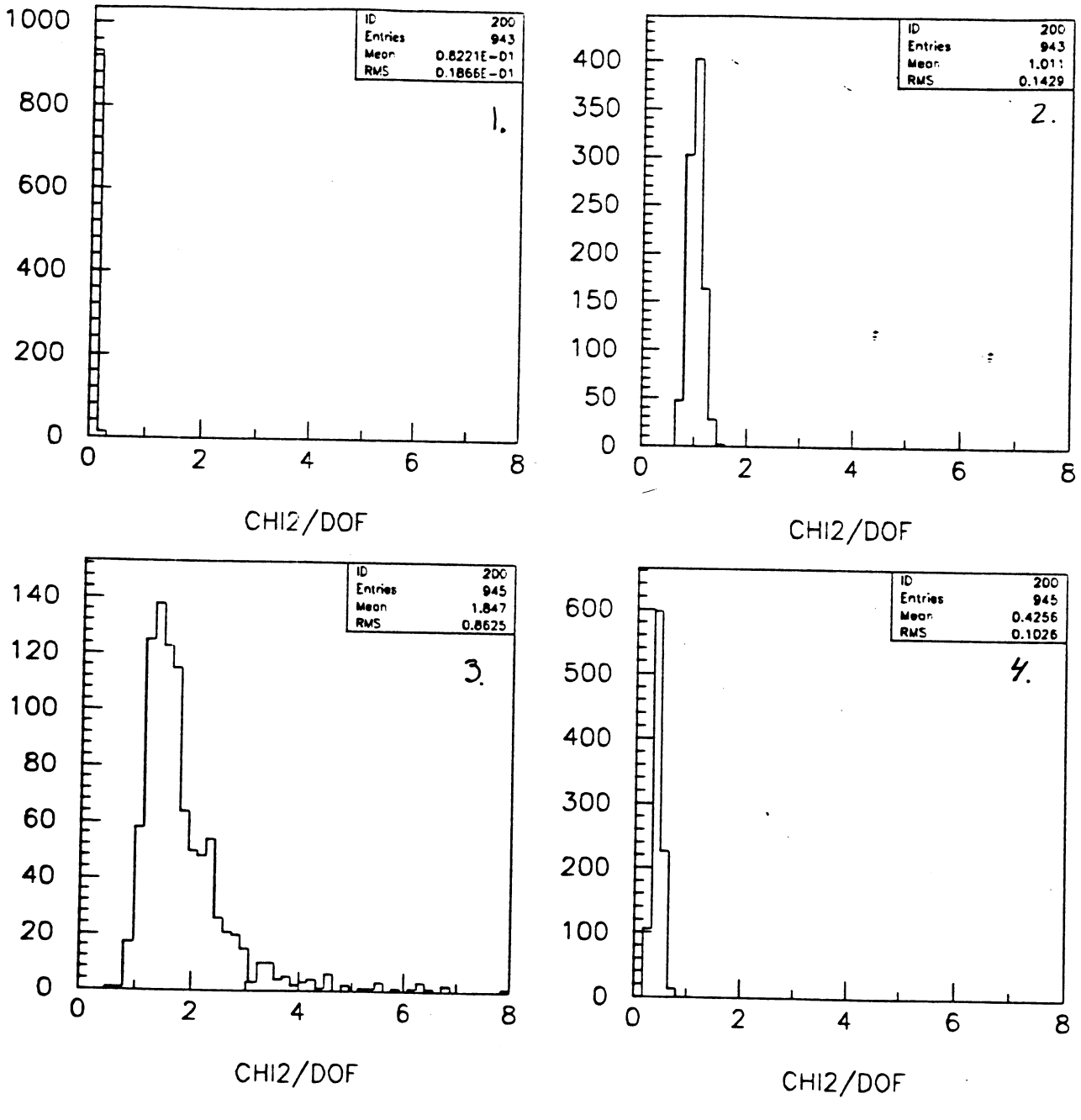

Figure 4.9: Chisquared distributions

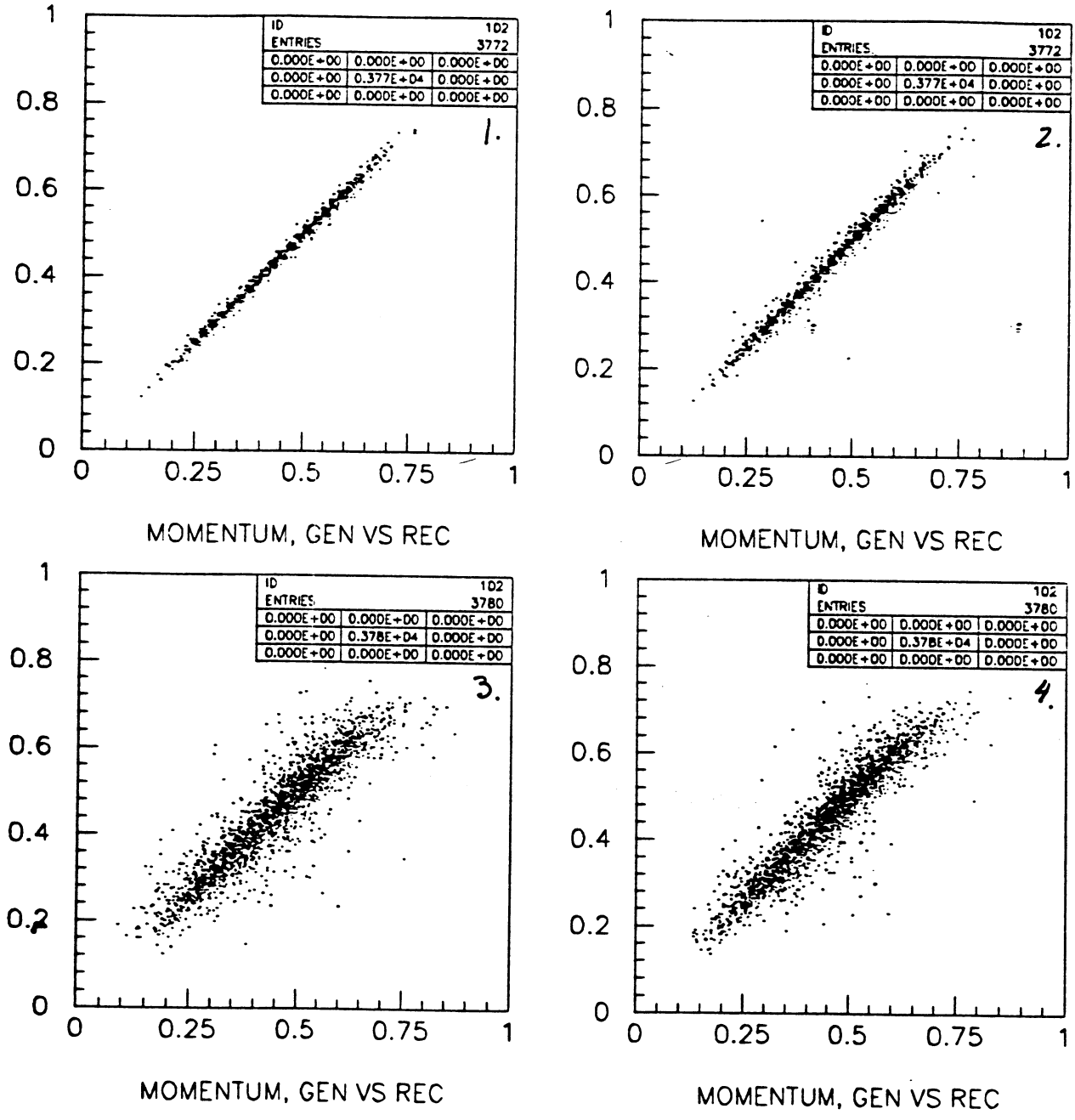

Figure 4.10: Momenta reconstructed/generated

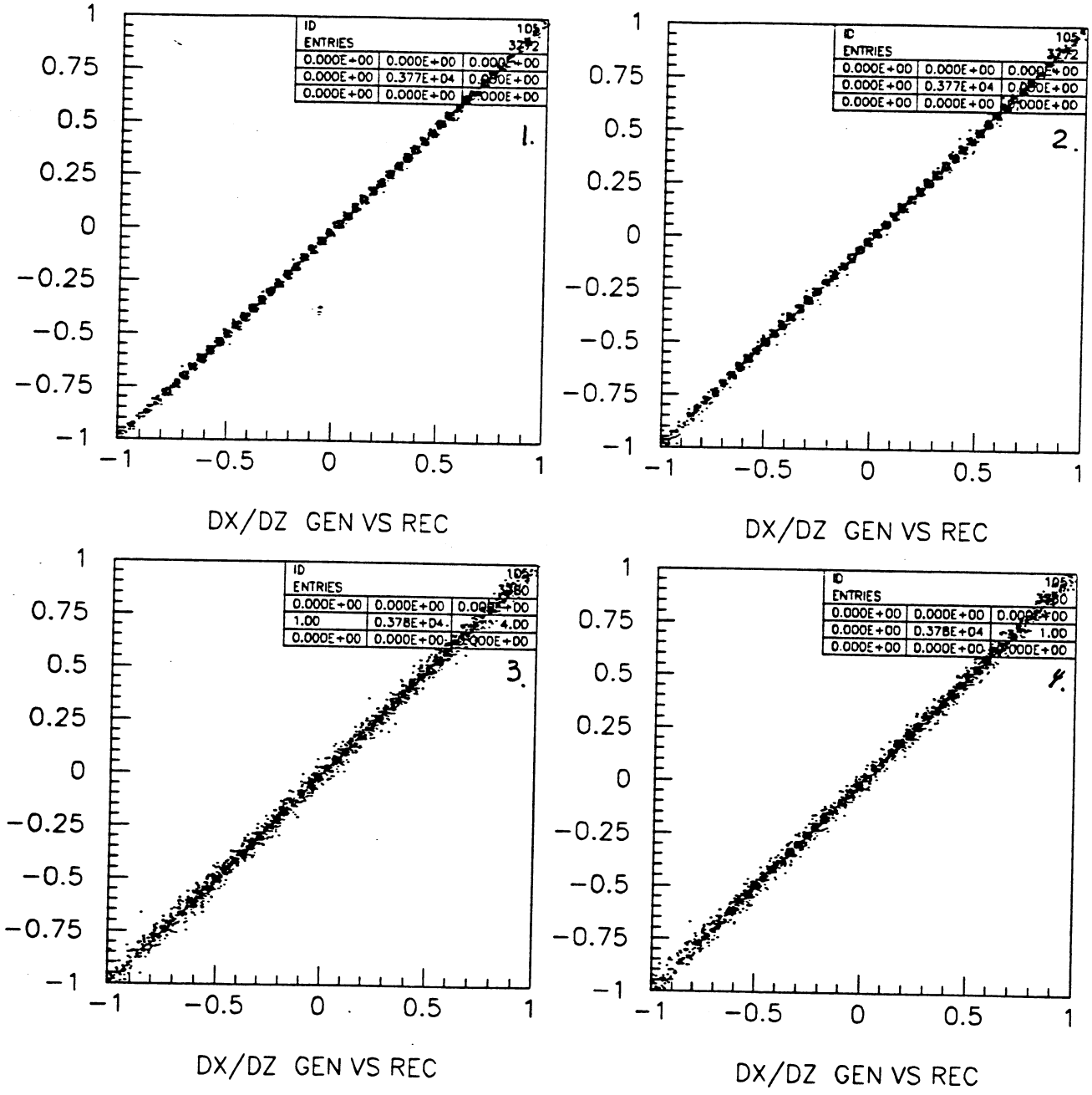

Figure 4.11: Directions reconstructed/generated

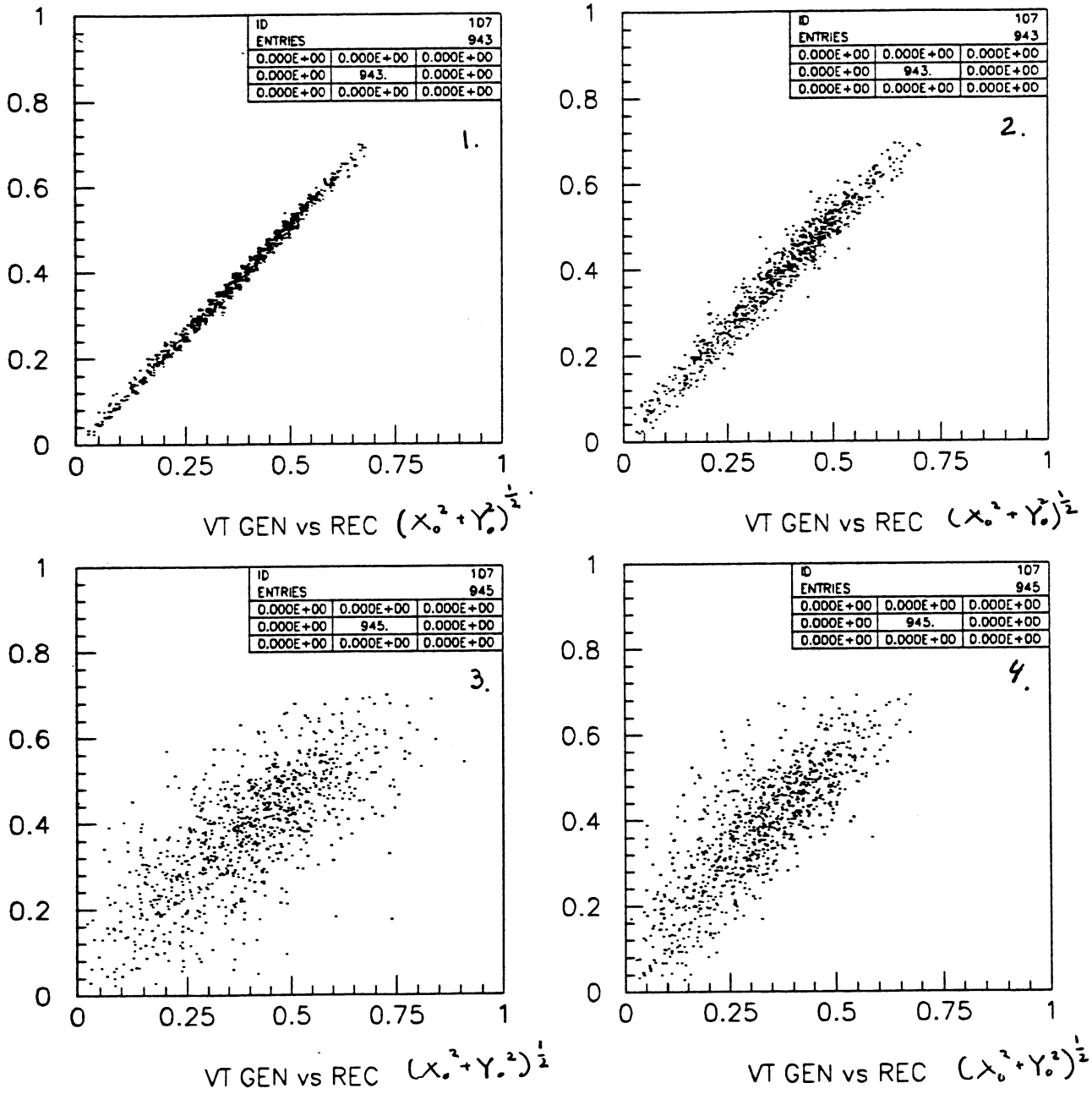

Figure 4.12: Vertex reconstructed/generated

Test	1	2	3	4
$(P_{gen} - P_{rec})(GeV)$	$0.62 \cdot 10^{-2}$	$0.78 \cdot 10^{-2}$	$2.9 \cdot 10^{-2}$	$2.5 \cdot 10^{-2}$
X^2/ν	0.08	1.01	1.85	0.43
$M(GeV)$	1.02	1.02	1.02	1.02
FWHM(dist) (GeV)	$0.8 \cdot 10^{-3}$	$0.8 \cdot 10^{-3}$	$5.2 \cdot 10^{-3}$	$5.6 \cdot 10^{-3}$
RMS(dist) (GeV)	$0.9 \cdot 10^{-3}$	$0.22 \cdot 10^{-2}$	$0.85 \cdot 10^{-2}$	$0.74 \cdot 10^{-2}$
$\mu(gaussfit)$ (GeV)	1.02	1.02	1.02	1.02
$\sigma(gauss)$ (GeV)	$0.71 \cdot 10^{-3}$	$0.97 \cdot 10^{-3}$	$0.49 \cdot 10^{-2}$	$0.44 \cdot 10^{-2}$

Table 4.5: Results from RETNREC

above, for the first three conditions for the track reconstruction in a magnetic field, but have so far not tried to calculate the multiple scattering errors.In the simulation, a magnetic field strength of 1.5 T is used.The results are shown in table 4.6. We see that the difference between reconstructed, and generated momenta is larger than was the case for the fit with only directions.The χ^2 is also larger than the theoretical value, this is due to some problems with deciding the proper weights for the virtual Z-planes.In the case of a magnetic field, we have two constraints on the momentum, both from curvature, and from conservation of four momentum.We hope that with a proper kinematical fit, it will be possible to do a better reconstruction. Another important point is that in this case, we don't have to make any assumptions of the particle mass, as we must do if we want to find the momenta from only the particles directions.

4.6 Multiple Scattering

The multiple scattering through the detector material will give a contribution to the error $\epsilon = \epsilon_{meas} + \epsilon_{msc}$.This means that we must use a different covariance matrix in the reconstruction,$\Sigma = \Sigma_{meas} + \Sigma_{msc}$.When a particle enters a straw it has already passed through the beam pipe, inner scintillators ,the endcap and other straws.Table 4.6 shows how much these detector elements will contribute to the scattering in terms of radiation lengths.

Since we have only a small amount of multiple scattering in each straw

Test	1	2	3
$\overline{(P_{gen} - P_{rec})}$ (GeV)	$0.6 \cdot 10^{-2}$	$1.7 \cdot 10^{-2}$	$4.8 \cdot 10^{-2}$
$\overline{X^2/\nu}$	0.04	1.4	1.94
$\overline{M}$ (GeV)	1.02	1.02	1.02
FWHM(dist) (GeV)	$0.4 \cdot 10^{-3}$	$2.4 \cdot 10^{-3}$	$5.6 \cdot 10^{-3}$
RMS(dist) (GeV)	$0.6 \cdot 10^{-3}$	$0.6 \cdot 10^{-2}$	$1.1 \cdot 10^{-2}$
$\mu(gaussfit)$ (GeV)	1.02	1.02	1.02
$\sigma(gauss)$ (GeV)	$0.6 \cdot 10^{-3}$	$0.2 \cdot 10^{-2}$	$0.78 \cdot 10^{-2}$

Table 4.6: Results from HELREC

Element	Material	Thickness,x	Radiation length,x_0	$\frac{x}{x_0}$
Beam pipe	Steel	0.015 cm	1.760 cm	0.0085
Scintillator	Plastic	0.2 cm	47.8 cm	0.0042
Straw walls	Aluminium	0.003 cm	8.9 cm	0.00034
Endcap	Aluminium	0.4 cm	8.9 cm	0.045

Table 4.7: Contributions to multiple scattering

we will not use this in the covariance matrix,but only calculate the scattering when the particle passes the beam pipe and the endcap.

4.6.1 Scattering Theory

Neglecting large angle scattering,multiple scattering can be described with a gaussian with mean $\overline{\theta} = 0$,and standard deviation

$$\Delta\theta = (\overline{\theta^2})^{1/2} = \frac{zE_s}{p\beta c}\sqrt{\frac{\Delta X}{X_0}} \tag{4.63}$$

where

p = momentum
β = speed v/c = p/E
z = charge of the particle
E_s = 21 MeV
$\frac{\Delta X}{X_0}$ = length of material passed /radiation length

The scattering angle projected onto a perpendicular plane containing the incident trajectory is

$$\Delta\theta_{proj} = \frac{\Delta\theta}{\sqrt{2}} \tag{4.64}$$

4.6.2 The Scattering Covariance Matrix

Estimates of Errors

We call the beampipe/scintillator scatterer number 1,and the endcap scatterer number 2.From figure 4.14 we see that at position z the deviation in x from scatterer no.i will be

$$\epsilon_{msc,x} = \frac{\theta_{i,x}(z - z_i)}{\cos^2\theta}$$

compared to the non scattered impact point,where

z_i = position where the particle crosses the scatterer
θ = polar angle for the particles momentum
θ_i = scattering angle,

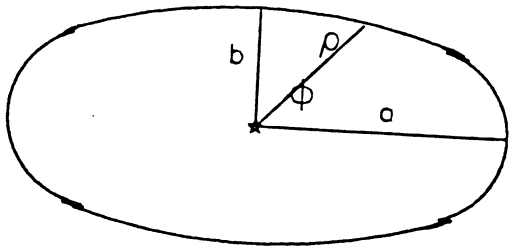

Figure 4.13: $\rho(\phi)$ for ellipse

The expression for the deviation in y will of course be identical.The errors in x and y will be independent, but with the same mean value and standard deviation. To find z_1 we have to calculate the position where the particle crosses the elliptic beam pipe.The following equation holds for an ellipse with centre at the origin

$$\rho = \frac{b}{\sqrt{1 - \epsilon^2 \cos^2 \phi}}$$

where

$\epsilon = e/a$
a, b = large and small half axis ,and e the eccentricity
ϕ = azimuthal angle for the momentum.

(See figure 4.13.) We finally get

$$z_1 = \frac{\rho}{\tan \theta}$$

Z_2 is only the position of the endcap.
The mean scattering angle will be $\theta_{msc} = \frac{14Mev}{p\beta}\sqrt{(x/x_0)_i}$
$(x/x_0)_1 = 0.0127/\sin\theta$, $(x/x_0)_2$=$0.045/\cos\theta$ (see fig 4.14).

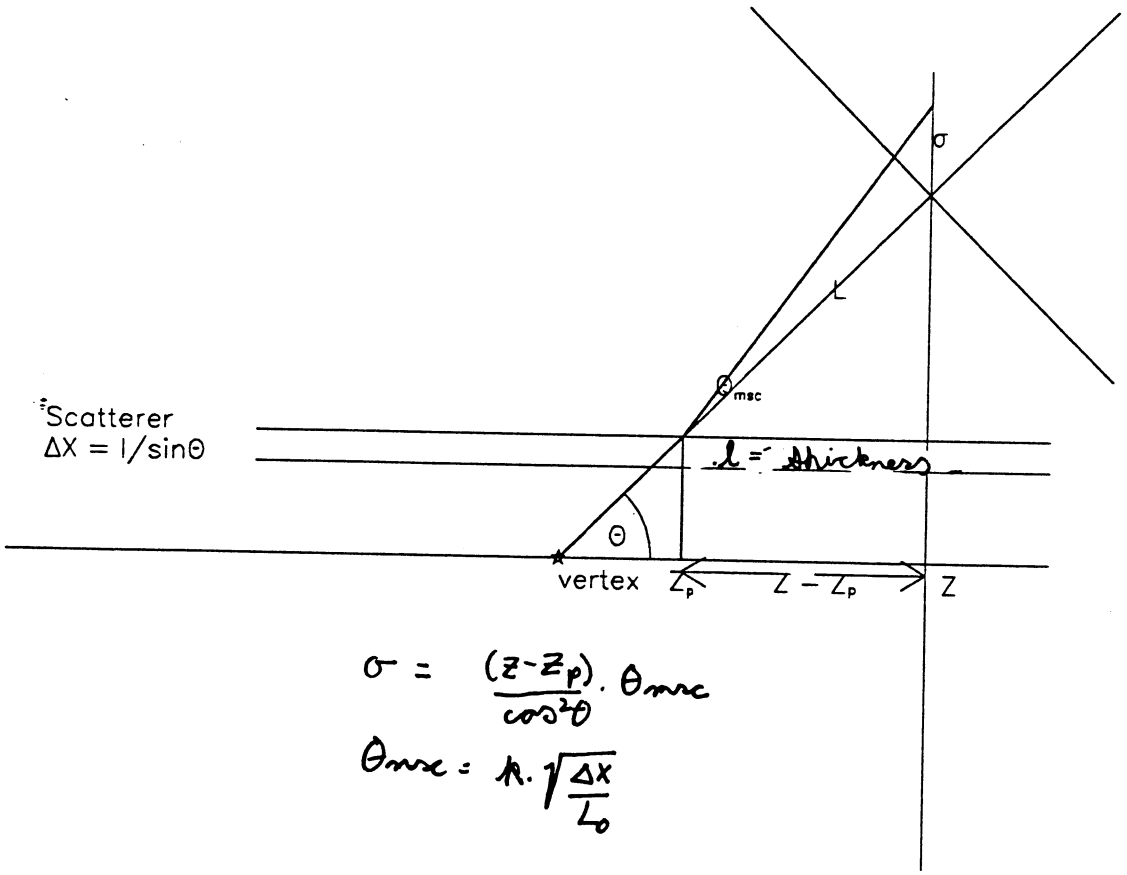

Figure 4.14: Error from multiple scattering

Covariance

The covariance of the two measured coordinate x_k and x_l is

$$cov(x_k, x_l) = \sum_{i(k,l<i)} \frac{(z_l - z_i)(z_k - z_i)\theta^2_{msc,i}}{(\cos\theta)^4} \tag{4.65}$$

For two coordinates x_l,and y_k perpendicular two each other the covariance is zero,since we assume that the two projected angles are independent.In general,for tilted planes with measured $u_i = x_i \cos\alpha_i + y_i \sin\alpha_i$,or the perpendicular $v_i = -x_i \sin\alpha_i + y_i \cos\alpha_i$

$$cov(u_k, u_l) = \sum_{i(k,l<i)} \frac{(z_l - z_i)(z_k - z_i)\theta^2_{msc,i}(\cos\alpha_k \cdot \cos\alpha_l + \sin\alpha_k \sin\alpha_l)}{(\cos\theta)^4}$$

$$cov(u_k, v_l) = \sum_{i(k,l<i)} \frac{(z_l - z_i)(z_k - z_i)\theta^2_{msc,i}(-\cos\alpha_k \cdot \sin\alpha_l + \sin\alpha_k \cos\alpha_l)}{(\cos\theta)^4}$$

$$cov(v_k, v_l) = \sum_{i(k,l<i)} \frac{(z_l - z_i)(z_k - z_i)\theta^2_{msc,i}(\cos\alpha_k \cdot \cos\alpha_l + \sin\alpha_k \sin\alpha_l)}{(\cos\theta)^4}$$

To take the multiple scatterig errors into account we must use a different covariance matrix. If we want to use a nondiagonal covariance matrix, we must use a different procedure from that described on page 4.3.1.This will take longer computer time since the matrix $\Sigma = \Sigma_{msc} + \Sigma_{meas}$ must be calculated and inverted for each event,as well as the matrix **A**,of derivatives and **Res**,the vector of residuals. Instead of doing this, we have used the same procedure as before (section 4.3.1), and only use the diagonal elements of the covariance matrix to calculate the new weights.The results of this improved fit are shown in the last column of table 4.5,and in the figures 4.9 to 4.12.

4.7 Mass Reconstruction

We want to reconstruct the mass of the ϕ particles, and see what resolution we obtain for the reconstructed mass. The mass of the ϕ is

$$M_\phi = \sqrt{E^2_{phi} - P^2_{phi}} \tag{4.66}$$

If we have the reaction $\phi_1 \rightarrow K_1K_2, \phi_2 \rightarrow K_3K_3$, then the energy and momenta of the first ϕ-particle,is given by

$$E_{phi} = E_{K_1} + E_{K_2}$$

$$P_{phi} = \sqrt{\sum_{i=1}^{3}(P^i_{K_1} + P^i_{K_2})^2}$$

When we try to reconstruct the masses of the ϕ's from the energy and momenta of the kaons we will get one right combination,with $M_1 = M_2 = M_\phi = 1.02GeV$, for a true $\phi\phi$ event, with a small error depending on how good the momentum reconstruction works. Depending on whether the charge is known we will get one or two wrong combinations,which will give a combinatorial background.

Fig 4.15 shows the distribution of the reconstructed mass,with only the right combination.For the same conditions as in section4.5.1 We have tried to fit the distribution to a gaussian curve

$$f(x) = \frac{1}{\sigma\sqrt{2\pi}} \exp[-\frac{(x-\mu)^2}{2\sigma^2}] \tag{4.67}$$

where

$\sigma^2$is the variance
μ is the mean value of the mass.

Table 4.5 lists both the average value, full width-half maximum and r.m.s. for the distribution,and μ and σ for the gaussian. We see that the distribution is not exactly gaussian.From the figure we see that we have a narrow peak, and many events with a large deviation from the mean value. I don't know if we should expect a perfectly gaussian distribution, but deviations could be caused by problems with the mass reconstruction, that we some times might have chosen a wrong solution . Note that in the generation of this reaction the width of the $\phi(\Gamma = 4.2MeV)$ is neglected.

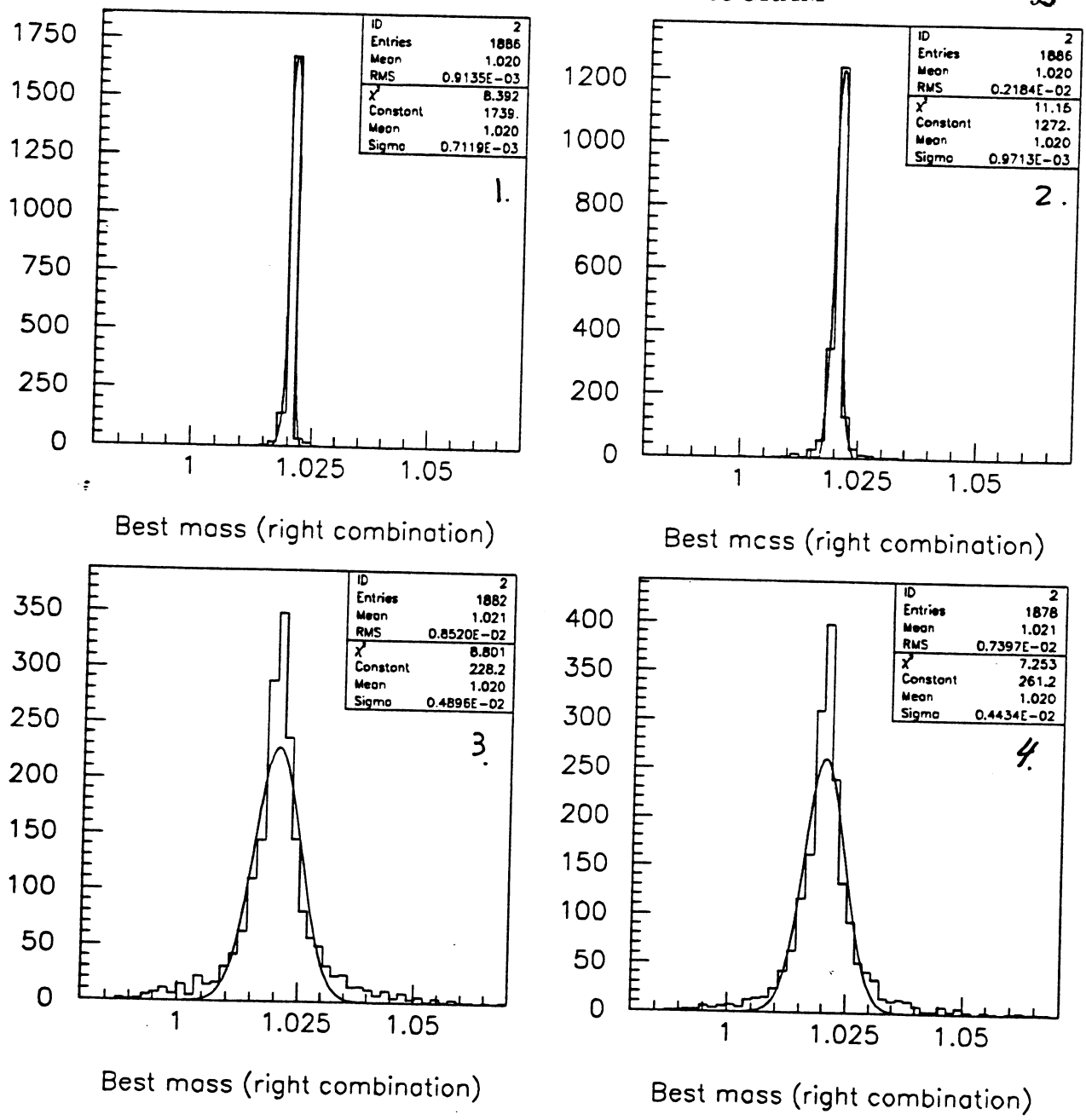

Figure 4.15: Reconstructed mass,right combination

Chapter 5

Monte Carlo Results

We will here present some results from applying the data analysis (track fitting , momentum and invariant mass reconstruction) on data obtained with the most recent Monte Carlo simulation of the detector (see [19]). Track fitting has been done with the straw measurements as described in chapter 4 , both with and without a magnetic field. We have also studied the background rejection from trigger and mass cuts.

5.1 Non Magnetic Detector

We have reconstructed tracks with polar angle $\theta\epsilon[15, 45]$, and required at least four hits for each track. In this case the track fit gives only the directions of the particles. When we try to reconstruct the momenta from the directions we will often find two solutions that agrees with the track fit, and gives momentum and energy conservation.To select the correct solution we must use the silicon dE/dx detectors. We have in this chapter assumed them to be "perfect",we always chose the right solution. The effect on the reconstruction from these detectors is discussed in [10], (appendix).

Figure 5.1 shows the mass resolution (rms. for the distribution, and sigma for the gaussian curve fitted to it),with two different values for the thickness of the straw walls,as a function of beam momentum. We have also investigated how the mass resolution depends on the detector resolution.The results are show in table 5.1, for three different values of σ_{res},at fixed beam momentum of 1.5 GeV.

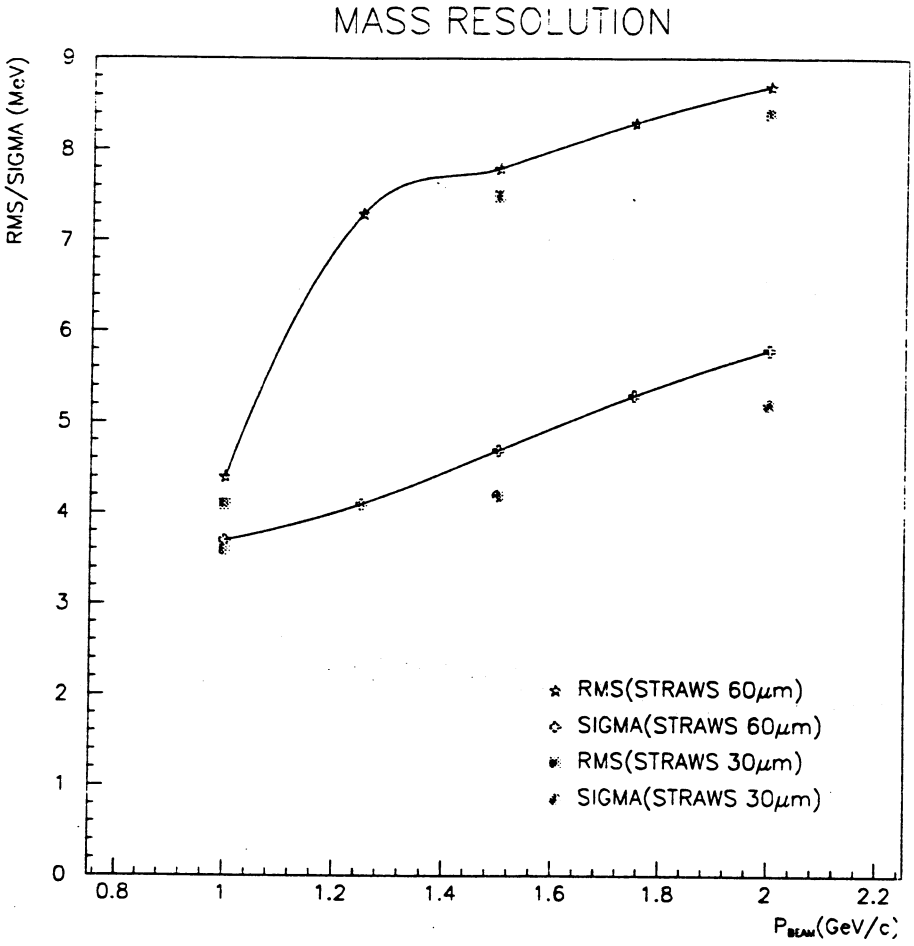

Figure 5.1: Mass resolution as a function of the momentum

$\sigma_t, \sigma_l(cm)$	0.02 ,0.2	0.04,0.2	0.02,0.4
RMS(MeV)	7.6	7.7	8.0
SIGMA(Mev)	4.5	4.6	4.8

Table 5.1: Mass resolution, different detector resolutions.

We see that the main contribution to the error in the reconstruction comes from multiple scattering in the beam pipe and inner detectors.

5.2 Trigger and Acceptance Studies

We have studied various reactions with four charged particles,and applied some of the trigger conditions discussed in section 2.4. After generation of an event in EVGEN,the subroutine ANALYS is called. Here the following cuts are applied

- Acceptance:Events with particles which have a polar angle less than 8 degrees are rejected.These particles will go inside the beam pipe and not be detected.
- Trigger1:Not more than one particle with $\theta > 45^{\circ}$ (in barrel).
- Trigger2:Not more than one particle with $\beta > 0.8$, the cerenkov limit.We have assumed an efficiency of 0.95 for the cerenkov detector.
- Trigger3:The sum of the polar angles.$100 < \theta < 160$.
- Masscuts

The values of β and θ are calculated directly from the FOWL output.This will give us an idea of the ratio between the signal and background events .

Background

We have assumed cross sections for $\phi\phi$ and the most important backgound reactions as listed in table 5.3. Table 5.2 shows the number of events left after the various cuts. In each case 10 000 events are generated. In figures 5.2 ,5.3 and 5.4 we can see the distribution of polar angle, (for the accepted events), beta (for events passed trigger1) ,and sumtheta (for events passed trigger2). The events with 4π and $2\pi 2K$ all have a lot of particles with high θ,so a lot of them will be rejected by the first trigger condition. These events also have high β,'s so this gives an even better rejection and almost all the 4π events are rejected. However,the 4K and $2\pi p\overline{p}$ look very similar to $\phi\phi \rightarrow 4K$,so the rejection efficiency will not be too good. Most of the $\pi\pi KK$ events and about half of the remaining $2\pi p\overline{p}$ will be rejected by the $\sum\theta$ condition.

reaction $P_{beam} = 1.0GeV/c$	$\phi\phi$	$4K$	4π	$\pi\pi KK$	$p\bar{p}\pi\pi$
$\theta > 15$	3206	3492	8278	7732	
$\leq 1, \theta > 45$	3204	3491	251	553	
$\leq 1, \beta > 0.8$	3204	3491	1	76	
$100 \leq \sum\theta \leq 160$	3131	3378	0	0	

reaction $P_{beam} = 1.5GeV/c$	$\phi\phi$	$4K$	4π	$\pi\pi KK$	$p\bar{p}\pi\pi$
$\theta > 15$	5528	4199	7702	7004	899
$\leq 1, \theta > 45$	5303	4089	556	1151	888
$\leq 1, \beta > 0.8$	5305	4088	1	46	884
$100 \leq \sum\theta \leq 160$	5305	4064	0	1	494

reaction $P_{beam} = 2.0GeV/c$	$\phi\phi$	$4K$	4π	$\pi\pi KK$	$p\bar{p}\pi\pi$
$\theta > 15$	6108	4116	7113	6343	2162
$\leq 1, \theta > 45$	5822	4007	979	1920	1991
$\leq 1, \beta > 0.8$	3497	2300	0	47	1454
$100 \leq \sum\theta \leq 160$	3497	2291	0	8	1166

Table 5.2: Number of events after cuts

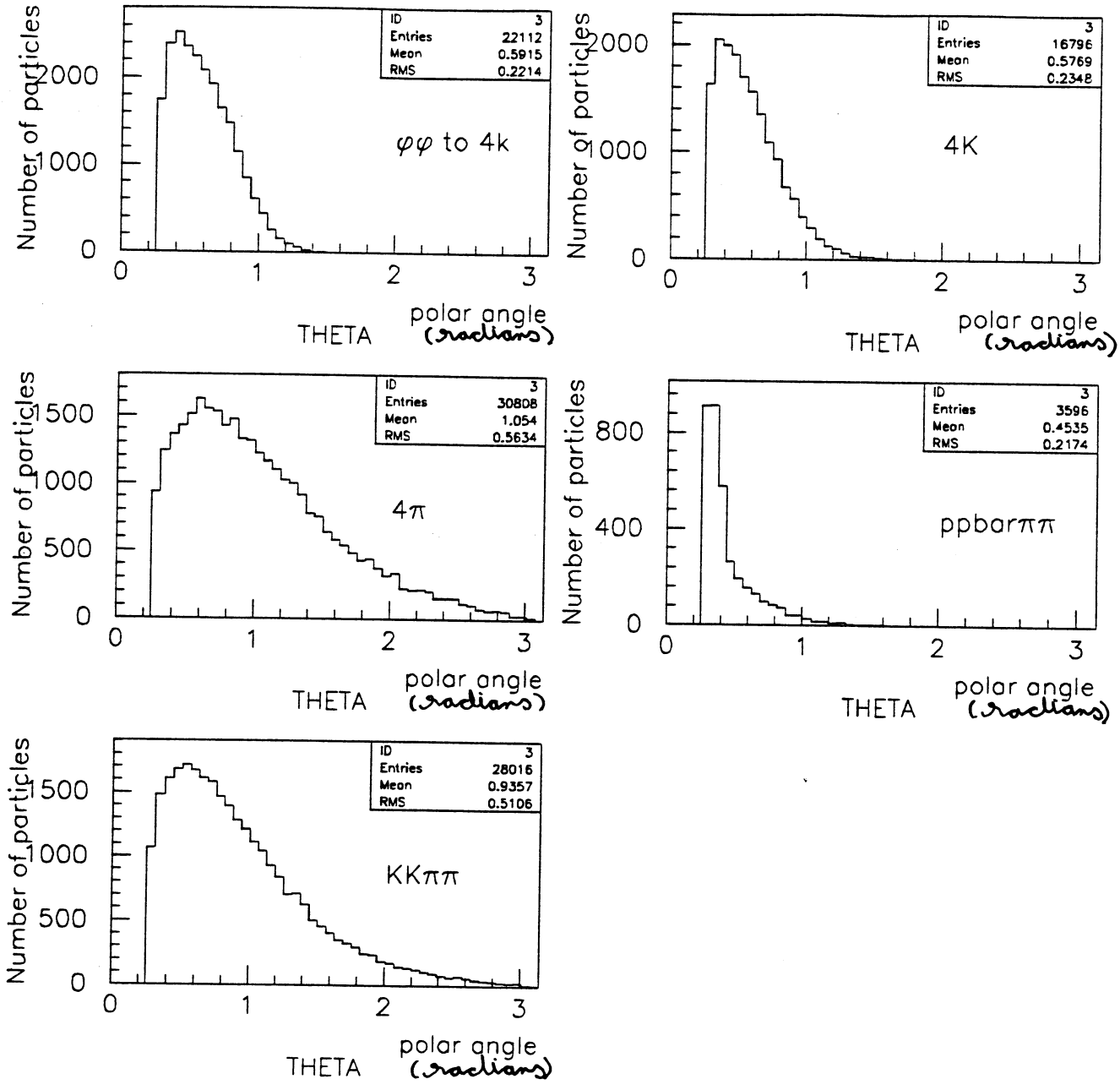

Figure 5.2: Theta distibutions

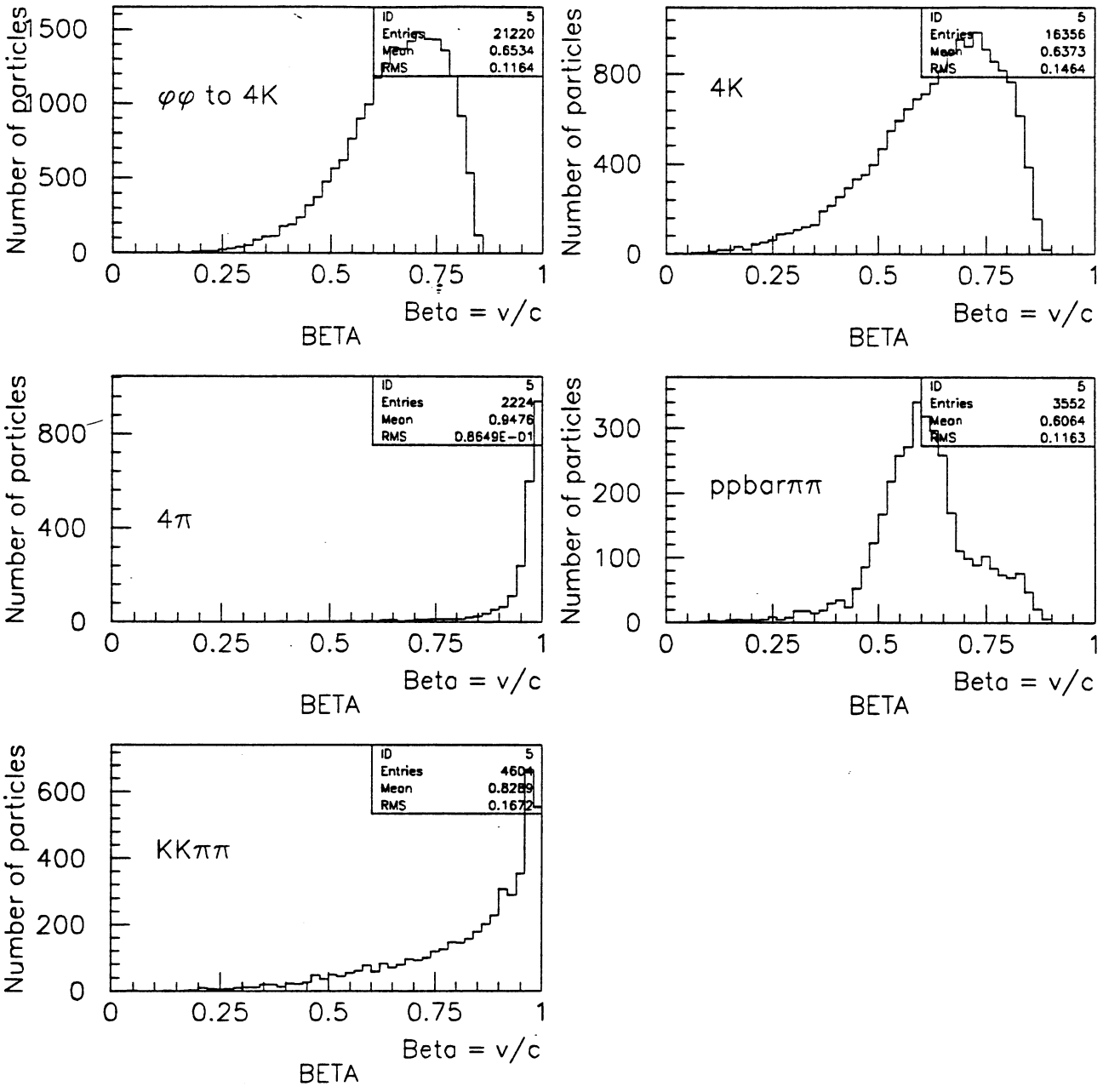

Figure 5.3: Beta distibutions

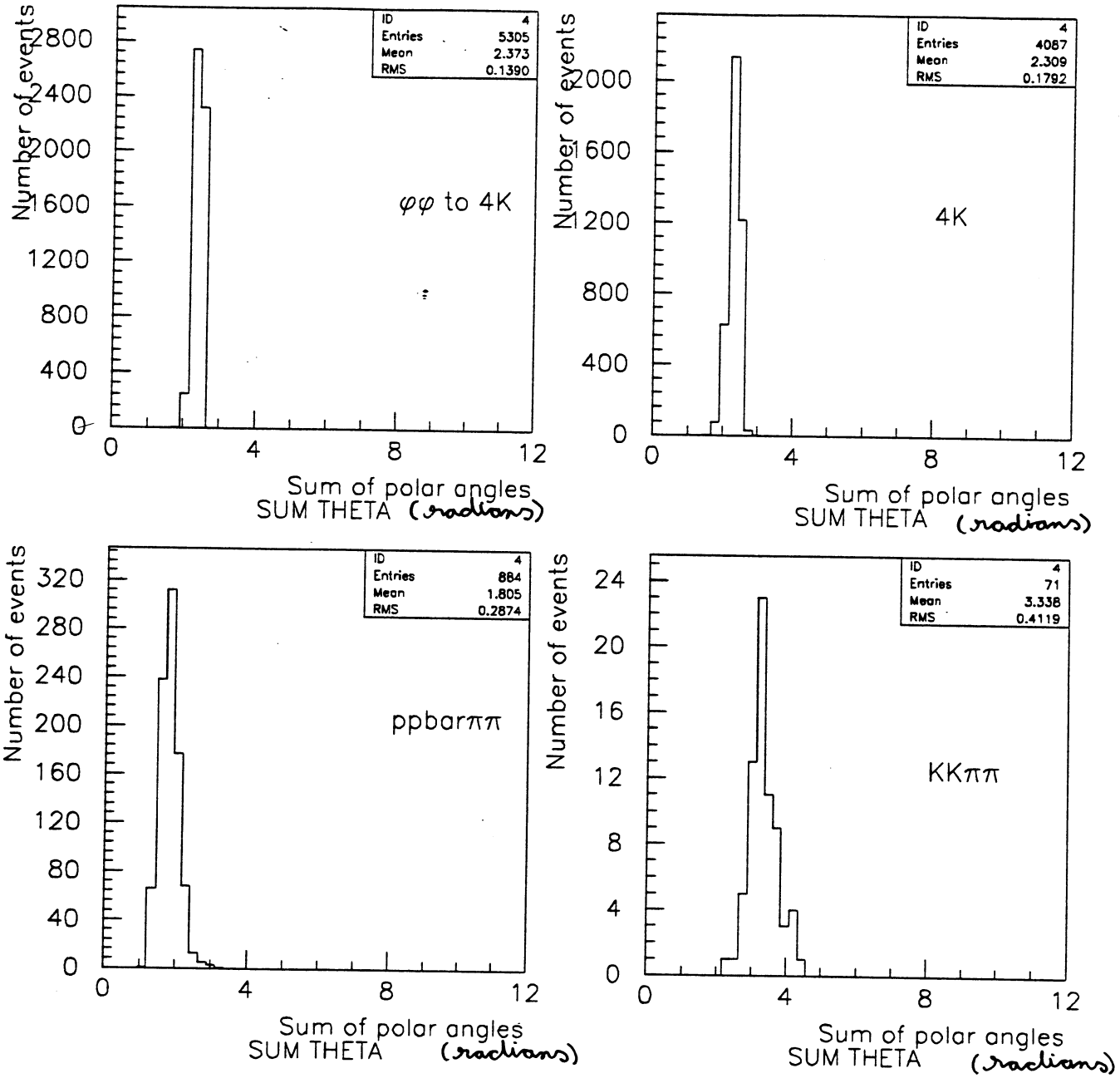

Figure 5.4: $\sum\theta$ distributions

$P_{\overline{P}}$	1.0 Gev/c	1.5 GeV/c	2.0 Gev/c
$\phi\phi$	0.1 μb	0.25 μb	0.5 μb
4K	1.0 μb	3.0 μb	4.0 μb
4π	3600 μb	2300 μb	1700 μb
$p\overline{p}\pi\pi$	-	5.0 μb	380 μb
$\pi\pi K^- K^+$ μb	410 μb	390 μb	380 μb

Table 5.3: Cross sections for $\phi\phi$ and background events (σ for 4K and $\phi\phi$ are assumptions)

5.3 Signal to Background Ratios

We have seen in table 5.2 that a large amount of $4K$ and some $p\overline{p}\pi\pi$ events will be accepted by the trigger. To separate 4K events from $p\overline{p}\pi\pi$ we can use the dE/dx detectors (see [10]).This will be useful for a measurement of the 4K cross section. If we want to get rid of the direct channel 4K as well, we must apply some mass cuts.If two particles come from a ϕ particle then their invariant mass will be $M_\phi \pm \sigma$,where σ is the width of the ϕ. The reconstructed mass will have a distribution as discussed in section 5.1. For each event we combine pairs of tracks, and calculate their invariant mass, assuming that the tracks are from kaons.Three possible combinations can be made for each event, and the figure 5.5 shows the results with the two masses plotted against each other . For the background reactions we have used the generated directions, and then assumed a mass equal to M_K in the momenta from directions fit (also for pions and protons). For $\phi\phi$ events we have done the same, but using the reconstructed directions and momenta. In figure 5.6 we see the $\phi\phi$ peak against a background of 4K reactions. Then we have applied the following condition for each event: $(M - M_{phi}) <$ (masscut) for both pairs in one of the combinations .
Table 5.4 shows the number of events left after applying first trigger cuts and then various mass cuts,for 10^4 events. Since the number of produced events is proportional to the cross section σ_k, the ratio of the accepted $\phi\phi$ events to

$P_{beam}(GeV)$	1.0	1.5	2.0
$4K, \Delta m = 4MeV$	148	12	2
$4K, \Delta m = 6MeV$	316	29	4
$4K, \Delta m = 16MeV$	753	255	43
$2\pi p\overline{p}, \Delta m = 4MeV$	0	0	0
$2\pi p\overline{p}, \Delta m = 6MeV$	0	0	0
$2\pi p\overline{p}, \Delta m = 16MeV$	0	0	0
$\phi\phi, \Delta m = 4MeV$	1330	1982	1211
$\phi\phi, \Delta m = 6MeV$	1781	2708	1617
$\phi\phi, \Delta m = 16MeV$	2207	4182	2734

Table 5.4: Number of events after mass cuts (of 10 000)

$P_{beam}(GeV)$	1.0	1.5	2.0
$\Delta m = 4MeV$	0.9	13.8	75.8
$\Delta m = 6MeV$	0.6	7.8	51.0
$\Delta m = 16MeV$	0.13	1.4	7.9

Table 5.5: Signal to background ratios

background events is

$$S/B = \frac{\sigma_{\phi\phi} \cdot N_{acc}(\phi\phi)}{\sum_{background} \sigma_{background} \cdot N_{acc}(background)} \tag{5.1}$$

Table 5.5 shows the results obtained.

5.4 Magnetic Field Studies

In a later phase of JETSET,the detector will also have a magnetic field. We have studied the reconstuction also in this case,and compared a non magnetic field, with different values of the magnetic field. Magnetic fields make it easy to filter out background particles, like pions and protons, because when we know both, the momentum and beta (from the dE/dx counters) we can

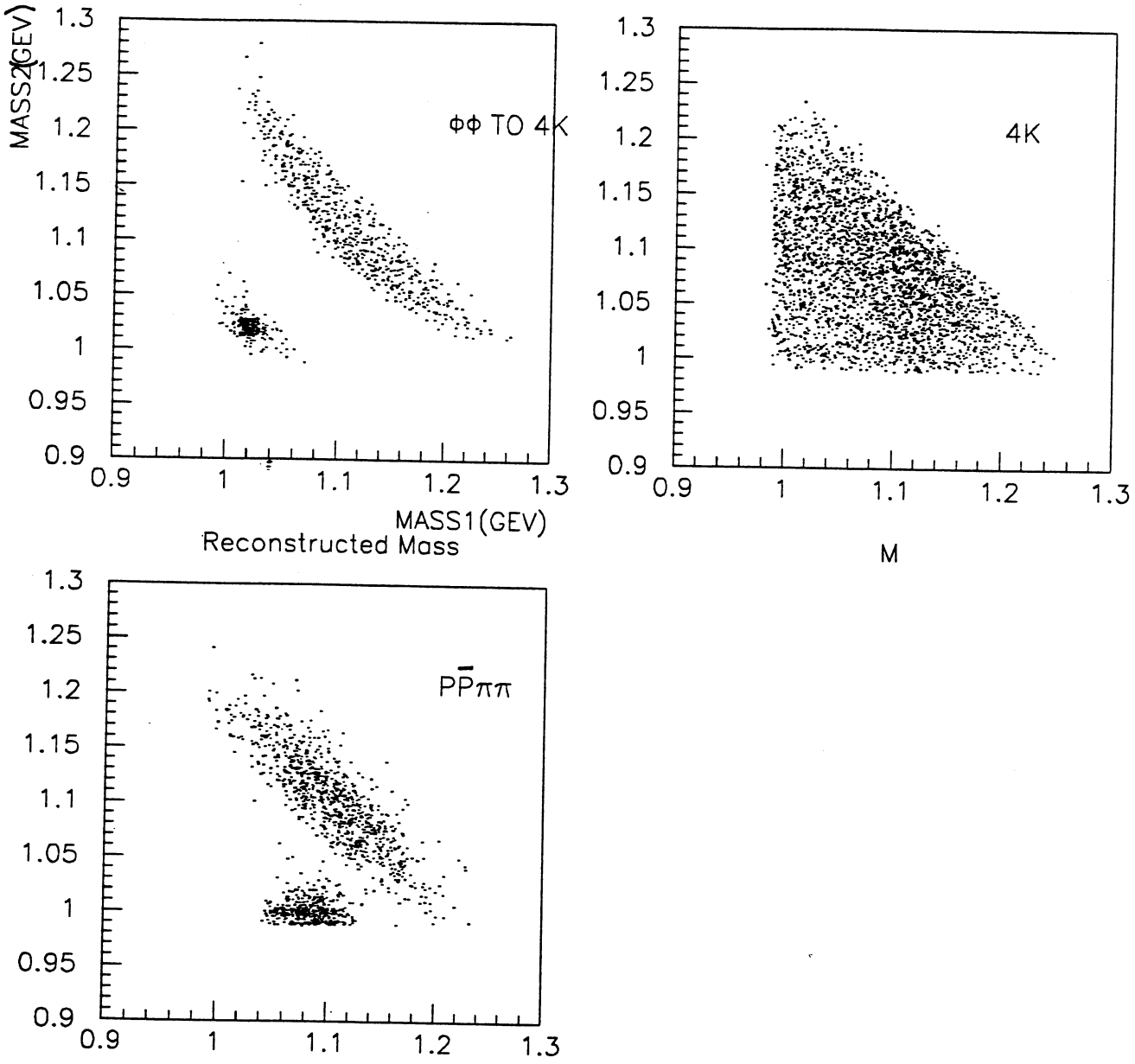

Figure 5.5: Reconstructed mass $\phi\phi$ and background

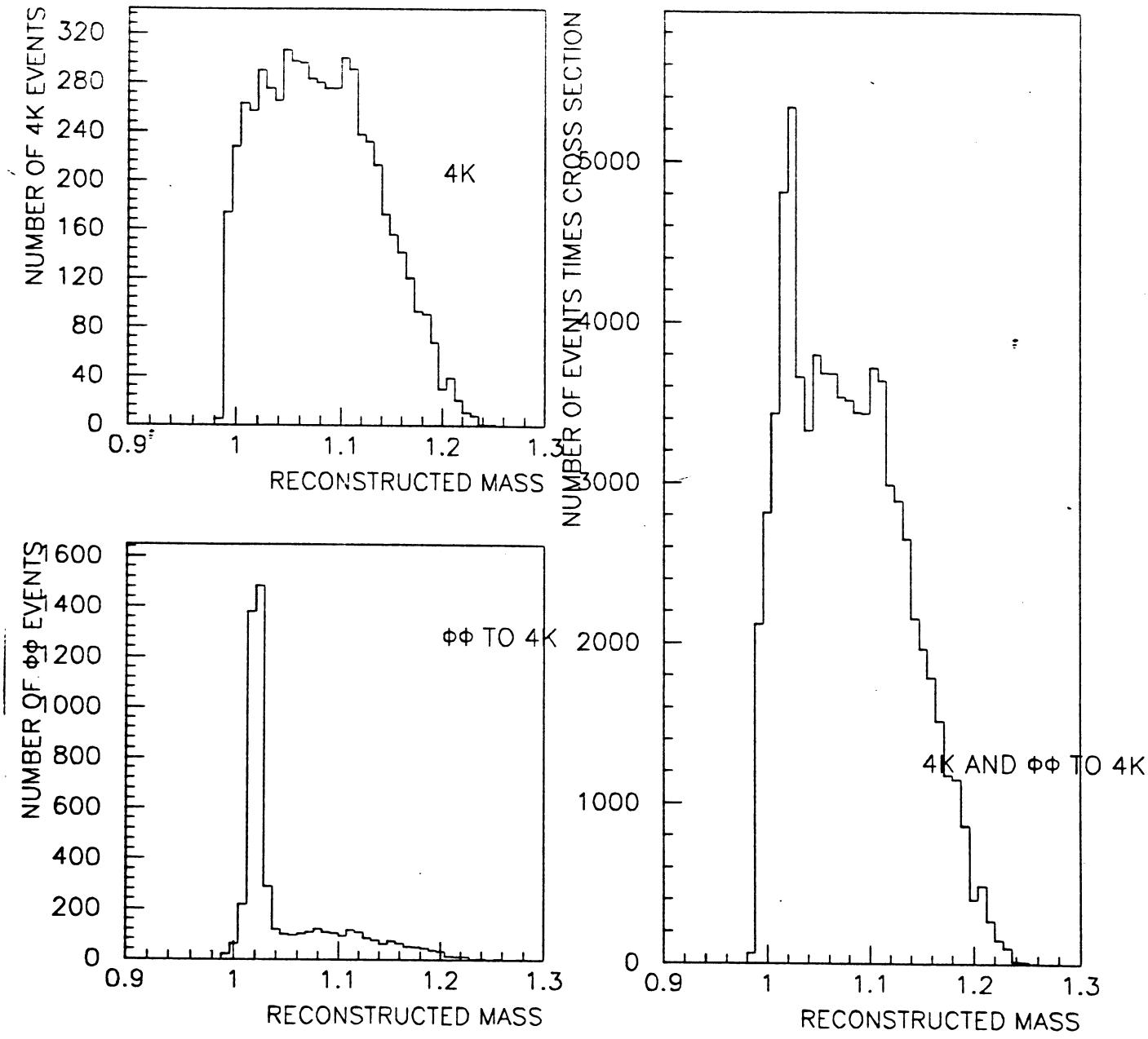

Figure 5.6: $\phi\phi$ and 4K mass distributions.

Field strength	0.5 T	1.5 T	4.0 T
RMS (MeV)	11.5	12.6	11.5
Sigma (Mev)	8.3	9.6	8.3

Table 5.6: Mass reconstruction in magnetic field

calculate the mass. Light particles like δ-rays will have very small radius of curvature, and will therefore make less of a problem in pattern recognition. Table 5.6 shows the mass resolution with beam momentum 1.5 GeV without a magnetic field,and with some different values for the magnetic field. Since the errors are smaller for 0.5 T, than for 1.5 T, this indicates that a measurement of the directions is more important than momentum measurements in the mass reconstruction.

5.5 Conclusion

The data analysis programs developed so far seems to give an acceptable method both to get rid of all backgound events to the two possible 4K reactions, and to filter out the reaction $p\overline{p} \rightarrow \phi\phi \rightarrow 4K$ both with and without a magnetic field. The main background channel will be the direct reaction $p\overline{p} \rightarrow 4K$. The reconstruction of the ϕ mass will have an error of about

$$\frac{RMS_\phi}{M_\phi} = 0.01$$

,which will enable us to apply mass cuts. Among the remaining problems are to improve the reconstruction for curved tracks, and to make a pattern recognition program . In this study we have neglected effects due to energy loss and secondary interactions. These effects turn out to be large (see thesis of E.Bergan to be finished in 1990).

Appendix A

Mass reconstruction in JETSET with straw tubes and silicon planes

Mass Reconstruction in JETSET with Straw Tubes and Silicon Planes

Helen Korsmo
University of Oslo

February 8, 1990

1 Introduction

We present the results from a simulation of the JETSET detector, and the preliminary offline data analysis program.We have studied the mass resolution for ϕ particles in the reaction $p\overline{p} \rightarrow \phi\phi \rightarrow 4K$ in a non magnetic detector with straw tubes and silicon detectors. The JETSET detector simulation program is described in [1]. With this program we tracked 1000 $\phi\phi$ events trough the detector. All the events had the four final kaons within a forward cone $\theta\epsilon[15^o, 45^o]$, and β less than 0.8. The beam momentum was varied between 1 and 2 GeV/c. All physical processes except multiple scattering were turned OFF. Then the preliminary JETSET data analysis program [2] was used to reconstruct the events.We have also studied rejection efficiencies of background events like $p\overline{p}\pi\pi$ with the silicon detectors.

2 Track and Momentum Reconstruction

The geometrical fit to straight lines coming from the same point is done with the measurements in the straw tubes.Figure 1 shows the number of hits for each track in the barrel and forward detectors, and figure 2 the number of hits vs polar angle.. At least 4 hits per track was required in order to accept the event for reconstruction. For four tracks the directions dx/dz dy/dz and vertex x_0, y_0, z_0 are fitted with a least square fit.From momentum and energy conservation we can then calculate the momenta assuming that the outgoing particles are kaons.(see [3]).We get 0,1 or 2 solutions that satisfy

$$(P_\mu)_{p\overline{p}} = (P_\mu)_{4K} \tag{1}$$

$$P_X/P_Z, P_Y/P_Z = d_X/d_Z, d_Y/d_Z \tag{2}$$

For the case that we have 2 solutions we must have a method to chose the correct solution.

Element	Material	Thickness, x	Radiation length, x_0	$\frac{x}{x_0}$
Beam pipe	Steel	0.015 cm	1.760 cm	0.0085
Scintillator	Plastic	0.2 cm	47.8 cm	0.0042
Straw walls	Aluminium	0.003 cm	8.9 cm	0.00034
Endcap	Aluminium	0.4 cm	8.9 cm	0.045

Table 1: Contributions to multiple scattering

$\sigma_t, \sigma_l(cm)$	0.02 ,0.2	0.04, 0.2	0.02, 0.4
RMS(MeV)	7.6	7.7	8.0
SIGMA(Mev)	4.5	4.6	4.8

Table 2: Mass resolution, different detector resolutions.

3 Errors in the Reconstruction

The errors on the measured coordinates will come from both measurement errors and multiple scattering.The measurement errors were assumed to be:
σ_t = 0.02 cm ,
σ_l = 0.2 cm ,
for the transverse(drift time) measurements, and longitudinal(charge division) measurements.The value for σ_l was probably to optimistic, however as shown in table 2 this does not give a very big difference in the final results. The contribution to multiple scattering in terms of radiation lengths is shown in table 1.

4 Mass Resolution

Combining the four particles in two pairs (there are three possible combinations when the charge is unknown) and plotting the invariant masses against each other, we get the result shown in figures 3 a,c. for $P_{beam} = 1.5GeV/c$ (using one or two silicon planes to choose the solution, see section 5). The mass distribution for the correct combination is shown in figures 3 b,d with a fit to a gaussian curve. The fit is not too good, it is clear that the distribution has long tails.

In studying the mass resolution we always chose the correct solution for the kinematics. Figure 4 shows the mass resolution as a function of the beam momentum, with two different values for the thickness of the straw walls. Since the main deviations on the measured track from the perfect track comes from the scattering in the beam pipe, the straw thickness will not be a very important

factor. In table 2 we have varied the detector resolution, at constant beam momentum $P_{beam} = 1.5GeV/c$.

5 The Silicon dE/dx Detectors

The silicon detectors will be essential to choose the right solution to the kinematics, and to get rid of background events. Furthermore the energy loss measurement will be important when estimating the amount of background in the event sample passing all cuts. For a given solution we can calculate the following quantity [4]:

$$X^2 = \sum_{i=1}^{ntracks} \left(\frac{(dE/dx)_{meas} - (dE/dx)_{calc}}{res \cdot (dE/dx)_{meas}}\right)^2 \quad (3)$$

Here the calculated energy loss will be given by a curve calibrated from measurements of the energy loss in the silicon at known beta . Only tracks at a polar angle less than 45 degrees are accounted for, since the dE/dx detectors will only be in this region of the setup. The simulation of the silicon detectors is described in section 5.1.

This gives a energy loss distribution as shown in figure 5, for the two cases.In the two figures at the left we can see that with two planes the long Landau tail has disappeared. The two figures at the right shows the mean energy loss as a function of β^{-2}.This can be fitted to a straight line so the calculated energy loss in equation 3 will be of the form

$$dE/dx = A\frac{1}{\beta^2} + B$$

and the measured energy loss simulated as described below. We can then choose the solution with lowest X^2, and make a cut for high X^2 values (to get rid of background). From the X^2 distributions shown in figures 6 (one silicon plane), and 7 (two planes) we see that most of the events have X^2 less than 20 for one plane, and less than 25 for two planes. In table 5 we show the number of events [out of 1000] with 0 ,1 or 2 solutions to the kinematics. In the case of two solutions, it is shown how many times the right/wrong solution is chosen (with one or two silicon planes). The number of events rejected by a X^2 cut ($X^2 < 20$ with 1 plane , $X^2 < 25$ with 2 planes) is also given.

The condition for one solution to the kinematics was that the minimum value of $\Delta = E_{inc} + E_{target} - \sum_{j=1}^{ntrack}(m_j^2 + P_j^2)^{1/2}$ was between 0 and 50 MeV, if it was larger than this the event was not accepted (0 solutions).See [3]

5.1 Simulation of the Silicon Detectors

The measured signal from the silicon detectors was simulated in the following way:

P_{beam}	1.0	1.5	2.0
0 solutions	0	2	6
1 solution	120	138	154
2 solutions	547	709	729
1 plane, right sol.chosen	501	630	620
1 plane, wrong sol.chosen	46	79	109
1 plane, too high X^2	22	3	0
2 planes, right sol.chosen	519	660	664
2 planes, wrong sol.chosen	28	49	65
2 planes, too high X^2	49	14	0

Table 3: Solution statistics

1. The geometrical efficiency of the detectors was assumed to be 0.913.

2. The mean energy loss,$< E >$, for the given β and δx (thickness 0.028 cm for the silicon), was calculated from the Bethe-Block formula.

3. Fluctuations were added according to Landau theory(see [5]). From the CERN library routine RANLAN a random number λ following the Landau distribution was generated.Then the energy loss is given by

$$E =< E > +\lambda \cdot \xi + \xi(\beta^2 + 1 - C + \ln \frac{\xi}{E_{max}}) \qquad (4)$$

where

$$\xi = 153.4 \frac{1}{\beta^2} \frac{Z}{A} \rho \delta x (keV)$$

$$E_{max} = \frac{2m_e^2(\beta\gamma)^2}{1 + 2\gamma\frac{m_e}{M_x} + (\frac{m_e}{M_x})^2}.$$

$C = 0.577215$, Euler's constant.

$M_x =$ particle mass.

4. A gaussianly distributed electronic noise N = S/8.5 was added.

5. If we had two silicon planes we did this procedure twice, and used the lowest value as the measured energy loss.

reaction $P_{beam} = 1.5GeV/c$	$4K$	$p\bar{p}\pi\pi$
$\theta > 15$	4199	899
$\leq 1, \theta > 45$	4089	888
$\leq 1, \beta > 0.8$	4088	884
$100 \leq \sum\theta \leq 160$	4064	494
0 solutions	21	42
1 solution	37	153
2 solutions	4005	299
$X^2 <$ cut(2 planes)	4001	73
$X^2 <$ cut(1 plane)	4036	164
Rate (2 planes)	12000	365

reaction $P_{beam} = 2.0GeV/c$	$4K$	$p\bar{p}\pi\pi$
$\theta > 15$	4116	2162
$\leq 1, \theta > 45$	4007	1991
$\leq 1, \beta > 0.8$	2300	1454
$100 \leq \sum\theta \leq 160$	2291	1174
0 solutions	19	184
1 solution	47	381
2 solutions	2233	609
$X^2 <$ cut(2 planes)	2273	401
$X^2 <$ cut(1 plane)	2280	572
Rate (2 planes)	9092	138700

Table 4: Number of events after cuts, 10 000 events generated

6 Background reactions

It is possible to distinguish the $\pi\pi p\bar{p}$ reaction from 4K by applying a cut on X^2.In figure 8 of the X^2 distribution for this background reaction we see that the values are much higher. To study the rejection efficiency, we generated 10^4 events of the $\bar{p}p\pi\pi$ reactions, and the non resonant 4K reaction and applied the following conditions:

- Acceptance:Events with particles which have a polar angle less than 8 degrees are rejected.
- Trigger1:Not more than one particle with $\theta > 45^o$ (in barrel).
- Trigger2:Not more than one particle with $\beta > 0.8$, the cerenkov limit.We have assumed an efficiency of 0.95 for the cerenkov detector.
- Trigger3:The sum of the polar angles.$100 < \theta < 160$.
- X^2 cuts , as described above, in the reconstruction we assumed that the particles were kaons.

In table 4 we see that these conditions will reject a lot of the $\bar{p}p\pi\pi$ reactions.We have assumed the following cross sections:

P_{beam}/reaction	1.0 Gev	1.5 Gev	2.0 Gev
4K	1.0 μb	3.0 μb	4.0 μb
$\bar{p}p\pi\pi$	0	5.0 μb	380.0 μb

when calculating the relative rates. Defining the X^2 cuts better, one could get even better signal to background ratios.

From the invariant mass we can distinguish between the direct channel 4K, and the $\phi\phi \rightarrow 4K$. Figure 9 shows the $\phi\phi$ events against a background of 4K, which shows a clear peak at the ϕ mass.

For the results obtained from applying mass cuts on the 4K , as well as more trigger tests see [2]. This reference also gives more details about the simulation and analysis programs.

References

[1] Bjarne Stugu. *Jetset-geometry description using the GEANT package* . JETSET NOTE JETSET 44, University of Oslo, 1989.

[2] Helen Korsmo. *An experiment to search exotic resonances in proton antiproton collisions at Cern's LEAR. A track reconstruction program and its application to simulated data.* Cand.Scient.thesis, University of Oslo, 1990.

[3] M.Ferro-Luzzi and J.-M.Perreau. *Study of the detector* . JETSET Note, CERN, 1988.

[4] A. Buzzo et al. *A silicon pad dE/dx detector for PS202.* JETSET NOTE JETSET 88-23, CERN, 1988.

[5] R. Brun et.al. *GEANT3 users guide.* CERN DD division, 1988.

List of Figures

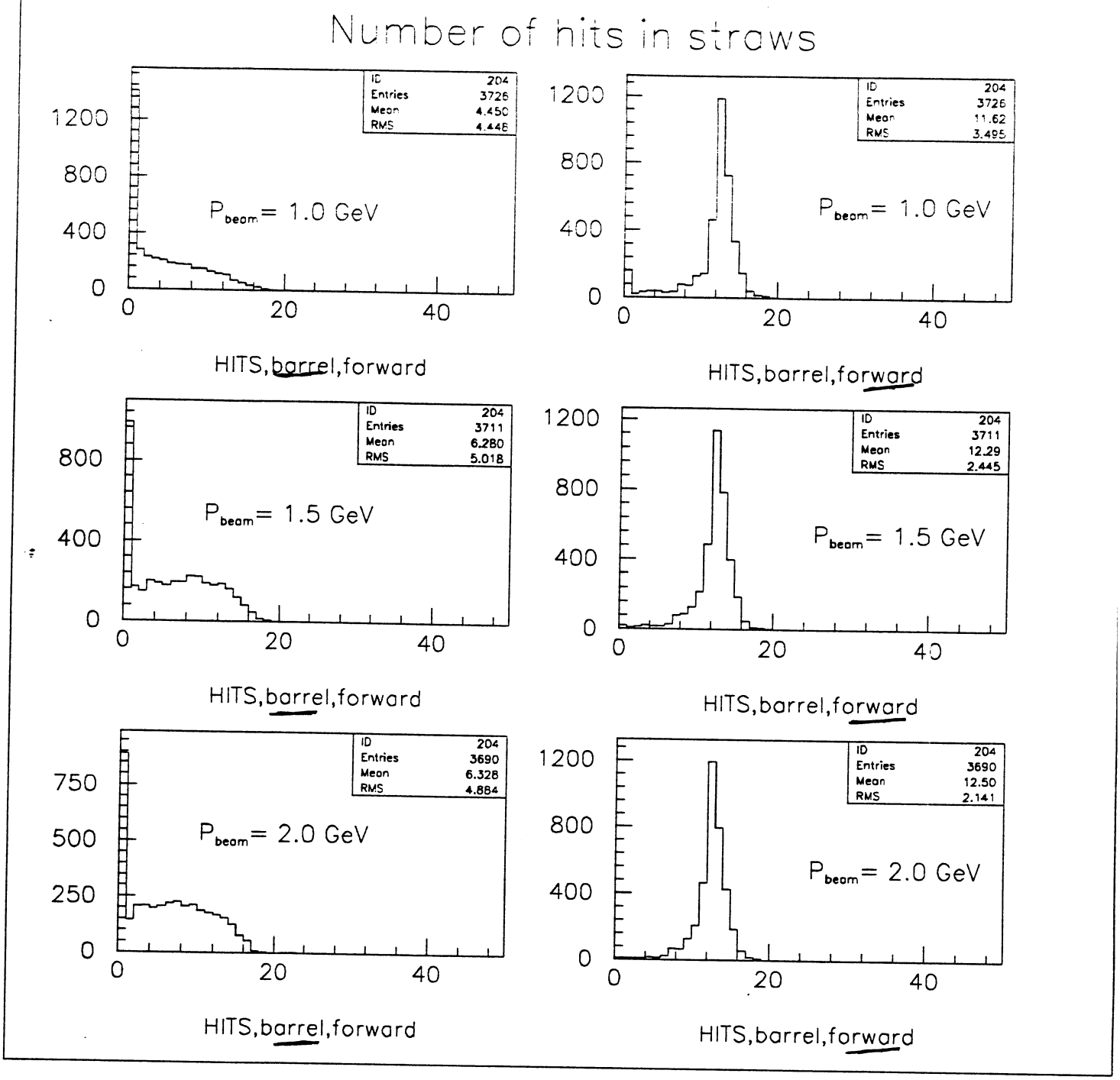

Figure 1: Number of hits for each track

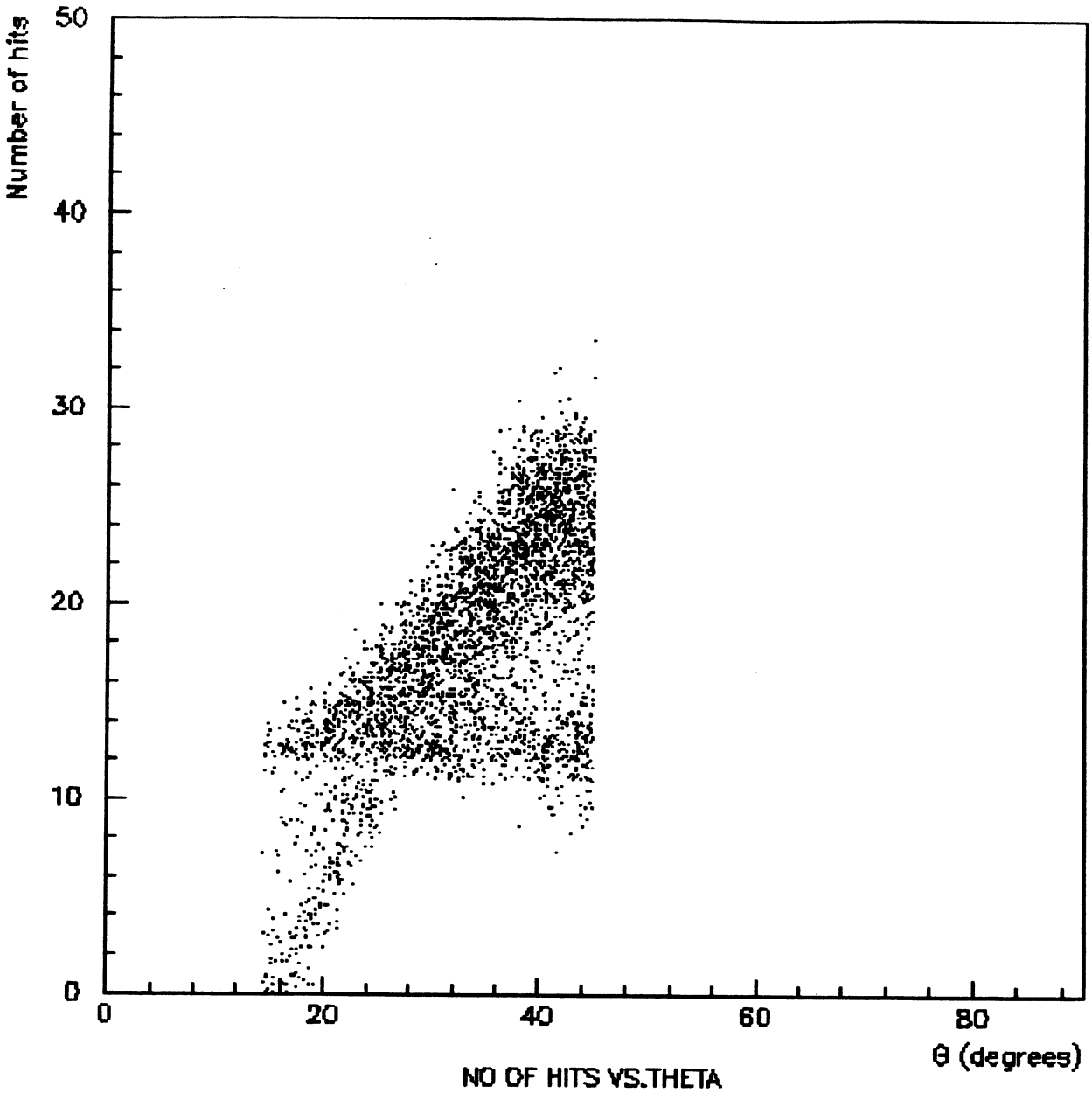

Figure 2: Number of hits vs theta

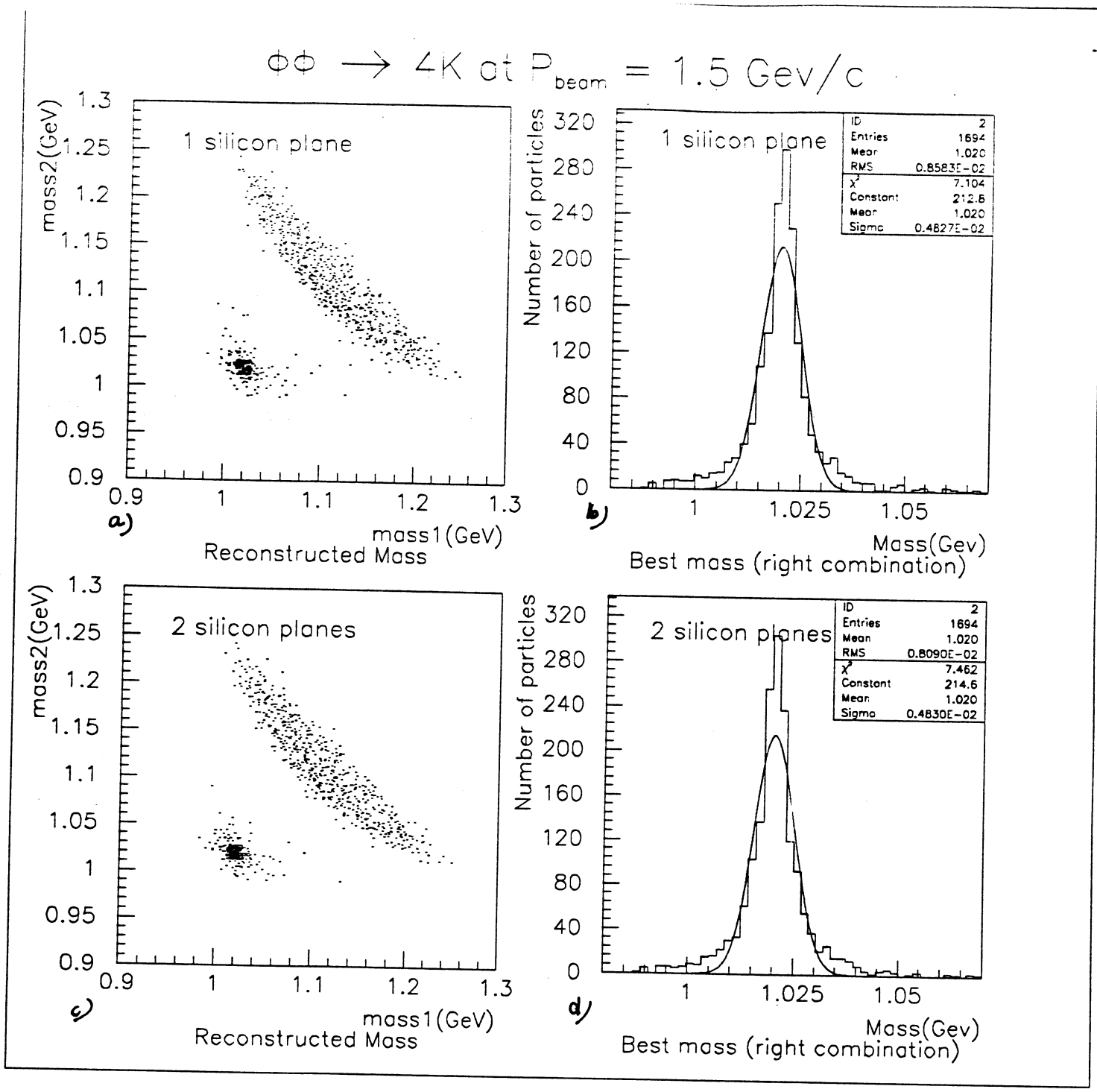

Figure 3: Invariant mass for kaon pairs

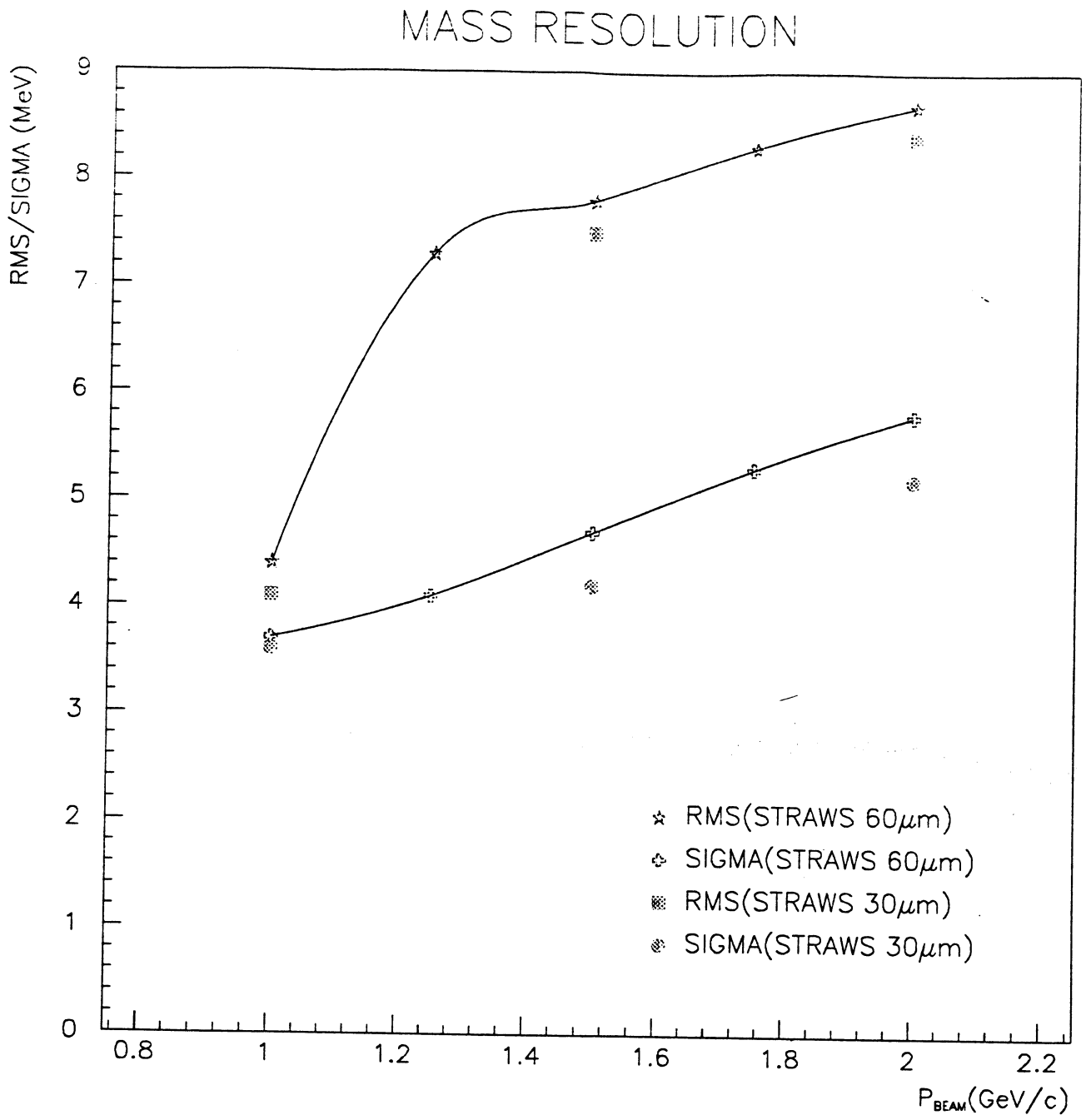

Figure 4: Mass resolution as a function of the momentum

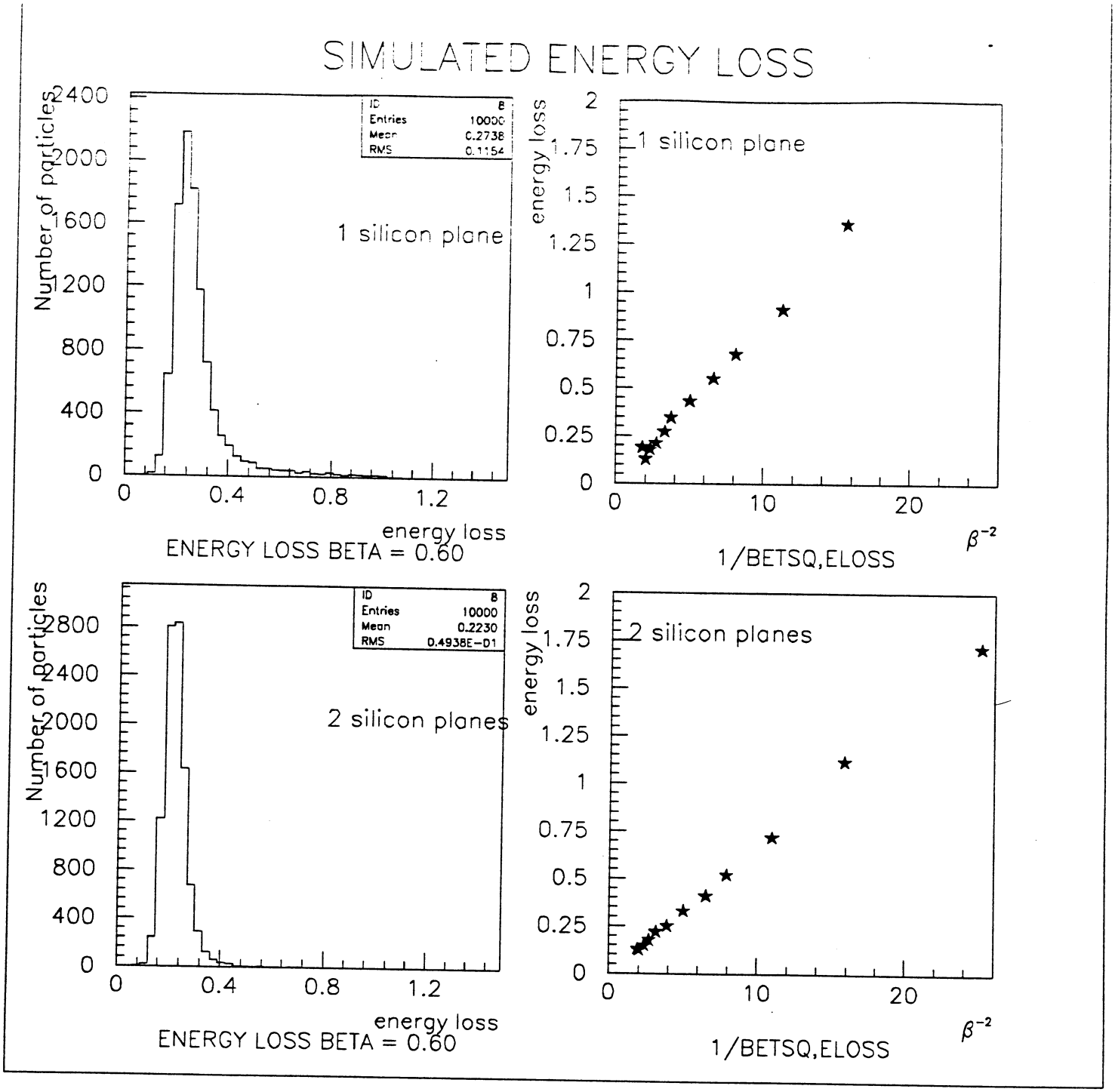

Figure 5: Energy loss in silicon detector

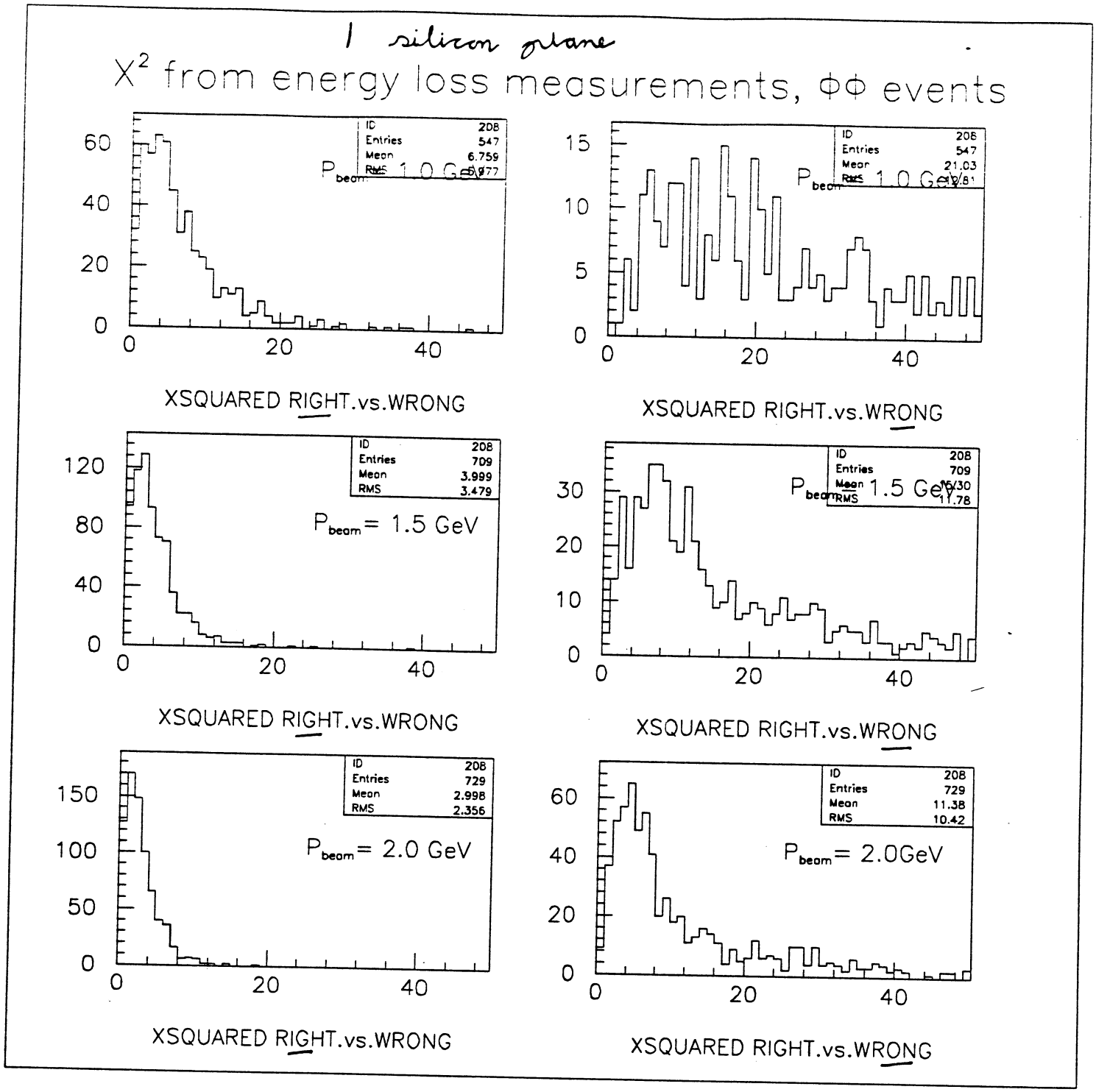

Figure 6: X^2 distributions

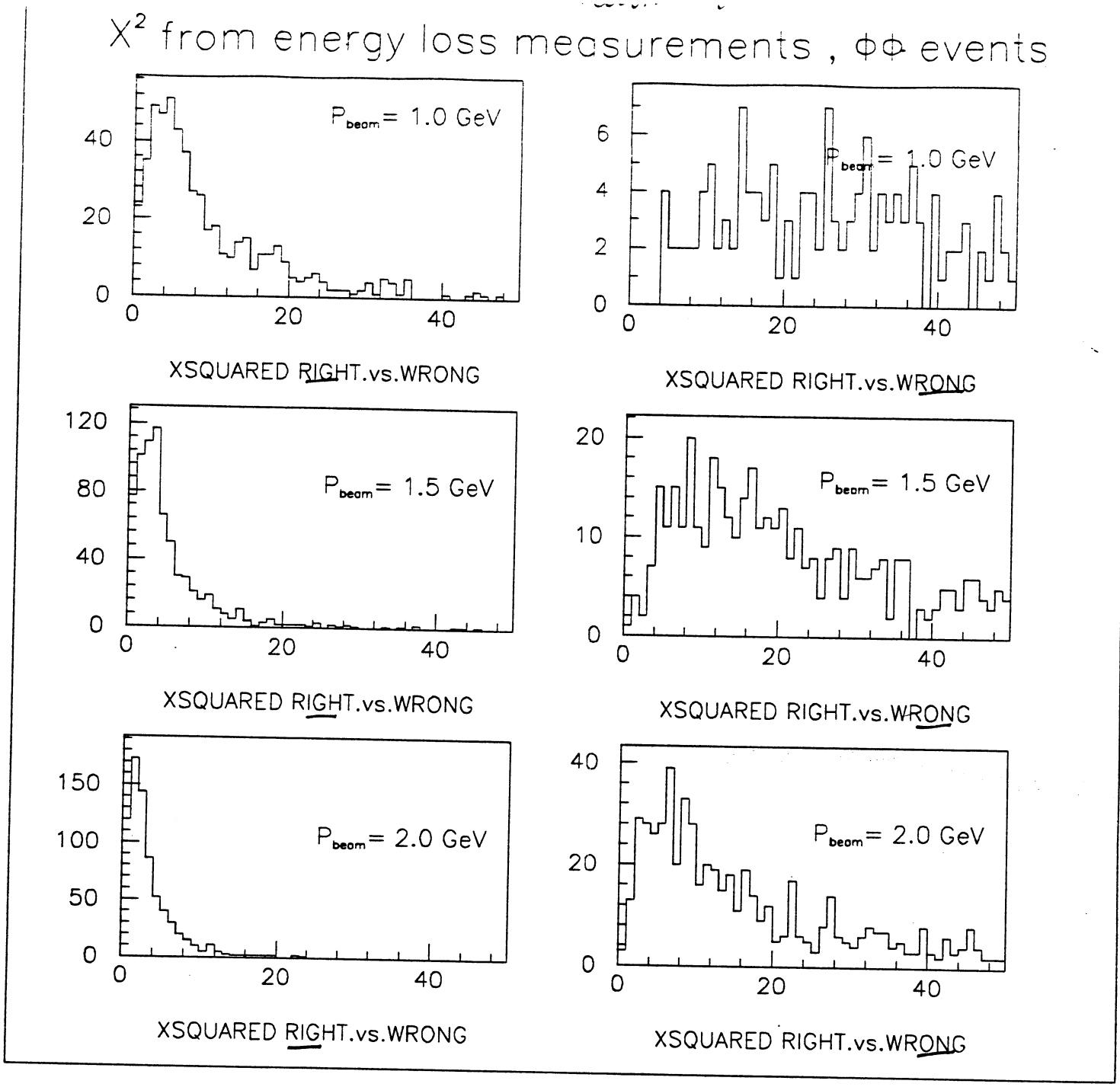

Figure 7: X^2 distributions

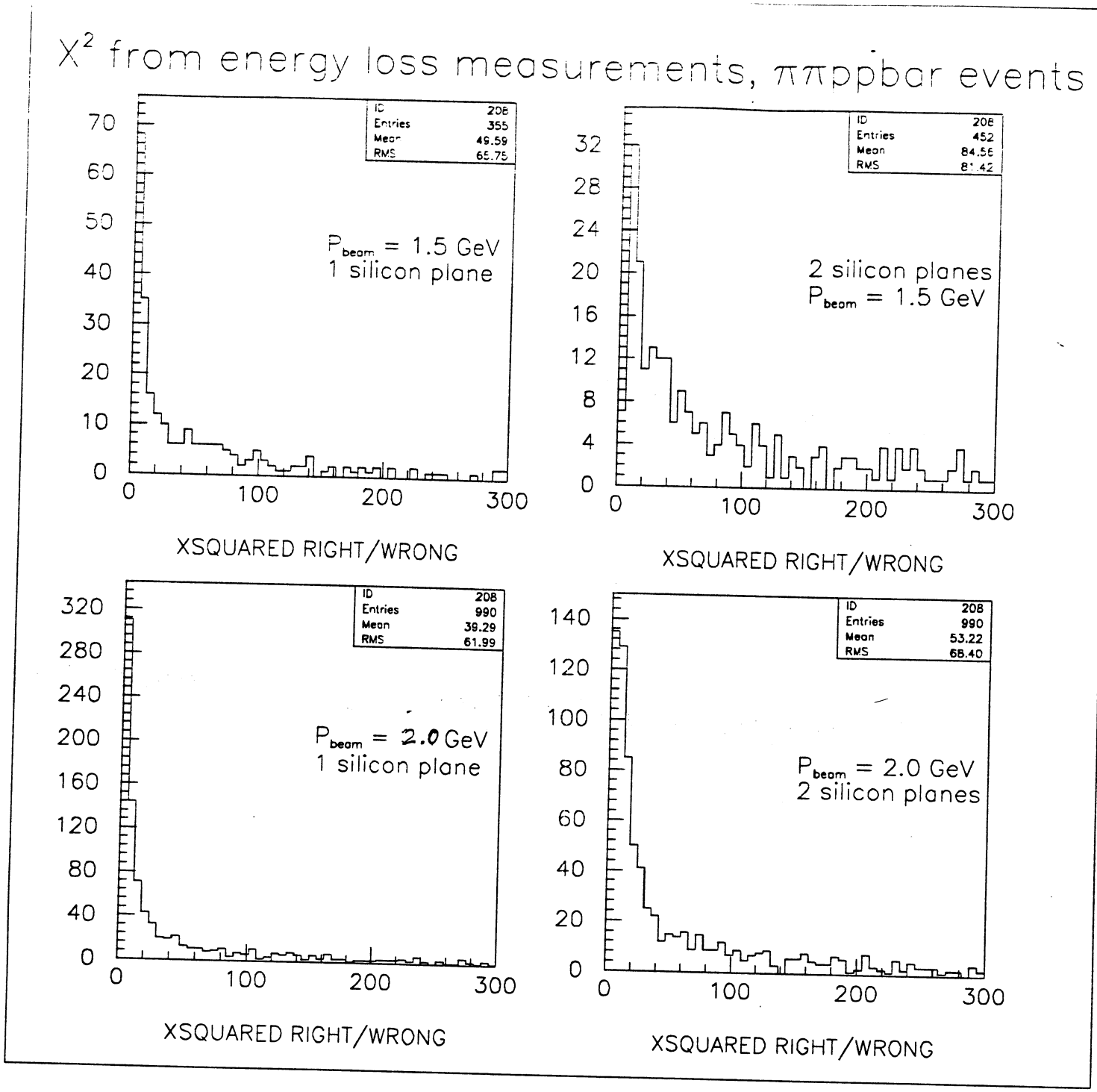

Figure 8: X^2 distribution for background reaction

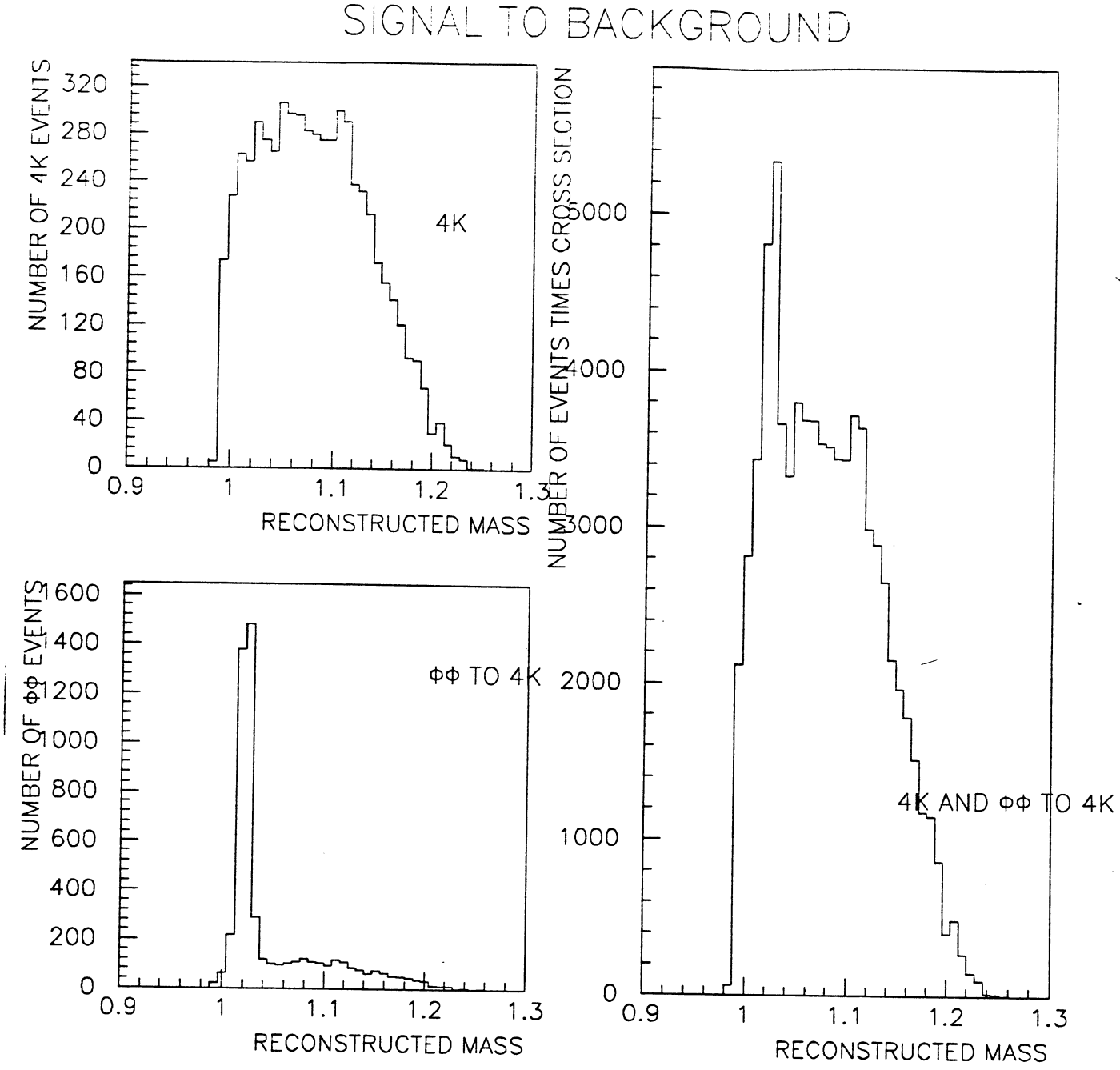

Figure 9: Mass distribution for 4K and $\phi\phi$ events

Bibliography

[1] B.Diekmann. Spectroscopy of mesons containing light quarks(u,d,s) or gluons. *Phys.rep.*, (159):171–185, 1988.

[2] D.Robson. A basic guide for the glueball spotter. *Nuclear Physics.*, (B130):328–348, 1977.

[3] R. A. Eisenstein. *The JETSET experiment at LEAR* . Technical Report, Status report to the PSCC, 1988.

[4] D.Hertzog et al. *Test of prototype PB/scifi eloctromagnetic calorimeter modules'.* JETSET NOTE JETSET 89-08, University of Illinois, 1989.

[5] F.E.Close. Gluonic hadrons. *Rep.Prog.Phys*, (51):833–880, 1988.

[6] F.Halzen and A.D.Martin. *Quarks and Leptons.* John Wiley and Sons,Inc., 1984.

[7] Ian S. Hughes. *Elementary Particles.* Cambridge, 1984.

[8] J.Cornwall and A.Soni. *Phys.lett.*, (120B), 1983.

[9] J.Kirkby and T.Taylor. *A 1.5 tesla warm magnet for jetset* . JETSET NOTE JETSET 88-10, CERN, 1988.

[10] Helen Korsmo. *Mass reconstruction in Jetset with straw detectors and silicon planes.* JETSET Note, University of Oslo, 1990.

[11] R. Ley. Lear statistics. In C.Amsler., editor, *Physics at LEAR with low energy antiprotons. Proceedings of the fourth LEAR workshop.*, 1987.

[12] M.Ferro-Luzzi and J.-M.Perreau. *Study of the detector* . JETSET Note, CERN, 1988.

[13] Antimo Palano. *The search for gluonic matter.* Technical Report CERN-EP/87-92, CERN, 1987.

[14] D.Hertzog P.E.Reimer, R.Tayloe. *More on 'More on the trigger pixel saga'.* JETSET NOTE , University of Illinois, 1989.

[15] P.Lefevre. Lear -present status,future and devlelopment. In C.Amsler., editor, *Physics at LEAR with low energy antiprotons. Proceedings of the fourth LEAR workshop.*, 1987.

[16] Meinhard Regler. Data analysis techniques in high energy physics experiments. 1988.

[17] R.v.Frankenberg and W.Oelert. *Beam tests of the JETSET scintillation trigger detectors.* JETSET NOTE JETSET 88-36, CERN, 1988.

[18] Richard Slansky. Particle physics and the standard model. In *Particle Physics, A Los Alamos Primer.*, pages 69–70, Cambridge, 1988.

[19] Bjarne Stugu. *Jetset-geometry description using the GEANT package* . JETSET NOTE JETSET 44, University of Oslo, 1989.

[20] T.Barnes. *Z.Phys.*, (10), 1981.

[21] Walther H. Toki. *BNL Glueball rewiew.* Technical Report SLAC-PUB-4824, SLAC, 1988.